The Use and Characterization of Composite Alumina-Titania-Zirconia-Silica Ceramic Membranes for Gas Separation

By

Berna TOPUZ

A Dissertation Submitted to the
Graduate School in Partial Fulfillment of the
Requirements for the Degree of

MASTER OF SCIENCE

Department: Materials Science and Engineering
Major: Materials Science and Engineering

İzmir Institute of Technology
İzmir, Turkey

September, 2002

ACKNOWLEDGEMENTS

ABSTRACT

The preparation, characterization and pure gas permeation of sol-gel derived alumina and silica membranes were investigated in this work. The effects of various parameters on sol particle size and unsupported membranes pore structure were investigated by laser light scattering particle size and N_2 adsorption-desorption analysis.

γ-alumina membranes were prepared on ZrO_2 supports by successive dipping into boehmite sols. Almost proportional decreases in sol particle size and membrane pore diameter were determined with increasing acid content during the boehmite sol preparation. Increasing the H^+/Al^{3+} mole ratio from 0.1 to 0.25 caused the hydrodynamic particle size and BJH pore size to decrease from 65 to 30 nm and 3.6 to 2.9 nm, respectively. The pore size increased from 2.8 nm to 3 nm upon increasing the calcination temperature from 500 to 600°C. Unsupported membranes were heat treated in the 200 to 1200 ^{o}C range for the characterization of the phase structure. Boehmite was the dominant phase below 500 ^{o}C, gamma being the dominant phase up to 900 ^{o}C and pure α-Al_2O_3 phase was obtained upon heat treatment at 1200°C. Pinhole and crack free alumina membranes about 3 μm (double layer) in thickness were observed from SEM pictures with insignificant infiltration. The CO_2 permeability through the double layer γ-Al_2O_3 membrane calcined at 600 ^{o}C was about $2.25*10^{-7}$ mol/m^2.s.Pa, and had a slight pressure dependence which may indicate Knudsen Diffusion and Laminar Flow as the effective transport mechanisms. Upon the calcination of a similar double layer alumina membrane at 500°C, the CO_2 permeability decreased to $1.51*10^{-8}$ mol/m^2.s.Pa and was independent of pressure.

Silica membranes were prepared by a sol-gel technique. These sols were prepared by acid catalysed hydrolysis and condensation of tetraethylorthosilicate in the presence of a solvent. The effects of processing parameters like the acid type and amount utilized during sol preparation, sol aging, heat treatment conditions, dipping time on the membrane pore structure and the permeation of pure gases were investigated. The supported membranes were heat treated in the 50-400 ^{o}C range. The N_2 and CO_2 permeabilities of silica membranes varied in the $2.2 * 10^{-10} - 2.7 * 10^{-8}$ mol / m^2.s.Pa and $1.2*10^{-9} - 6.95*10^{-8}$ mol / m^2.s.Pa range for single layer membranes dipped for 10 seconds into the sol. The sols became viscous and gelled in 16 hours at 50 ^{o}C. The O_2 permeability increased with aging time. The optimum dipping time during

processing was determined to be 10 seconds. The permeabilities of these membranes increased significantly with the sol acid content. The thickness of the silica membranes were determined to be about 2μm and significant infiltration into the support was observed from the SEM pictures.

ÖZ

Bu çalışmada alumina ve silika membranların sol-jel yöntemiyle hazırlanması, karakterizasyonu ve gaz geçirgenliği incelendi. Çeşitli parametrelerin sol parçacık boyutuna ve desteksiz membran gözenek yapısına olan etkileri lazer ışık saçınım parçacık boyut analizi ve azot adzorpsiyon-dezorpsiyon analizi ile incelendi.

γ-alumina membranlar zirkonya desteklerin böhmit soluna ard arda daldırılmasıyla hazırlandı. Böhmit solunun hazırlanması aşamasında asit içeriğinin artmasıyla sol parçacık boyutunda ve membran gözenek çapında orantılı azalış belirlendi. H^+/Al^{3+} mol oranının 0.1'den 0.25'e çıkması sırasıyla hidrodinamik sol parçacık boyutunun ve BJH gözenek boyutunun 65'den 30 nm'ye ve 3.6'dan 2.9 nm'ye düşmesine neden oldu. Gözenek boyutu ısıl işlem sıcaklığının 500'den 600 ^{o}C'ye çıkarılmasıyla 2.8'den 3 nm'ye arttı. Desteksiz membranlar faz yapısı karakterizasyonu için 200-1200 ^{o}C aralığında ısıl işleme tabi tutuldu. 500 ^{o}C'nin altında böhmit, 900°C'ye kadar γ-Al_2O_3 ve 1200 ^{o}C'nin üzerinde α-Al_2O_3 hakim faz olarak elde edildi. Kusursuz alumina membranların yaklaşık 3μm (iki katman) kalınlığında olduğu ve önemsiz sayılabilecek miktarda destek içine nüfuz ettiği SEM fotoğraflarıyla belirlendi. 600 ^{o}C'de ısıl işleme tabi tutulmuş iki katmanlı γ-Al_2O_3 membranların CO_2 geçirgenliği yaklaşık 2.25*10^{-7} mol/m^2.s.Pa'dır ve az miktarda basınca bağlı olması etkin aktarım mekanizmalarının Knudsen difüzyon ve laminar akış olabileceğini gösterdi. 500 ^{o}C'de ısıl işlemin uygulandığı benzer iki katmanlı alumina membranlarda CO_2 geçirgenliği basınçtan bağımsız olarak 1.51*10^{-8} mol/m^2.s.Pa' a düşmüştür.

Silica membranlar sol-jel tekniği ile hazırlandı. Bu sollar çözücü ortamında tetraetilortosilikatın asit ile katalizlenmiş hidroliz ve yoğunlaşma tepkimeleriyle hazırlandı. Sol hazırlanmasında kullanılan asit çeşidi ve miktarı, sol yaşlandırma, ısıl işlem koşulları ve daldırma zamanı gibi proses parametrelerinin membran gözenek yapısı ve gaz geçirgenliğine etkileri incelendi. Destekli membranlara 50 ile 400 ^{o}C aralığında ısıl işlem uygulandı. Sol içerisine 10 saniye daldırılmış tek katmanlı silica membranların N_2 ve CO_2 geçirgenlikleri sırayla 2.2 * 10^{-10} – 2.7 * 10^{-8} mol/m^2.s.Pa ve 1.2*10^{-9}–6.95*10^{-8} mol/m^2.s.Pa aralığındadır. Solların 50 ^{o}C'de 16 saat yaşlandırılmasıyla akışkanlığı azaldı ve jelleşti. O_2 geçirgenliği yaşlandırma zamanıyla arttı. Proses boyunca optimum daldırma zamanı 10 saniye olarak belirlendi. Bu memranların geçirgenlikleri sol asit içeriğinin artmasıyla önemli oranda arttı. Silika

membranların yaklaşık 2µm kalınlığında olduğu ve önemli sayılabilecek oranda destek içine nüfuz ettiği SEM fotoğraflarından gözlendi.

TABLE OF CONTENTS

LIST OF FIGURES

LIST OF TABLES

CHAPTER I

INTRODUCTION

The superior thermal/chemical/mechanical stability and the ability of ceramic membranes in affecting the transport rates of chemical species through their processing controllable pore structures make them very attractive for many separation problems. Inorganic membranes have been used for a very long time in many applications and this reduces the operating costs for users. In addition, pore dimension and pore size distribution are controllable and inorganic membranes are easy to shape which is an important parameter for separation processes. On the other hand, the most important disadvantage is their brittle character. To overcome this problem membranes can be coated on a macroporous support.

Inorganic membranes are classified into two groups, porous and non-porous. The non-porous membranes have chemical, mechanical, electrical functions and are used as a device. The porous inorganic membranes are mainly used in separation processes (e.g. microfiltration, ultrafiltration, reverse osmosis, gas separation and pervaporation), where the control of microstructure is an important factor.

Gas separation membranes can be described as a semi-permeable barrier capable of separating gases by a driving force. The driving force may be pressure difference across the membrane. Design of defect free asymmetric composite ceramic membranes that are composed of different layers with a gradual decrease in layer thickness and pore size, is the key parameter since gas transport through the inorganic porous membranes depend on the pore microstructure unlike polymeric membranes. Three keys to membrane production are (i) avoidance of cracks, pinholes and other defects that reduce the selectivity, (ii) precise pore size control and (iii) maximisation of porosity and minimisation of the membrane thickness in order to maximise the flux. In order to obtain an effective gas separation membrane, the membrane should be highly permeable and the selectivity should be high.

The nature of the pore structure is one of the most important factors along with molecular properties and the interaction with the pore walls of gaseous species during their transport through porous membranes. Transport of gases through porous membrane is mainly by Knudsen Diffusion, Surface Diffusion and Micropore Diffusion, depending on the average pore size and also on the interaction with the

membrane materials. For membranes with pores in the small mesopore to micropore region, knudsen diffusion and micropore diffusion are important. Gas separation according to knudsen diffusion is based on differences in molecular velocity of different components in a mixture. Surface diffusion and micropore diffusion can provide higher separation efficiencies. To achieve high level of separation using micropore diffusion and surface diffusion mechanisms, pore size in the microporous range must be closely controlled and porosity must be high.

The most selective thin top layers with a small effective thickness (in the micron or sub-micron range) such as Silica and Zeolites can be synthesised from either sol-gel or chemical vapor deposition (CVD) processes.

Sol-gel processes attract most attention due to their excellent processibility and their potential to the towards close control of pore microstructure. The preparation of metal oxide ceramic membranes are generally conducted by sol-gel techniques and posses the following characteristics; (i)the thickness of the membrane can be in the order of micrometers, (ii) homogeneous membranes with relatively separation surfaces can be realised, (iii) membranes with a variety of chemical composition can be prepared. Consequently, sol-gel processes have been the focus of many studies and a variety of strategies have been identified.

The preparation, characterization and pure gas permeation of sol-gel derived alumina and silica membranes on zirconia support discs were investigated in this work. N_2 adsorption-desorption isotherms, thermogravimetric analysis and FTIR were used to investigate the effects of water/alkoxide ratio, H^+/alkoxide ratio on the catalysis of the hydrolysis and condensation reactions and the peptisation process. The performance and the potential use of these membranes in gas separation applications mainly depend on the ability in control/design of the microstructure-pore network in these materials. The effects of processing parameters like the acid type/amount and water amount utilized during sol preparation, sol aging, heat treatment conditions, dipping time on the thin film pore structure and the permeation of pure gases were investigated. Defect free microporous top silica layers with high selectivity and high flux were prepared by using sol-gel dip-coating process.

CHAPTER II

INORGANIC MEMBRANES AND SEPARATION PROCESSES

Membranes can be classified as separative and non-separative ones. A separative membrane can be described as a semipermeable barrier between two phases preventing intimate contact. This barrier must be permselective which means that it restricts the movement of molecules in a very specific way. The flux of liquids or gases is in most cases driven by a (partial) pressure gradient or by an electric field gradient.

The barrier can be solid, liquid or gas and the permselectivity can be obtained by means like; size exclusion, molecular sieving mechanisms, and differences in bulk or surface diffusion, adsorption and/or reactivity on internal surface, solubility or vapour pressure, and electrical charge between surface and permeating species. Membranes can be used for, separation of mixtures (liquids, gases or liquid-solid mixtures), and manipulation of chemical reactions. Possibilities are the increase of the conversion of a reaction by shifting away from the equilibrium conditions or increasing the conversion and/or selectivity of a catalytic reaction. Non separative membranes form a new group which is used for; immobilization of enzymes or biological molecules in a bioreactor, in photo-electrochemical or photocatalytic cells and as sensors for example, in diagnostic kits or selective gas monitors.

Membranes have some advantages over the conventional separation techniques. Membranes are very fast, efficient and economical in many cases. Membrane separation takes place without phase changes. Many different types of membranes are in use these days with different sizes, structures and shapes.

Membrane separation involves partially separating a feed containing a mixture of two or more components by use of a semipermeable barrier (the membrane) through which one or more of the species moves faster than another or other species. As shown in Figure 2.1 , the basic process of the membrane separation involves a feed mixture separated into a *retentate* (part of the feed that does not pass through the membrane, i.e., is retained) and a *permeate* (part of the feed that passes through the membrane).

Although the majority of time the feed, retentate, and permeate are usually liquid or gas, they may also be solid. The optional sweep is a liquid or gas, used to help remove the permeate.

Feed Mixture
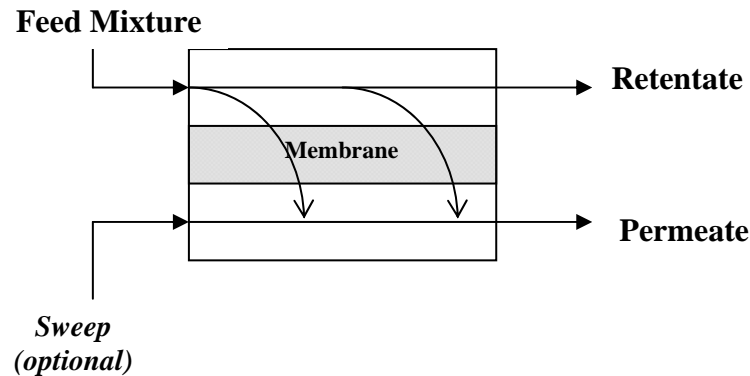
Figure 2.1. Basic Membrane Separation

The membrane selectivity, which expresses the preferential passage of one of the components, has to be as high as possible. Permeability has to be the highest too. This latter requirement led to the concept of the permselective layer with a small thickness that needs a support to provide mechanical properties.

The energy is required for separation process. These energy may be only of mechanical nature, such as in the process of microfiltration, ultrafiltration, reverse osmosis, gaseous diffusion, gaseous permeation, but energy may be also of electrical nature such as in the electrodialysis process.

The classification of membranes can be made in two main groups and many subgroups. Main groups are inorganic and polymeric and such a classification of membranes according to materials is given in Figure 2.2.

Asymmetric polymeric membranes consist of a very dense and non-porous 0.1-0.5 μm thick layer supported by a porous sublayer of thickness 50-150 μm and have been extensively used for industrial applications. Various polymers have been used including polyether sulfone, polycarbonate, polydimethylsiloxane (PDMS) and polytrimethylsilylpropyne. In such membranes, high flux is achieved by low separation or vice versa. In other words, quality of the final product is always compromised by production throughput.

Polymeric membranes are currently used in industry for most separation processes, but ceramic membranes that are composed substantially of inorganic materials, offer several advantages over polymeric membranes. One of the disadvantages of the polymeric membranes is the relatively short service life. Ceramic

Classification of Membranes

INORGANIC

POLYMERIC

Dynamic

Dense

Porous

Glassy

Rubbery

Metallic

Ceramic

Glass

Molecular
Sieving

Symmetric

Asymmetric
Composite
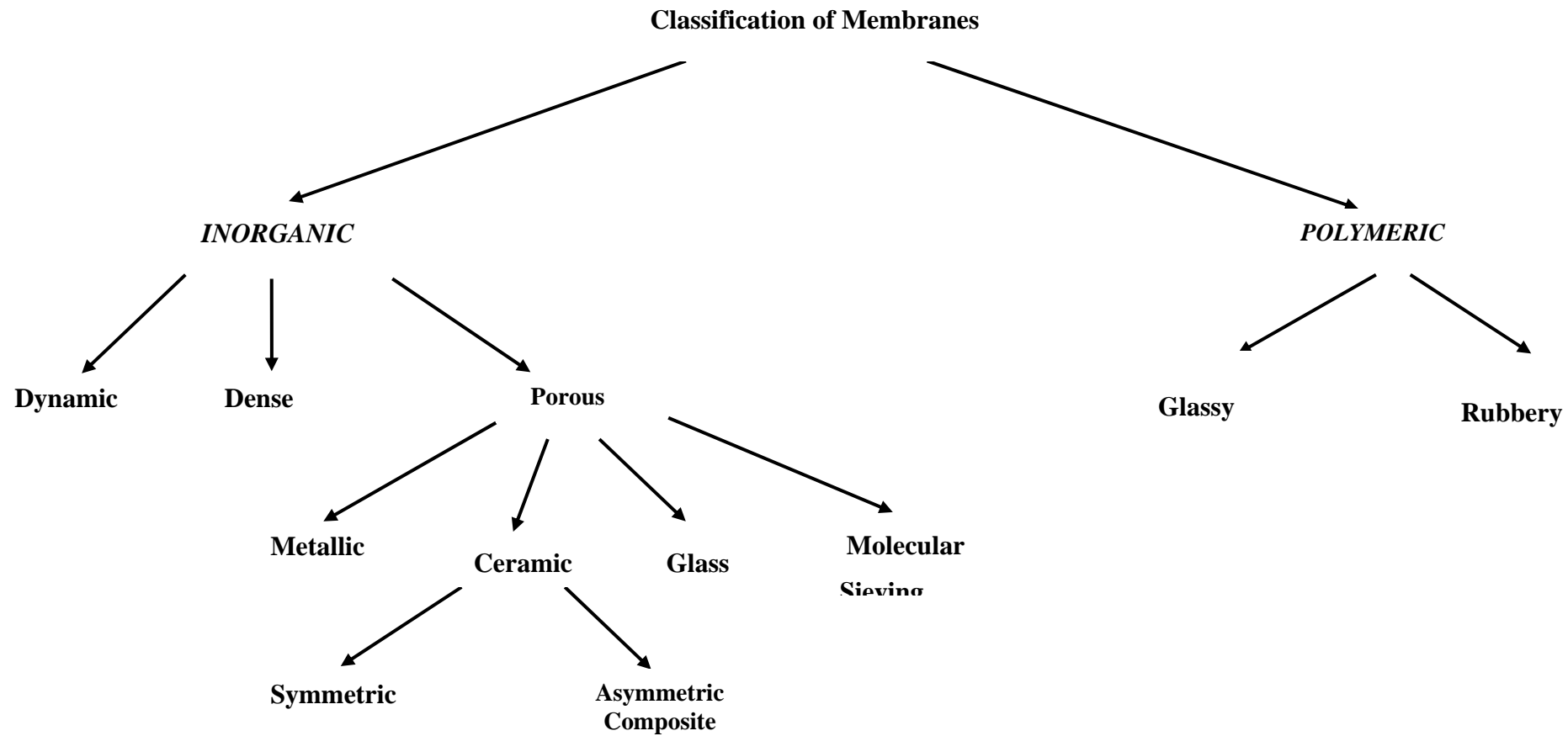
Figure 2.2. Classification of membranes based on the materials and structure.

membranes are more resistant than polymeric membranes to organic solvent, chlorine and in some cases, extremes of pH. Ceramic membranes are also inherently more stable at high temperatures, thus allowing more efficient sterilisation of process equipment than is possible with polymeric membranes. Ceramic membranes are generally quite resistant to microbial or biological degradation, which can occasionally be a problem with polymeric membranes. And also ceramic membranes are also mechanically more stable under high pressures. Due to these disadvantages of the polymeric membranes, the range of applications are limited.

2.1. Inorganic Membranes

Inorganic membranes can be classified as shown in Table 2.1. The dense inorganic membranes consist of solid layers of metals (Pd, Ag, alloys) or oxidic solid electrolytes which allow diffusion of hydrogen or oxygen. Another category of dense membranes consist of a porous support in which a "liquid" is immobilised. The liquid fills the pores completely and is semipermeable. Interesting examples are molten salts immobilized in porous steel or ceramic supports and semipermeable for oxygen.

Very high selectivities can be obtained but permeabilities are relatively low with dense membranes. This can be improved by decreasing the membrane thickness and by improving the sorption and surface reactions which limit the permeation processes in thin membranes (Bhave,1991).

Inorganic porous membranes have been developed over the last fifty years primarily for the separation of uranium isotopes. It remains a technical challenge to produce defect-free inorganic membranes to separate gases. However, in the 1980s, the advantages of chemically inert ceramic membranes with well defined pore structure encouraged researchers to investigate the separation properties and application of inorganic membranes. Inorganic materials used for membrane preparation include zeolites, metals, glass and silica, alumina, etc.

Table 2.1. Types of Inorganic Membrane (Bhave,1991).

INORGANIC MEMBRANES	*MAIN CHARACTERISTICS*
	Metal foil
DENSE	*Oxidic solid electrolyte*
	Liquid immobilised (LIM)
	Permanent
DYNAMIC	*Nonpermanent*
POROUS METAL OR NONMETALLIC	*Symmetric, asymmetric*
	Supported, nonsupported
	Pore shape, morphology and size
	Chemical nature of pore surface
COMPOSITE	*Two phase particle mixture*

2.1.1. Porous Inorganic Membranes

In porous membranes the permeability and the selectivity in liquid and gas separations depends on the separation mechanism which in turn is a function of the pore diameter and of the size of the molecules to be separated. Transport properties are selectively influenced by the interaction of the mobile species with the internal pore surface. Strong effects can be obtained in very small diameter, generally smaller than 2 nm pores.

2.1.1.1. Metallic Membranes

Microporous metallic membranes can be prepared from metal alloys such as Ni, Al, Au, Cr, Pt, Pd by subsequent leaching of one component. These membranes have found their main application in gas separation processes. Porous metals are commercially available for particulate filtration. They are used in some cases as microfiltration membranes that can withstand harsh environments or may be supports for dynamic membranes.

Another important application of metallic membranes is in the supply of highly pure hydrogen for semiconductor production. Nonporous metallic membranes are used for this purpose, operating at elevated temperatures. Pd and especially Pd- Ag alloys are particularly suitable membrane materials (Bhave 1991, Hsieh,1988).

2.1.1.2. Alumina Membranes

The market activities of alumina membranes thus far have provided the bulk of the momentum for making inorganic membranes an acceptable and viable separations tool in many applications.

Currently, those alumina membranes having a pore diameter greater than approximately 0.1 μm are made of α-alumina which is known to exhibit good thermal, chemical and mechanical stability. Although it is stable up to above 1000 °C, the α-alumina membrane modules which contain other auxiliary materials such as gaskets and end seals are generally recommended below 140 °C for those applications where steam sterilisation is required (Hsieh, 1988).

In contrast, transition- alumina membranes, which are characteristically small in pore size are much less resistant to, for example, strong acids and bases, and can be dissolved in those chemicals with time. Therefore, they are not recommended for applications where strong acids or bases are either present in the feed streams or required as part of the cleaning procedure (Bhave 1991, Hsieh,1988).

Alumina membranes have been used in a variety of applications like concentration of whole skimmed milk, clarification and sterilisation of fruit juices, wine, beer and malt, microfiltration of water, sterilisation in biotechnology and oil-water separation. The porous alumina membranes have been used for gas separation in the isotopic separation and enrichment of uranium (Charpin et al.,1987).

Two types of alumina membranes can be prepared 1) unsupported 2) supported ones. Membranes can be synthesised by using slip casting and sol-gel method. Unsupported and supported α-alumina membranes can be prepared from boehmite colloidal suspensions. Boehmite sols were prepared by adding aluminum trisecbutoxide to distilled water then diluted nitric acid was added for peptization. The pore size of the alumina membranes can be tailor made by varying acid/hydroxide ratio, water/alkoxide ratio, acid type used in the preparation of the sol. (Chang et al.,1994,Changrong et al.,1996, Yoldas,1975a, 1975b).

Dipping time, the viscosity of the sol and the sintering temperature were effective in the formation of the membrane from the alumina sol. Many experimental studies showed that dipping time, number of dipping, alumina sol concentration at dipping, control the membrane morphology, membrane thickness and permeability (Okuba et al.,1990,de Lange et al.,1995a).

Heat treatment schedules also affect pore size distributions and the pore structures of alumina gels. Another factor is the use of drying chemical control additives such as PVA, which can be added to boehmite sols and modify the drying and calcination procedures (Lin et al.,1991, Uhlhorn et al.,1992).

2.1.1.3. Silica Membranes

In order to decrease the pore size of an ultrafiltration membrane for the introduction of specific properties necessary for gas separation, modification with amorphous silica is one of the options. Pore diameters smaller than 1 nm is necessary for gas separation. One way to make a microporous structure with such small pores is to use nanometer sized particles or polymers which are packed very effectively. The size and the shape of particles or polymers play important role. Particles or polymers with a more linear structure are preferred (Munoz-Aguado and Gregorkiewitz,1996, Nair et al., (1997b).

The preparation of submicrometer monodisperse particles by controlled hydrolysis of metal alkoxides have been widely investigated for a number of ceramic materials. In particular, recent research efforts were concentrated on sol-gel processes involving the formation of particulate materials or glass-precursor gels from silicon alkoxides such as tetraetylorthosilicate (TEOS) and tetrametoxysilane (TMOS). Silica sols and gels can be produced very easily both by the colloidal suspension and by the polymeric gel route. (de Vos and Verweij, 1998, Munoz-Aguado and Gregorkiewitz,1995, Fujii et al.,2001).

2.1.1.4. Molecular Sieve Membranes

The most commonly known molecular sieve membranes are carbon and zeolite membranes. Initial development work carried out on carbon molecular sieve membranes injected further interest in membrane research. Carbon Molecular Sieve membranes are synthesised from different polymeric materials including cellulose acetate, polyaramides and polyimides. Pore size (3-6 A^o) can be controlled under pyrolysis temperatures ranging from 500 to 1000 ^{o}C. Carbon molecular sieve membranes have high selectivities whilst fluxes are not compromised to the same extent as in polymeric membranes. The control of pore size is fundamental in producing high quality products or achieving high separation rates (da Costa et al., 1998 a).

Zeolites have well defined uniform pore structures. Zeolite based materials offer the potential to organise matter and manipulate molecules at the nanometer scale. Most zeolite membranes are prepared using hydrothermal methods, which are relatively simple but have difficulties in controlling the thickness of the membrane layers and the orientation of the particles. Another major difficulty is how to control the calcination process in order to provide crack-free membranes (Vroon et al., 1998). Various researchers have worked on ceramic zeolite composite membranes for gas separation using template method. They used an in situ process where a layer of pure zeolite grows on the surface of a ceramic substrate and zeolite crack-free membranes of small surface areas were produced (Jia et al., 1994).

Microfiltration membranes have relatively large pores (100nm to few μm in size), Ultrafiltration membranes especially with pore size in the 1 nm- 100nm range. Nanofiltraion membranes for gas separation and pervaporation with pore size of 1nm or smaller. Membrane separation processes are summarised at Table 2.2.

Table 2. 2. Membrane separation processes.

Membrane Process	Separation Potential for	Driving force	Preferably permeating component
Reverse Osmosis	Aqueous low molecular mass solutions Aqueous organic solutions	Pressure difference	Solvent
Ultrafiltration	Macromolecular solutions, emulsions	Pressure difference	Solvent
Microfiltration	Suspension, emulsions	Pressure difference	Continuous phase
Gas permeation	Gas mixtures, water vapour-gas mixtures	Pressure difference	Preferably permeating component
Pervaporation	Organic mixtures, aqueous-organic mixtures	Permeate side: ratio of partial pressure to saturation pressure	Preferably permeating component
Liquid membrane	Aqueous low molecular mass solutions, aqueous-organic solutions	Concentration difference	Solute (ions)
Osmosis	Aqueous solutions	Concentration difference	Solvent
Dialysis	Aqueous solutions	Concentration difference	Solute (ions)
Electrodialysis	Aqueous solutions	Electric field	Solute (ions)

2.2. Synthesis of Porous Inorganic Membrane

Porous inorganic membranes especially those with a microporous structure are potentially useful in gas separation in emerging areas such as catalytic reactors, gasification of coal, molten carbonate and water decomposition by thermochemical reactions. In order to achieve effective separation of gases with small molecules, the pores should be smaller than 2 nm. Gases permeate with low selectivities through mesoporous or macroporous membranes.

Materials, structures and preparation processes for typical porous inorganic membranes are shown in Figure 2.2. Silica based membranes are produced by chemical vapour deposition, sol-gel and pyrolysis techniques (Nair et al., 1997 (b), Vercauteren et al.,1998,Morooka and Kusakabe,1999). Carbon membranes are produced by pyrolysis of precursor films and the zeolite membranes are formed by hydrothermal techniques.

Sol-gel processes have been more frequently utilised to prepare inorganic microporous membranes based on alumina, silica, titania and zirconia. Sol-gel chemistry appears to be well adapted for the synthesis of inorganic materials with nanometer size pore diameters.
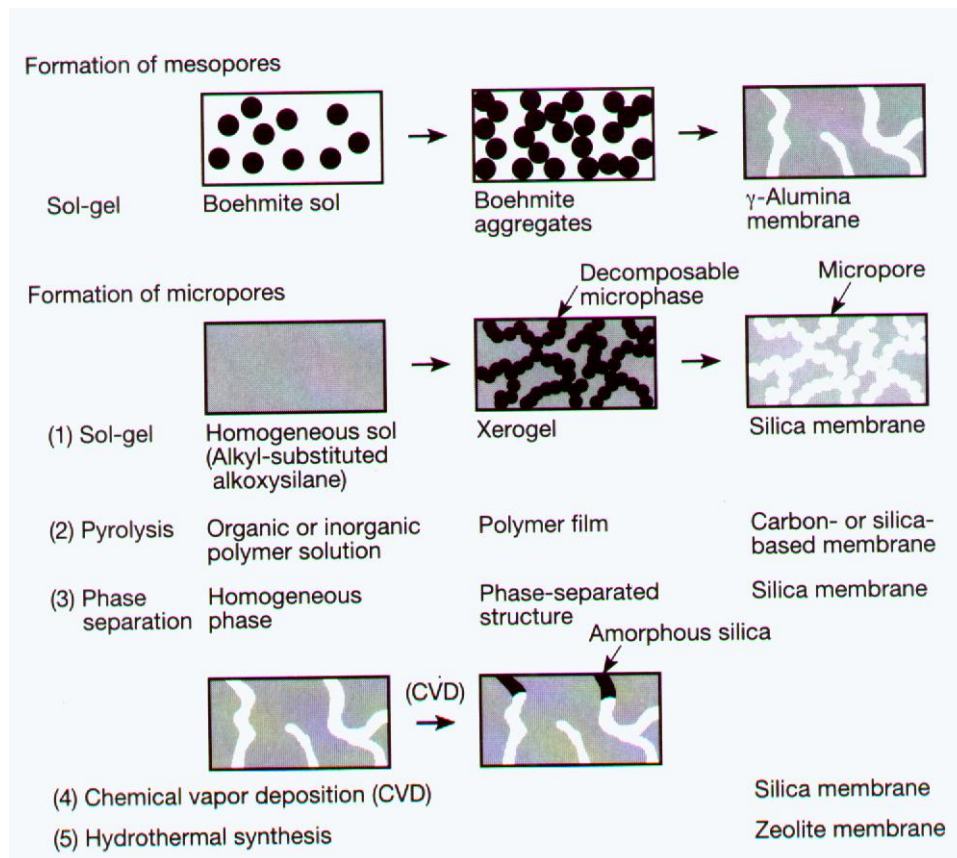
Figure 2.2. Formation of mesopores and micropores (Morooka and Kusakabe,1999).

CHAPTER III

SOL-GEL PROCESSING

Sols are defined as dispersions of solid particles, having at least one dimension in the range of 1-100 nm, in liquid media. The techniques used to induce gelation in these sols are now commonly termed as sol-gel techniques. Gels are defined as a three dimensional network of the dispersed solid particles in a liquid medium (Ward and Ko,1995).

The unique property of the sol-gel process is the ability to all the way from the molecular precursor to the product, allow a better control of the whole process and synthesis of tailor made materials. The sol-gel process appears attractive because it offers in principle the following advantages (Brinker and Scherer 1990, Zarzycki ,1997);

i.   Homogeneous multi-component systems can be easily obtained by mixing the molecular precursor solutions,

ii. The potential ability in a viscous liquid to minimise the sources of defects introduced in the processing of powders,

iii. The ability to visually examine many gel products for defects after drying,

iv. Temperatures required for glass and ceramic processing can be significantly reduced by mixing the precursors at the molecular level,

v.   The rheological properties of sols or gels allow the formation of fibers, films or composites by such techniques as spinning, dip coating or impregnation.

3.1. Sol-gel Chemistry

The sol-gel process involves the use of inorganic or metal organic precursors for the preparation of a sol followed by the formation of a gel. In aqueous or organic solvents the precursors are hydrolysed and condensed to form inorganic polymers composed of M–O–M bonds. The most commonly used organic precursors are metal alkoxides $[M(OR)_z]$, where R is an alkyl group. Normally the alkoxide is dissolved in alcohol and hydrolysed by the addition of water under acidic, basic or neutral conditions. Hydrolysis replaces an alkoxide ligand with a hydroxyl ligand:

$$M\,(OR)_z + H_2O \rightleftharpoons M\,(OR)_{z-1}\,(OH) + ROH \qquad (1)$$
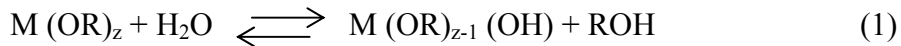
Condensation reactions involving the hydroxyl ligands produce polymers composed of M–O–M or M–OH–M bonds, and in most cases the by products are water or alcohol as shown below for silicate condensation:

$$Si\,(OR)_3\,OH + Si\,(OR)_4 \rightleftharpoons (RO)_3\,Si–O–Si\,(OR)_3 + ROH \qquad (2)$$

$$2Si\,(OR)_3\,OH \rightleftharpoons (RO)_3\,Si–O–Si\,(OR)_3 + H_2O \qquad (3)$$
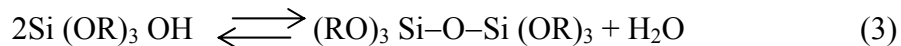
The reverse of reactions 2 and 3, siloxane bond alcoholysis and silioxane bond hydrolysis, promote bond breakage and reformation process that permit complete restructuring of the growing polymer.

Since metals or metalloids of interest for membrane and catalyst formation (Si, Al, Ti, etc.) have coordination numbers (C)>=4, complete condensation would lead to compact, particulate oxides. In fact, for electropositive metals such as Ti and Zr, it is difficult to avoid particle formation unless the alkoxide precursor is modified, e.g., chelated with slowly hydrolyzing ligands to reduce both the rates of hydrolysis and condensation. The metalloid, silicon, however, is substantially less electropositive. Hydrolysis and condensation of silicon alkoxides occur at much lower rates, and the condensation pathway can be more easily influenced by steric and chemical factors.

This description of sol gel chemistry identifies two key ideas. First, a gel forms because of the condensation of partially hydrolysed species into a three dimensional polymeric network. Second, any factors that affect either or both of these reactions are

likely to have an impact on the properties of the gel. These factors are called sol gel parameters that separate sol gel preparation from other methods. These parameters include, type of precursor, type of solvent, water content, acid or base content, precursor concentration and temperature (Ward and Ko,1995).They affect the structure of the initial gel and the properties of the material at all subsequent steps.

A gel which is a solid matrix encapsulating a solvent, needs to be dried to remove the solvent. A gel starts to age after its formation until its dried and is not static during aging where hydrolysis and condensation reactions can continue. Furthermore, *syneresis* which is expulsion of solvent due to gel shrinkage and *coarsening* which is the dissolution and reprecipitation of particles, also may occur during aging. Due to these phenomena, chemical and structural properties of the gel change.

Drying conditions have a significant effect on the properties of sol-gel derived materials. Conventional evaporative drying induces capillary pressure associated with the liquid-vapor interface within the pores. The presence of a pore size distribution, causes the formation of differential capillary pressures which collapses the porous network during drying. The dried sample is commonly known as a *xerogel*. To eliminate the formation of differential capillary pressures supercritical drying is used and the resultant materials are known as *aerogels* which generally have high surface areas and porous structures with low densities (Scherer,1988).

3.1.1. Hydrolysis and Condensation Reactions of Aluminates

The hydrolysis chemistry of aluminium has been of interest for over a century because of its relationship to soil chemistry and to the mineral bauxite as the main source of aluminium. Bauxite is composed of largely of aluminium hydroxides and oxo-hydroxides which have become of interest as precursors to transition aluminas recently. Furthermore, the discovery by Yoldas, in the late 1970s that hydrolysis and condensation of aluminium alkoxides could result in monolithic alumina gels was largely responsible for the development of the sol-gel research. Hydrolysis and condensation behaviour of Al(III) can be investigated in aqueous inorganic solutions and non-aqueous solutions derived from metal alkoxides.

3.1.1.1. Solution Chemistry of Inorganic Precursors

Al^{3+} with an ionic radious of 0.5 A^o, has a coordination number for water of N=6 and exists as the unhydrolysed species $[Al(OH_2)_6]^{3+}$ below pH 3. With increasing pH, $[Al(OH_2)_6]^{3+}$ can be hydrolysed extensively;

$$[Al(OH_2)_6]^{3+} + hH_2O \rightarrow [Al(OH)_h(OH_2)_{6-h}]^{(3-h)+} + hH_3O \qquad (4)$$

$$hH_3O^+ + hOH^- \rightarrow 2hH_2O \qquad (5)$$
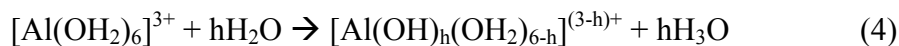
where h is defined as the molar ratio of hydrolysis, which is equivalent to the OH:Al ratio according to the net reaction. Subsequent condensation (via olation[1] or oxolation[2]) results in polynuclear hydroxides or oxo-hydroxides, which can be stable indefinitely, but which are in fact metastable with respect to the precipitation of bayerite α-Al(OH)$_3$. Metastable precipitates can form and redissolve slowly, the species distribution being very sensitive to the conditions of the hydrolysis procedure.
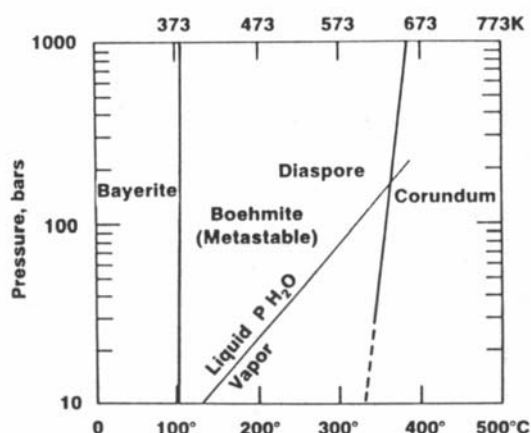
Figure 3. 1. Pressure temperature phase diagram of the Al$_2$O$_3$-H$_2$O binary system (Brinker and Scherer 1990).

The stable mononuclear species in solution corresponds to the series h=0-4, although the h = 2 and h = 3 species are significant only in very dilute solutions. The potentiometric study results indicate two small polynuclear species at low equivalent additions of base, $[Al_2(OH)_2(OH_2)_4]^{4+}$ and $[Al_3(OH)_4(OH_2)_9]^{5+}$ and higher base additions one large polynuclear species $[AlO_4Al_{12}(OH)_{24}(OH_2)_{12}]^{7+}$, the Al$_{13}$ ion. The

---

[1] olation is a condensation process in which a hydroxy bridge is formed between two metal centers.

[2] oxolation is a condensation reaction in which a oxo bridge (-O-) is formed between two metal centers.

existence of both the dimer and Al_{13} ion has been confirmed by X-ray crystallography of the corresponding sulfate salts. The Al_{13} ion has been attributed to the tetrahedrally coordinated aluminium located at the center of three layers of edge sharing octahedra.
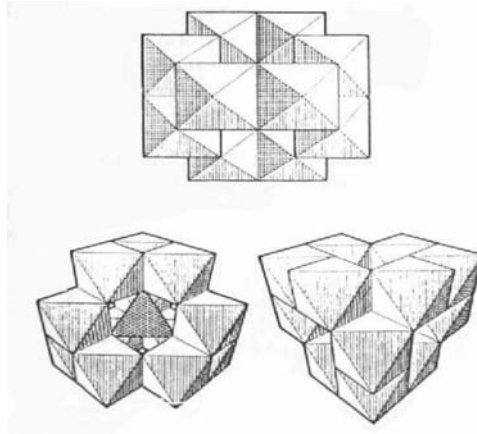
Figure 3. 2. The Al$_{13}$ ion (Brinker and Scherer 1990).

Above h = 2.46 (theoretical value for Al_{13}), rapid precipitation of more highly condensed, amorphous or weakly crystalline phase occurs. The common crystalline phase is pseudoboehmite (or gelatinous boehmite) shows broad lines that coincide with the major reflections of well crystallised boehmite, γ-AlO(OH). The degree of crystalline order, particle size and chemical composition of the gelatinous aluminas depends on temperature, rate of precipitation, final pH, ionic composition, concentration of starting solutions and time of aging.

The dimer consisting of two edge-shared octahedra forms via an olation reaction between two singly hydrolysed monomers (h = 1):

$$2[Al(H_2O)_6^{3+} - H^+ \rightarrow Al(H_2O)_5OH^{2+}] -2H_2O \rightarrow Al_2(OH)_2(H_2O)_8^{4+}$$
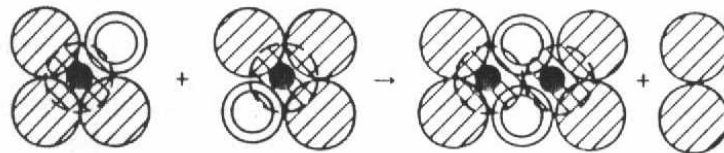
The structures of more condensed products can be understood on the basis of an aluminium hydrolysis model which predicts that the initial hydrolytic interactions of two aluminium cations will proceed along the reaction pathway that maximises their hydrogen bonding. According to this model, preferred condensation sites are those that maximise the interactions between lone pair electron on a bound hydroxide ligand on one aluminium species with a proton on a water bound to another aluminium species. The most acidic water ligand in the dimer is cis to existing bridging hydroxides. Therefore, deprotonation generates the following species:

h=1, monomer,[Al(OH)(OH$_2$)$_5$]$^{2+}$ **[Al$_3$(tri-μ-OH)(OH)$_3$(OH$_2$)$_9$]$^{5+}$**   **linear species**
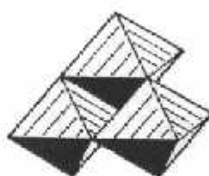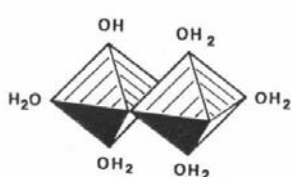
Nucleophilic attack by [Al$_3$(tri-μ-OH)(OH)$_3$(OH$_2$)$_9$]$^{5+}$ on a monomeric aluminium species initiates the condensation process that generates Al$_{13}$ ion. Due to the bulky nature of the tri-μ-OH trimer, this monomer is then forced to adopt tetrahedral coordination. The addition of two more tri-μ-OH trimers creates the Al$_{13}$ ion.

3.1.1.2. Metal Alkoxides

The Yoldas process outlined schematically in Figure 3.3 is the most common method of forming transparent, monolithic alumina gels. It consists of hydrolysing an aluminium alkoxide Al(OR)$_3$, normally Al (OBu^s)$_3$, in a large amount of water (water/alkoxide molar ratio = 100-200) at 80-100 ^{o}C, resulting in the precipitation of fibrillar boehmite, followed by peptization with a mineral acid (HNO$_3$) to yield a stable particulate sol. Cold water hydrolysis forms an amorphous precipitate that converts to bayerite upon aging through a dissolution–recrystallisation process. Gelation is generally achieved by concentration of the sol by boiling or evaporation. Yoldas observed that a minimum gel volume occurred with an acid:Al mole ratio of 0.07. Several studies have shown that changes in the water content, the acid content and the hydrolysis temperature results in a microstructural changes in the resulting xerogel products (Yoldas, 1975a, Changrong et al.,1996, Okubo,1990).

1 mole $Al(OC_4H_9)_3$
100 moles H_2O → Al-hydroxide precipitate

$T = 80\ ^oC$

0.07 mole HCl

PEPTIZATION

ETHER EXRACTION OF BUTANOL-2

Treated sol ← Alumina sol

$-H_2O$

$- H_2O, C_4H_9OH$

SOLVENT EVAPORATION

Wet gel

$-H_2O$ (molecular water)

DRYING

Dried gel

$-H_2O$ (structural water)

CALCINATION

Transition
aluminas γ, θ

$500\ ^oC$

T

$1200\ ^oC$

$\alpha\text{-}Al_2O_3$
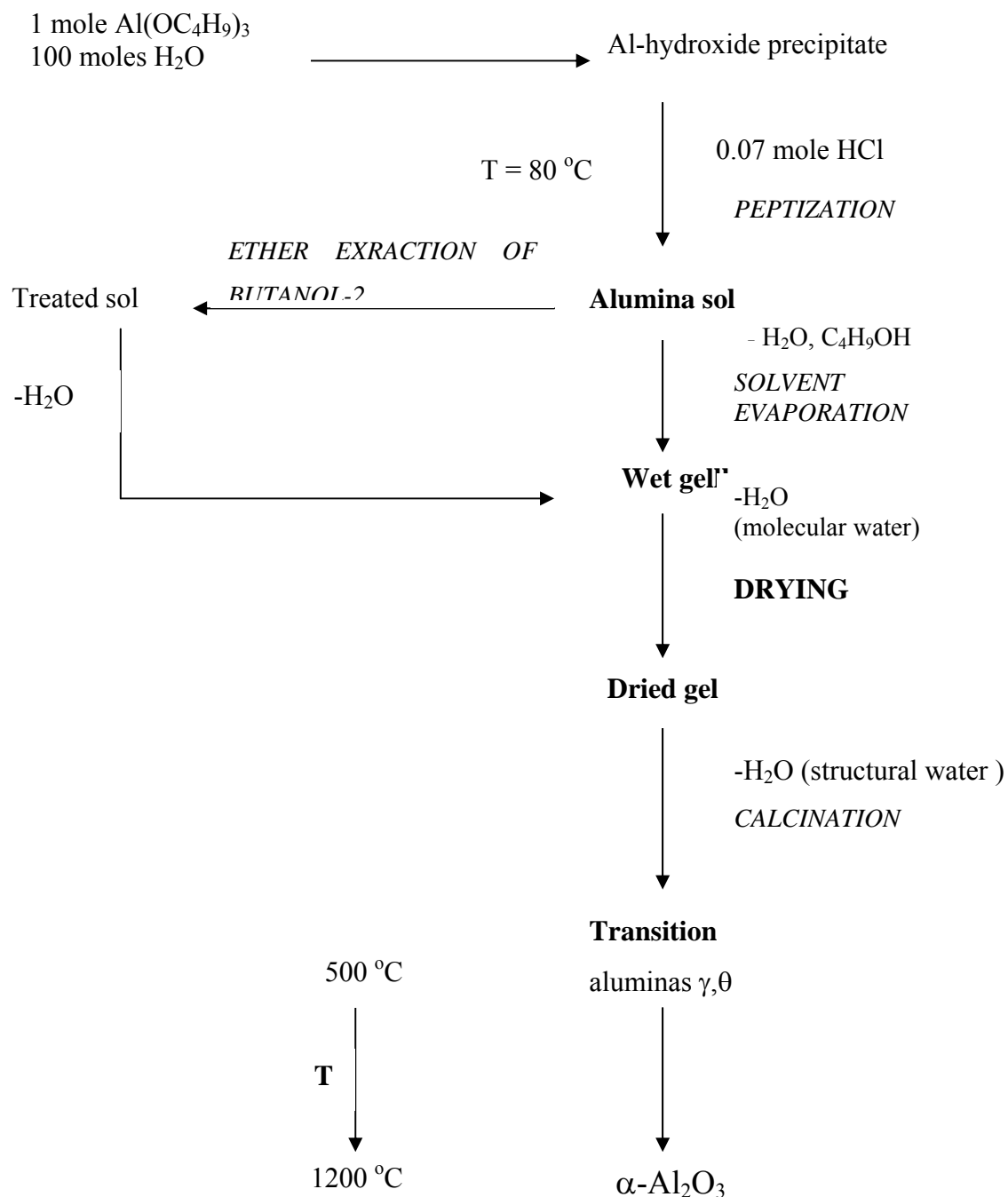
Figure 3.3. Flow chart of the Yoldas process for preparing alumina (Brinker and Scherer,1990).

The two fundamental differences in the hydrolysis and condensation mechanisms between the alkoxide system and the inorganic systems are as follows: (1) the unhydrolysed monomers often associate to form oligomers via alcolation, (2) OR ligands must be replaced by OH ligands for condensation to proceed further, so the effective functionality toward condensation may be reduced by employing low values of water amount.

The extent of oligomerization (molecular complexity) of aluminium alkoxides depends on the steric bulk of the alkoxide ligand. Steric crowding is reduced for alkoxide ligands exhibiting –O-CH$_2$- bonding to metal, resulting in symmetric molecules (Structure D). Sterically bulky OR groups inhibit the conversion of tetrahedral atoms to pentacoordinated or octahedral Al atoms, leading to the formation of less constrained linear species, either dimers or trimers (Structures A and B).
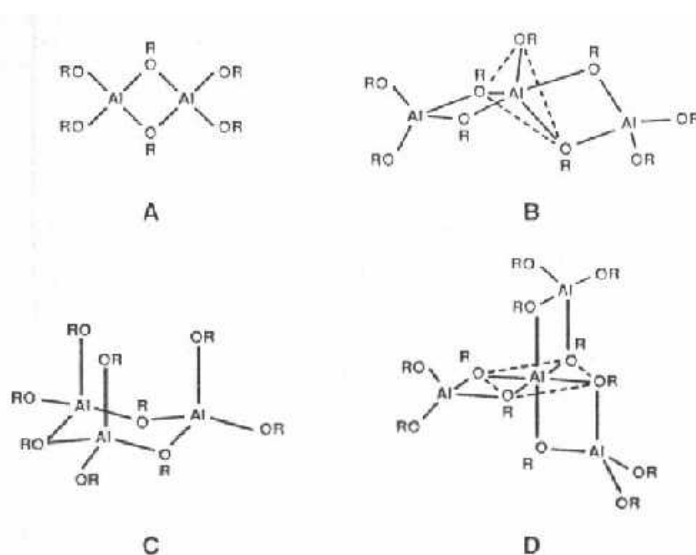
Figure 3.4 Various [Al(OR)$_3$]$_n$ oligomers (Brinker and Scherer 1990).

Under neutral conditions, it is expected that both hydrolysis and condensation occur by nucleophilic addition followed by proton transfer and elimination of either water or alcohol in a manner analogous to transition metal alkoxides as follows;

Hydrolysis;

$$H-O-H + M-OR \longrightarrow \begin{matrix}H\\ \searrow\\ O :\rightarrow M-OR\\ \nearrow\\ H\end{matrix} \longrightarrow HO-M \leftarrow O\begin{matrix}\nearrow R\\ \\ \searrow H\end{matrix} \longrightarrow M-OH + ROH \quad (6)$$

Alcoxolation;

$$M-O-H + M-OR \longrightarrow M-O:\overset{\nearrow H}{\rightarrow} M-OR \longrightarrow M-O-M \leftarrow O\begin{matrix}\nearrow R\\ \\ \searrow H\end{matrix} \longrightarrow M-O-M + ROH \quad (7)$$

Oxolation;

$$M-O-H + M-OH \longrightarrow M-O:\overset{\nearrow H}{\rightarrow} M-OH \longrightarrow M-O-M \leftarrow :O\begin{matrix}\nearrow H\\ \\ \searrow H\end{matrix} \longrightarrow M-O-M + H_2O \quad (8)$$
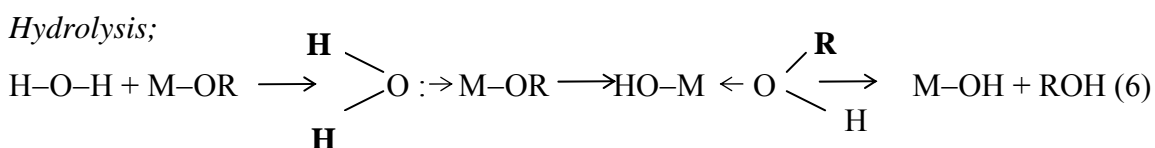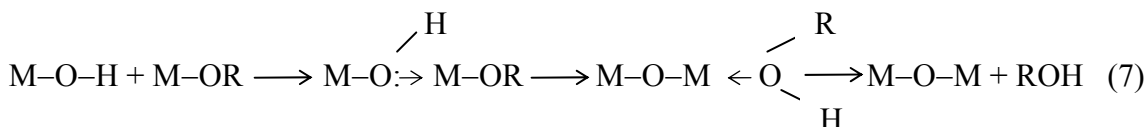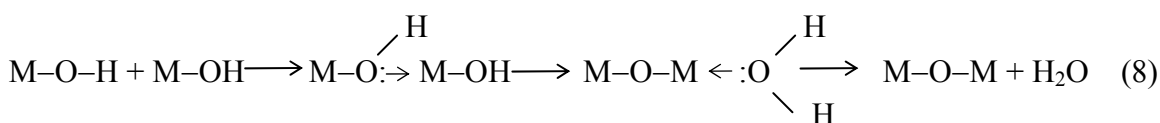
Likewise, both of these reactions are catalysed by addition of either acid or base;

$$M-OR + H_3O^+ \longrightarrow M^+ \leftarrow: O \begin{smallmatrix} \nearrow H \\ \searrow R \end{smallmatrix} + H_2O \qquad (9)$$

$$M-OH + :OH^- \longrightarrow M-O^- + H_2O \qquad (10)$$

Acids protonate OR or OH ligands creating good leaving groups and eliminating the requirement for proton transfer in the intermediate and bases deprotonate water or OH ligands creating strong nucleophiles.

Aluminium alkoxides may be coordinatively unsaturated and are able to adopt three stable coordination numbers kinetic, pathways of nucleophilic reactions should be quite facile. Consequently the rates of hydrolysis and condensation are greater than for silicon alkoxides which are coordinatively saturated and exhibit only one stable coordination number.

3.1.2. Sol-Gel Processing of Silicates

Silicon is the most abundant metal in the earth's crust and evidence of silicate hydrolysis and condensation to form polysilicate gels and particles are seen in many natural systems. For example, precious opal is composed of amorphous silica particles glued together by a lower density silicate gel (Iler,1979). The essential ingredients required to form opals are an abundant supply of readily soluble silica and a source of water. Repeated hydrolysis and condensation steps involving the soluble silica lead to aqueous polysilicate species that, under appropriate chemical conditions, evolve into spherical particles of essentially anhydrous SiO_2.

The discovery of the exceptional tendency of organosilicon compounds to form siloxane polymers containing organic side groups (silicones) caused an explosion of activity in the late 1930s that established a chemical and physical basis for understanding the process of hydrolysis and condensation. More recently, the rediscovery of monolithic gel formation and the low-temperature conversion of gels to glasses without melting has caused renewed interest in the topic of the hydrolysis and condensation of silicates.

This section reviews the hydrolysis and condensation of silicates in both aqueous and organic systems used in sol-gel processing of silica.

3.1.2.1. Aqueous Silicates

The +4 oxidation state (z=4) is the only important one in the chemistry of silicon in naturally occurring systems and the coordination number of silicon C, is most often four. Compared to the transition metals, silicon is generally less electropositive, therefore coordination expansion does not spontaneously occur with nucleophilic reagents. These factors make the kinetics of hydrolysis and condensation considerably slower than transition metals or Group III systems (Brinker and Scherer, 1990).

Silicon is hydrolysed even in dilute acid as expected from its small ionic radius (0.42 A^o), and Si(OH)$_4$ is the predominant mononuclear solution species below pH 7. Above pH 7 further hydrolysis produces anionic species:

$$Si(OH)_{4(aq)} \rightarrow SiO_x(OH)_{4-x}^{x-} + xH^+ \qquad (11)$$
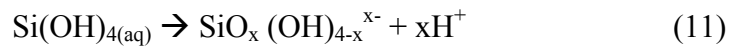
where SiO(OH)$_3^-$ is the predominant mononuclear species above pH 7. Because SiO(OH)$_3^-$ is a very weak acid, SiO$_2$(OH)$_2^{2-}$ is observed in appreciable quantities only above pH 12 (Brinker and Scherer, 1990).

Polymerization occurs in three stages (Iler, 1979);

i. Polymerization of monomer to form particles,

ii. Growth of particles,

iii. Linking particles into chains, then networks that extend throughout the liquid medium, thickening it to a gel.

Condensation takes place to maximize the number of Si−O−Si bonds and minimize the number of terminal hydroxyl groups through internal condensation. Thus rings are quickly formed to which monomers add, creating three dimensional particles. These particles condense to the most compact state leaving OH groups on the outside. According to the Iler the three dimensional particles serve as nuclei. Further growth occurs by an Ostwald ripening mechanisms whereby particles grow in size and decrease in number as highly soluble small particles dissolve and reprecipitate on larger, less soluble nuclei. Growth stops when the difference in solubility between the smallest and largest particles becomes only a few ppm. Growth continues to larger sizes at higher temperature at especially above pH 7 due to greater solubility.

Iler divides the polymerization process into three approximate pH domains: < pH 2, pH 2-7, and > pH 7. pH 2 appears as a boundary, since the point of zero charge (PZC), where the surface charge is zero, and the isoelectic point (IEP), where the electrical mobility of the silica particles is zero, both are in the range of pH 1-3. pH 7 appears as a boundary because both the silica solubility and dissolution rates are maximized at or above pH 7 so that particle growth occurs without aggregation or gelation.

pH 2 represents a metastability region where the observed gel times are quite long. Below pH 2, polymerization rate proportional to $[H^+]$. In this region, the formation and aggregation of primary particles occur together and ripening contributes little to growth after the particles exceed the size of 2 nm diameter. Developing gel networks are composed of exceedingly small primary particles as shown in Figure 3.5.
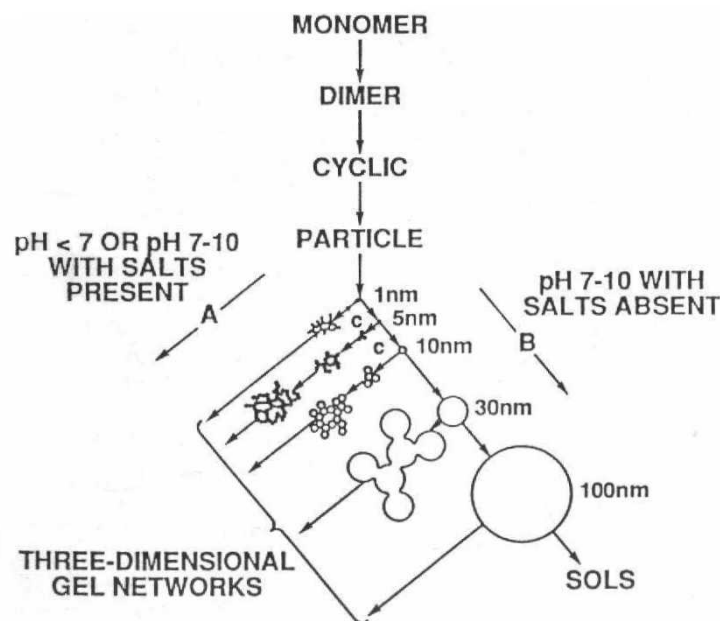
Figure 3.5. Polymerization behaviour of aqueous silica. In basic solution (B) particles grow in size with decrease in number; in acid solution or in the presence of salts (A), particles aggregate into three dimensional networks and forms gel (Iler,1979).

Since the gelling times decrease steadily between pH 2 and pH 6, it is generally assumed that above the IEP the condensation rate is proportional to [OH⁻] as in the following reaction sequence (Brinker and Scherer, 1990):

$$\equiv Si-\text{OH} + \text{OH}^- \xrightarrow{fast} \equiv \text{Si}-\text{O}^- + \text{H}_2\text{O} \qquad (12)$$

$$\equiv Si-\text{O}^- + \text{HO}-\text{Si} \xrightarrow{slow} \equiv \text{Si}-\text{O}-\text{Si}\equiv + \text{OH}^- \qquad (13)$$
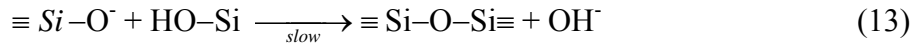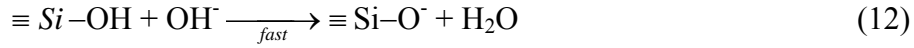
In any given distribution of silicate species, the most acidic silanols are those contained in the most highly condensed species. Therefore, condensation according to Eq. 13 occurs preferentially between more highly condensed species and less highly condensed, neutral species. This means that the rate of dimerization is low, but once dimers form they react preferentially with monomers to form trimers which in turn react with monomers to form tetramers. At this point, cyclization is rapid due to the proximity of the chain ends and the substantial depletion of the monomer population. Cyclic trimers may also form but the reduced Si-O-Si bond angles and the associated strain make them much less stable in this pH range (Curran and Stiegman,1999).

Further growth occurs by continued addition of lower molecular weight species to more highly condensed species (either conventional polymerization or ripening) and by aggregation of the condensed species to form chains and networks. Near the IEP where there is no electrostatic particle repulsion, the growth and aggregation processes occur together. In any case, since the solubility of silica is low in this pH range, particle growth stops when the particles reach 2-4 nm where the solubility and size dependence of solubility is greatly reduced.

Polymerization occurs by the same nucleophilic mechanisms above pH 7. However, because all the condensed species are more likely to be ionized and therefore mutually repulsive, growth occurs primarily by the addition of monomers to more highly condensed particles rather than by particle aggregation. Particles 1-2 nm in diameter are formed in a few minutes above pH 7.

Due to the greater solubility of silica and greater size dependence of solubility in this region, growth of the primary particles continues by Ostwald ripening. Particles grow rapidly to a size that depends mainly on the temperature. Since growth occurs by the dissolution of smaller particles and deposition of soluble silica on larger particles, the growth rate depend on the particle size distribution.

3.1.2.2. Hydrolysis and Condensation of Silicon Alkoxides

Silicate gels are most often synthesised by hydrolyzing monomeric tetrafunctional alkoxide precursors employing a mineral acid or base as a catalyst. At the functional group level, three reactions are generally used to describe the sol-gel process:

$$\equiv Si-OR + H_2O \xrightleftharpoons[Esterification]{Hydrolysis} \equiv Si-OH + ROH \qquad (14)$$

$$\equiv Si-OR + HO-Si \xrightleftharpoons[Alcoholysis]{Alcohol\ Condensation} \equiv Si-O-Si\equiv +ROH \qquad (15)$$

$$\equiv Si-OH + HO-Si\equiv \xrightleftharpoons[Hydrolysis]{Water\ Condensation} \equiv Si-O-Si\equiv + H_2O \qquad (16)$$
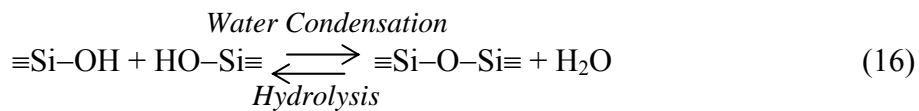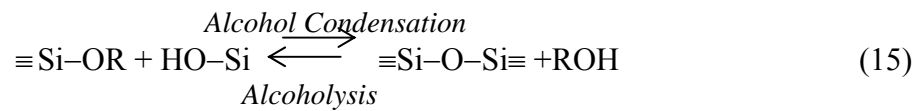
where R is an alkyl group. The hydrolysis reaction replaces the alkoxide groups (OR) with hydroxyl groups (OH). Subsequent condensation reactions involving the silanol groups (Si-OH-Si) produce siloxane bonds (Si–O–Si) plus the by-products alcohol (ROH) or water. Under most conditions, condensation commences before hydrolysis is complete (Brinker, Scherer 1990).

Because water and alkoxysilanes are immiscible, a mutual solvent such alcohol is normally used as a homogenizing agent (Brinker, Scherer 1990).However, gels can be prepared from silicon alkoxide-water mixtures without added solvent, since alcohol produced as the by product of the hydrolysis reaction is sufficient to homogenize the initially phase separated system. It should be noted that alcohol is not simply a solvent. As indicated in the reverse of Eqs. 14 and 15, it can participate in *esterification* and *alcoholysis* reactions. It is evident from Eqs. 14–16 that the structure of sol-gel silicates evolves sequentially as the product of successive hydrolysis reactions (and the reverse reactions: esterification and alcoholic or hydrolytic depolymerisation) (Brinker, Scherer, 1990).

Hydrolysis occurs by the nucleophilic attack of the oxygen contained in water on the silicon atoms as evidenced by the reaction of isotopically labelled water with TEOS (Tetraethylorthosilicate) that produces only unlabelled alcohol in both acid and base catalyzed systems.

$$Si-OR + H\,OH \; \rightleftarrows \; Si-OH + ROH \hspace{3cm} (17)$$
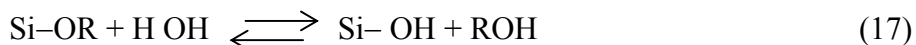
Tetraalkoxysilanes, organotrialkoxysilanes and diorganodialkoxysilanes hydrolyse upon exposure to water vapor. Hydrolysis is facilitated in the presence of homogenizing agents that are especially beneficial in promoting the hydrolysis of silanes containing bulky organic or alkoxy ligands, which when undiluted, remains unhydrolysed upon exposure to water vapor. However, the addition of solvents may promote esterification or depolymerization reactions according to the reverse of Equations 14 and 15.

Hydrolysis is most rapid and complete when catalysts are employed. The catalyst can either be protons (acid catalysis) or hydroxyl ions (base catalysis). Although mineral acids or ammonia are most generally used in sol gel processing, other known catalysts are acetic acid, KOH, amines, KF, HF, and the titanium alkoxides.

The rate and extent of the hydrolysis reaction is mostly influenced by the strength and concentration of the acid or base catalyst. Temperature and solvent are of secondary importance. All strong acids behave similarly, but weaker acids require longer reaction times to achieve the same extent of reaction.

The reaction rates and ratio between hydrolysis and condensation reactions depend on the process parameters in the reaction mixtures. The main parameters are temperature, TEOS concentration and the ratios of water to TEOS and the catalyst to TEOS. As mentioned above, the catalyst can either be protons (acid catalysis) or hydroxyl ions (base catalysis). Protons enhanced especially the hydrolysis rate, and the resulting gel is weakly branched. Hydroxyl ions especially the condensation rate. Base catalysis enhances condensation and so gel is highly branched gel and contains particles. Therefore protons are chosen as catalysts for a fast hydrolysis and slow condensation of the hydrolysed species. It should also be emphasised that the reaction rate for hydrolysis of the first OR− group of the TEOS molecule is order of magnitude larger than that of the second OR− group. The same holds for the third and fourth OR− groups. This means that completely hydrolysed TEOS molecules are almost not present (Nair et al., 1997b).

3.1.2.3. Sol-Gel Transition of Silicate System

A gel is a form of matter intermediate between a solid and a liquid. The hydrolysis and condensation reactions lead to the growth of clusters that eventually collide and link together into a gel. The sudden change in rheological behaviour is generally used to identify the gel point. The time of gelation t_{gel}, is defined as the point where the gel has a certain value of viscosity μ. Mainly, two types of gel are formed, *polymeric gel* that is derived from metal alkoxide synthesis and the *colloidal gel* that is prepared by the destabilization of an aqueous sol.

In the colloidal gel shown in Figure 3.6 more weakly crosslinked networks form when condensation commences before hydrolysis is complete. If all the monomer is quickly consumed to form dimers, trimers, etc. and possible condensation sites are limited by reducing the extent of hydrolysis and extended linear or randomly branched polymers would result rather than dense colloids. Furthermore, it is unlikely that linkage together of these weakly crosslinked polymers could ever result in macroscopic regions of fully crosslinked oxides, since complete coalescence would be sterically hindered.
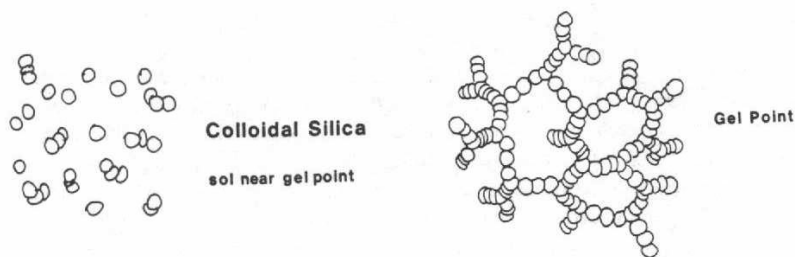
Figure 3.6. Colloidal gel (Brinker and Scherer, 1985).

Sequential polymer growth and gel formation are illustrated schematically in Figure 3.7 (a) and 3.7 (b) for the acid and base catalysed systems. Under acid catalysed conditions and especially at low additions of water, primarily linear or randomly branched polymers grow which entangle and form additional branches resulting in gelation. Under basic conditions and/or at higher additions of water more highly branched clusters are formed which do not interpenetrate prior the gelation and thus behave as discrete species. In the latter case gelation occurs by the linking together of clusters in a manner similar to colloidal gel formation.

(a)   (b)
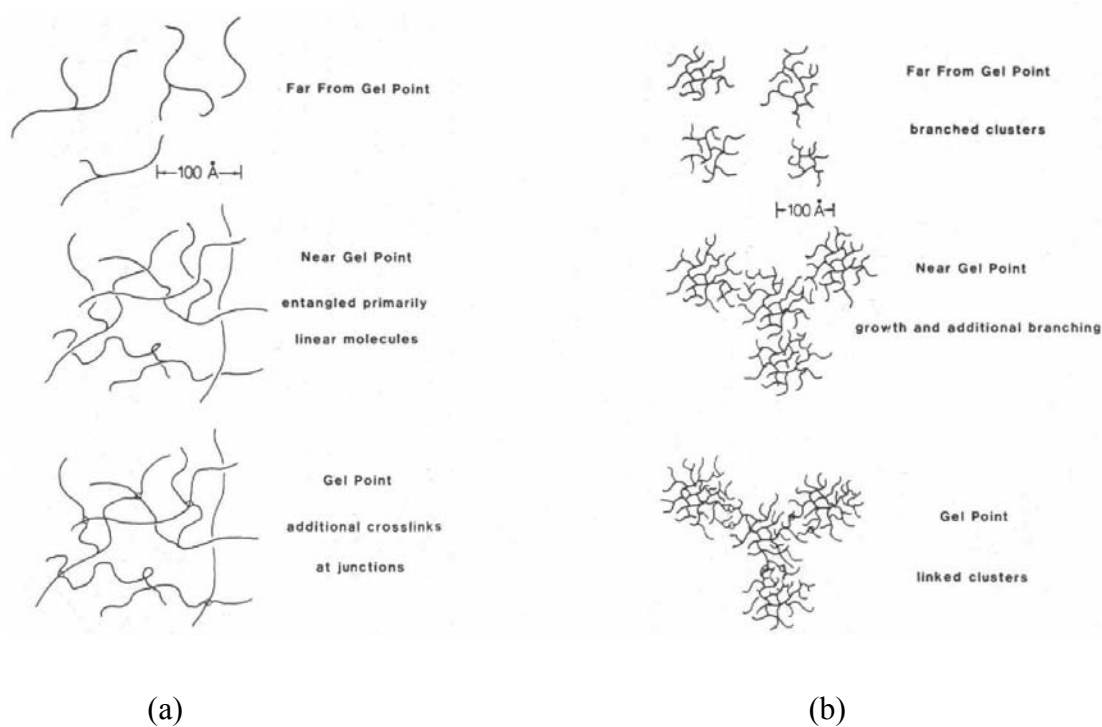
Figure 3.7. Polymer growth and gel formation in a) acid catalysed systems, b) base catalysed systems (Brinker and Scherer, 1985).

Although the sharp increase in viscosity which is accompanied by gelation essentially freezes in a particular polymer structure at the gel point (i.e. gelation may be considered as a rapid solidification process), this frozen-in structure may change appreciably with time (aging) depending on the temperature, solvent and pH conditions or upon the removal of solvent (desiccation). The processes of change during aging after gelation are categorized as polymerization (increase in connectivity of gel network), synerisis (shrinkage of the gel network with expulsion of liquid from the pores), coarsening (increase in pore size and reduction in surface area through dissolution and reprecipitation) and segregation (phase separation). The properties of the gel and its behaviour during subsequent processing are shown to be strongly affected by aging.

Much of the current interest in gels stems from the potential of forming monolithic pieces of glass. As a part of this process gels must be dried without cracking. Changes in gel structure during drying were described by Iler for colloidal systems. According to Iler, surface tension forces created during solvent removal cause the original extended network to fold   as the coordination number of the particle is

increased. Porosity develops when due to additional crosslinking or neck formation, the gel network becomes sufficiently strengthened so that it resists to the compressive forces of surface tension. The amount of shrinkage that occurs during drying is dependent on the stiffness of the network as indicated schematically in Figure 3.8 (Iler,1979).
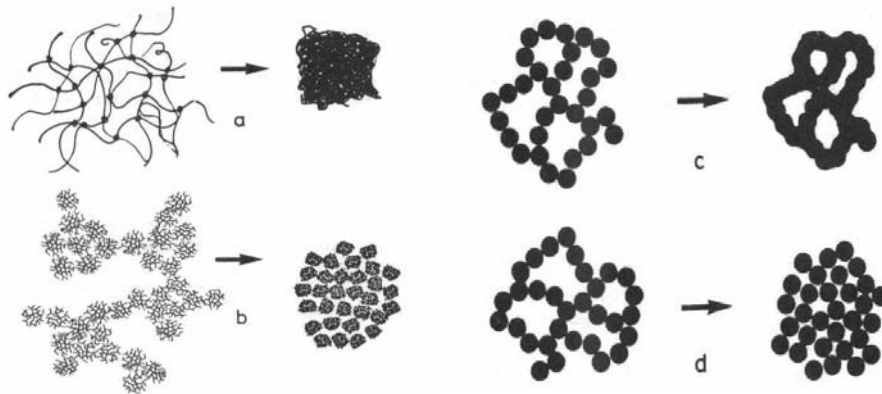
Figure 3.8. Schematic representation of gel desiccation for (a) acid catalysed, (b) base catalysed, (c) colloidal gel under conditions of high silica solubility, (d) colloidal gel composed of weakly bonded particles (Scherer, 1988).

Figure 3.8 (a) represents a silicate gel made at low pH and water concentration which has low crosslink density. Figure 3.8 (b) shows a silicate gel made at moderate pH and water content which consists of more densely crosslinked clusters and Figure 3.8 (d) represents a colloidal gel. In all cases, drying causes shrinkage. Coarsening of the gel shown in Figure 3.8 (c) can occur if gel is aged in a solution in which the solid phase is slightly soluble. Dissolution and reprecipitation cause the neck formation and the stiffer gel produced by aging does not shrink as much when dried.

3.2. Sol-Gel Processing of Ceramic Membranes

The sol gel method is a very suitable technique for the production of mesoporous (e.g. γ-Al_2O_3) and microporous (e.g. SiO_2) membranes (de Lange et al., 1995a, West et al., 2002, Chu and Anderson, 1996). Ceramic membranes may be formed form particulate (colloidal) or polymeric species with a wide range of pore sizes and porosity by sol-gel processing which is schematically shown in Figure 3.9. In both cases a precursor is hydrolysed while simultaneously a condensation or polymerisation reaction occurs (Klein and Gallagher, 1988, Nair et al., 1997b).

```
                    ┌─────────────────┐
                    │   METAL SALT    │
                    │       OR        │
                    │    ALKOXIDE     │
                    └─────────────────┘

Colloidal Gel                          Polymeric Gel
   Route                                   Route

        Peptization          Control
                            Hydrolysis

   SOL                                        SOL

(Colloidal Species)                   (Polymeric Species)


                      DIPPING

                           Sol-gel Transition

                    GEL LAYER

                           Drying

       ORGANIC-INORGANIC MEMBRANE

                           Heat Treatment

             CERAMIC MEMBRANE
```
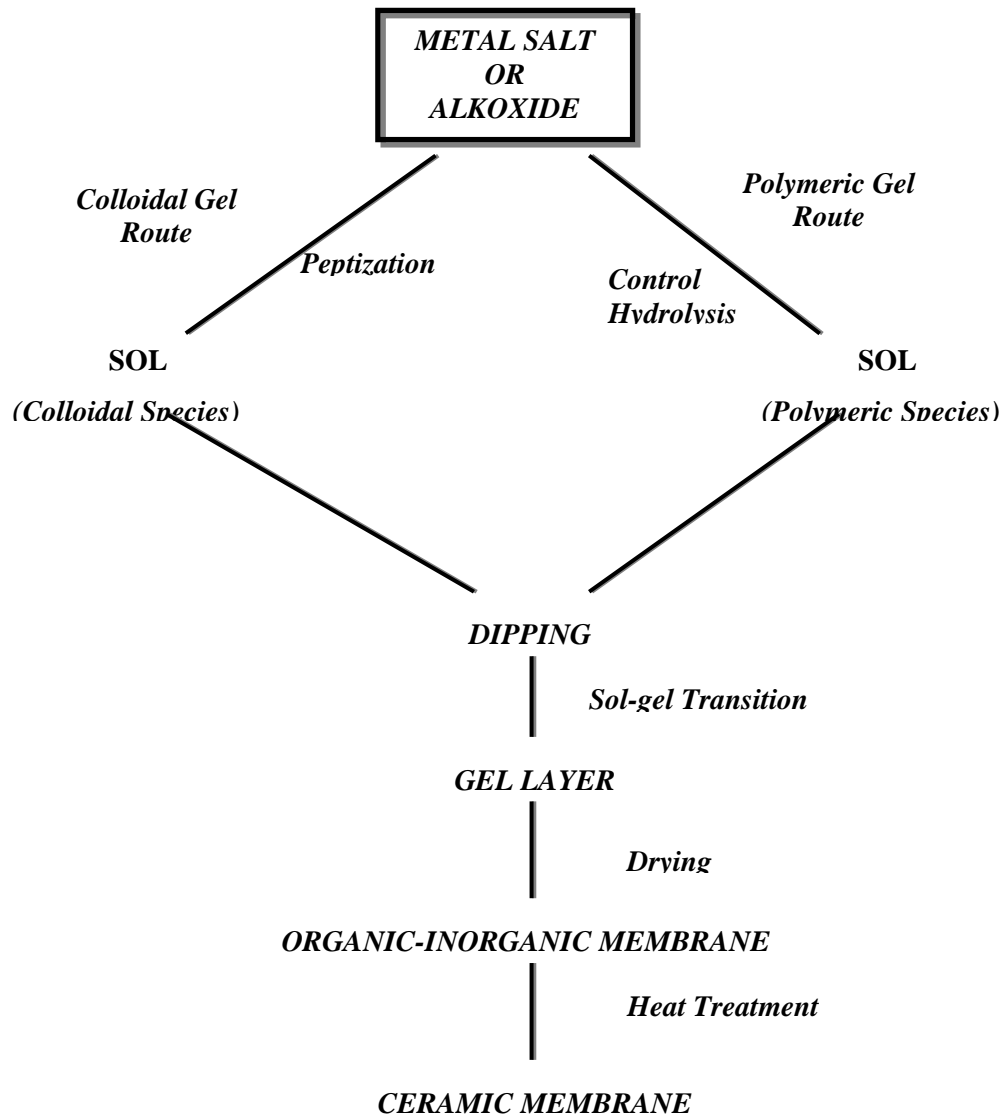
Figure 3. 9. Scheme of sol-gel routes (Bhave,1991).

In the colloidal route a faster hydrolysis rate is obtained by using a precursor with a fast hydrolysis rate and by reacting the precursor with excess water. A precipitate of gelatinous hydroxide or hydrated oxide particles is formed which is peptised in a subsequent step to a stable colloidal suspension. The elementary particle size varies, depending on the system and process conditions, in the 3-15 nm range and these particles form loosely bound agglomerates with sizes in the 5-1000nm range. The size of the agglomerates can be decreased by ultrasonification of the suspension and by manipulation of the electrical charge on the particles. By increasing the concentration of the suspension and / or manipulation of the surface (zeta) potential of the sol particles the colloidal suspension is transformed to a gel structure consisting of interlinked chains of particles or agglomerates. pH and the nature of the electrolyte has an important effect on the gelling point and volume, because they determine the mutual repulsion force which is necessary to obtain a stable colloidal suspension. The anion chosen for the electrolyte or peptising acid must not form a complex with the metal ion of the membrane to be formed. Gels with minimum volume are better suited to obtain monolithic structures and membranes for the case of alumina sols (Yoldas,1975a).This means that pH, counter-ion type and concentration must be chosen in such a way that the particles are just far enough from its points of zero charge (IEP) to prevent flocculation. With conditions too close to IEP a poorly densified film will be obtained.

Colloidal approach is suitable for preparing mesoporous alumina membranes. Alumina membranes have been extensively studied (Yoldas, 1975a, Leenaars et al.,1984, Huang et al., 1997). Yoldas conducted significant research on the fabrication of gamma-alumina membranes made by a sol gel process. Yoldas was able to achieve a relatively small particle size in the sols and was able to achieve porous membranes.

In the polymeric gel route the hydrolysis rate is kept low by adding successively small amounts of water and by choosing a precursor which hydrolyses relatively slowly. The final stage of this process is a strongly interlinked gel network with a structure different from that obtained from the colloidal route. The network formation takes place continuously within the liquid. The gel will form and shrink even within the liquid. It is not necessary to remove this liquid to obtain a gel as in the colloidal route. This means that concentrations of solid material in polymeric gels are usually smaller than in particle gel. Gelation process can be significantly changed by the nature of catalysis of the polycondensation / polymerization reaction (Iler,1979).

Generally, polymeric gel route can be realized for silica systems. The sols prepared by acid-catalysed hydrolysis and condensation of alkoxides (TEOS), with fractal dimensions in order of 1.3 and radii of gyration of 20-30 A^o leads the microporous crack-free membranes with a small pore size (Nair et al.,1997b). For nonsupported membranes a pore size distribution was calculated with a strong maximum at an effective pore diameter of 0.5 nm and a weak maximum present at 0.75 nm. And also these small pores give rise to molecular sieve like gas transport properties (de Lange et al.,1995, de Vos and Verweij, 1998).

In preparing the membranes, the precursor sol will be deposited onto the surface of the substrate to produce a coated substrate that is then dried and calcined to yield the supported inorganic membrane. It has been known that the quality of the underlying support determines, to a degree, the properties and the quality of the top selective microporous layer. Rough or large pore support surfaces would cause cracking of overlaying sol gel derived membranes due to stress development on film coating (Tsai et al. ,2000, Varcauteren et al.,1998).

Deposition of the sol onto the substrate is achieved by contacting the substrate with the sol so that the substrate is coated by a layer capable of collapsing during drying to produce a thin film. The substrate may be contacted with the sol using dip-coating process. There are many parameters that affect this process, such as, sol concentration, dipping time, number of dipping, pore size of the support and the type and the amount of the acid to the stabilize sol. The use of dilute sols reduced the membrane thickness which was proportional with the square root of the dipping time, to the order of surface roughness of the support. Dilute sol is effective in preparing thinner membranes with reduced cracking or peeling off the membrane during drying which happens occasionally in the case of thicker membranes (Cho et al., 1995).

The coating process which involves deposition and subsequent drying may be repeated as desired to produce a membrane comprising a number of coating layers on the support. It is found that under certain conditions, repeated coating and calcination steps can lead to better sieving characteristics, i.e. greater selectivity, with fewer defects for membranes (de Vos and Verweij, 1998).

Defect formation during preparation is a major problem in ceramic membrane processes. The size and the surface density of the defects in the ceramic membrane depend on, for instance, drying rate, amount and size of foreign particles in the atmosphere and the thermal processing regime. Both repeated coating and processing

under clean room conditions were applied for reducing membrane defects (de Vos and Verweij,1998).

3.2.1. Drying of Supported and Unsupported Membranes

The final porous microstructure in xerogels and membranes are established during drying. It is also very crucial because cracks tend to form during drying and this usually necessitates very slow controlled drying rates and processes. (Brinker et al.,1994). The extent of shrinkage of the solid network at the critical point has a determining role on the final pore volume - size distribution in the dried gel or xerogel. This in turn depends on a balance between the capillary pressures that tries to collapse the gel and stiffness of the gel that opposes it. For bulk gels this may take a lot longer (hours or days) than films (seconds or minutes) causing lower levels of condensation reactions in films during drying. Thus, capillary tension is higher causing greater collapse of the network in films. In summary films have lower pore sizes, pore volumes and surface areas than their bulk counterparts.

Drying process is composed of two successive stages. In the first stage, which is called the constant rate period, the loss of pore fluid is accommodated by shrinkage of the gel surface. In other words, the volume shrinkage will be equal to the volume of the pore fluid lost by evaporation. The driving force for this shrinkage is the capillary tension P developed in the liquid, which can be correlated to the pore radius through the Kelvin equation:

$$P = 2\gamma LV \cos\theta / r_p \qquad (18)$$

where ;

γLV: Liquid - vapor interfacial energy

θ = Contact angle

r_p = Pore radius

For wetting pore fluids ($\theta < 90º$) the meniscus is concave and the liquid is in tension (positive P). The reduced volume of liquid stretches to cover the solid surface so that the creation of the higher-energy solid-vapour interfaces is avoided.

This tension in the liquid causes the gel network to contract. Further shrinkage and condensation as the reactive terminal hydroxyl species are brought into closer contact continue up to the critical point. At this point shrinkage stops and tension is maximised. Contracting network is stiff and resists to further compaction. Further evaporation of the pore fluid causes the meniscus to go into gel interior, which is the beginning of the second stage of drying, the falling rate period, which can also be divided into two stages (Scherer,1990).

The stages of drying are illustrated schematically in Fig 3.10: a) Before evaporation begins, the meniscus is flat. b) Capillary tension develops in liquid as it stretches to prevent exposure of the solid phase, and network is drawn back into liquid. The network is initially so compliant that little stress is needed to keep is submerged, so the tension in the liquid is low and radius of the meniscus is large. As the network stiffens, the tension rises and, at the critical point (end of the constant rate period), the radius of the meniscus drops to equal the pore radius. c) During the falling rate period, the liquid recedes into the gel (Scherer,1990).
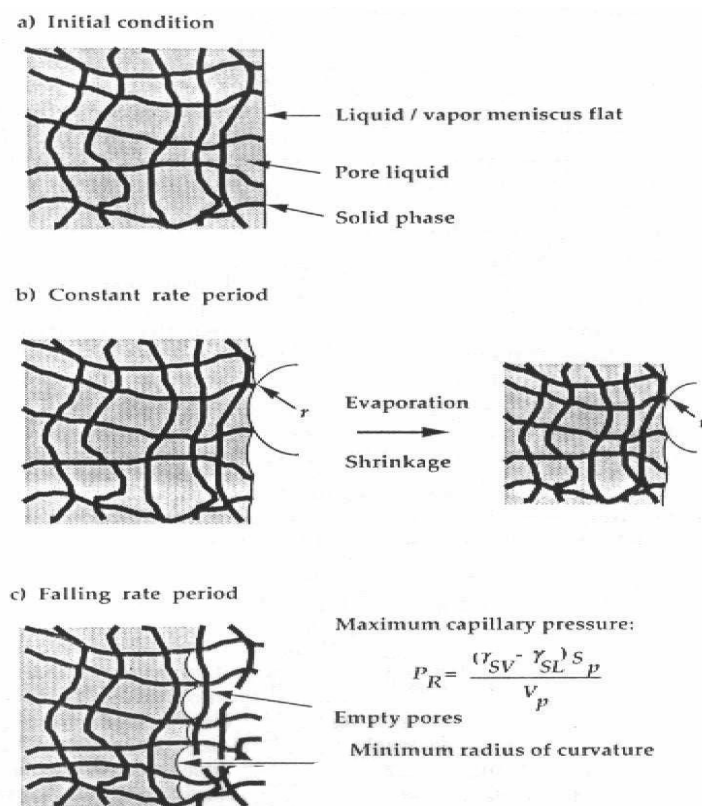
Figure 3.10. Schematic depiction of drying of gel. S_p and V_p are surface area and pore volume of pore, respectively (Scherer, 1990).

It has been argued that cracking result from the variation of pore sizes in the gel, because the higher capillary pressure in a smaller pore could fracture the wall separating it from a neighbouring larger pore (Scherer, 1988). Aging helps to reduce cracking of gels, but it is still necessary to dry very slowly to avoid cracking of any macroscopic piece. Several much more efficient approaches have been suggested, including surfactants "drying control chemical additives (DCCA)", supercritical drying and dialysis. Since differential strain arises from capillary pressure, it's evident that surfactants can reduce the stress by reducing the interfacial energy. Supercritical drying eliminates the liquid/ vapor interface by heating the gel under pressure to a point above the critical temperature and pressure of the solvent.

Organic additions called drying control additives (DCCA) can be used for controlling sol-gel derived gel-membrane-monolith fabrication and drying to prevent cracking problems (Munoz Aguado and Gregorkiewitz, 1996). These additives can control the rate of hydrolysis-polymerization reactions, reduce drying stresses, and affect the pore size distribution. Organics like formamide, glycerol, oxalic acid, PVA are known to be used for this purpose.

The use of formamide was reported to reduce the gelation, aging and drying times, drying stress, and increase the size of the gel monoliths in the preparation of SiO_2 gels from alkoxides. The formation of uniform particle sizes during sol formation and more uniform pore size distributions during drying are enhanced by the use of DCCA's. The DCCA's however must be removed during drying-calcination-densification before pore closure happens.

3.2.2. Heat Treatment of Membranes

Phase formation and/or grain growth can occur at different temperature for the currently used membrane materials like SiO_2, Al_2O_3, TiO_2, ZrO_2, etc. The membranes will become sinteractive at around 500-600 ºC for TiO_2, 900-1000 ºC for ZrO_2, 300-400 ºC for SiO_2 and a number of phase transformations will occur for Al_2O_3 in the 500-1200 ºC range. Initial stage sintering usually will coarsen the grains and increase the pore size and density of the structure. The variation of the pore size with temperature was shown to vary from 3 nm to 55 nm in the 400-1200 ºC range for Alumina membranes (Larbot et al.,1988). Doping the boehmite sol with lanthanum nitrate and PVA was observed to

stabilise the structure thermally at even 1200 ºC (Lin et al.,1991a, Lin and Burggraaf, 1991b).

3.2.3. Ceramic Membrane Support Systems

Preparation of composite or multilayer membranes starts with the fabrication of an appropriate support system. These support membranes are usually disc or tubular shaped but recently the use of ceramic hollow fibers has also been reported . Preparation techniques mainly include conventional powder pressing (uniaxial and isostatic), extrusion, tape and slip casting and spinning.

Support membranes can already be composed of different layers with a gradual decrease in layer thickness and pore size. Much is dependent on the layer which is applied on top of it and the requirements concerning the strength, the surface roughness, thermal stability and the compatibility with other materials. The quality of the support (or supporting layers) is critical for the quality of the membrane itself. Defects and irregularities in the support usually produce defects in the layer applied on it. Defects are, for example, pores much larger than the average pore diameter of the support. They will give rise to so-called "pin-holes" in the layer on top of the support. Furthermore, surface irregularities causing rough surfaces exclude the formation of defect-free thin and smooth top layers in a single step. The wetting behaviour of the surface is also important in layer formation processes. A lot of microporous top layers are prepared starting from a suspension or sol in water which is brought in contact with the surface of the support. Several local changes in wettability can result in pinhole formation.

Consequently, high-quality supports should be smooth, have constant and homogeneous surface characteristics (wettability) and preferably should have sufficient mechanical strength which does not age with time.

The use of macroporous support with an intermediate layer such as γ-Al_2O_3, can be advantageous for some reasons. Usually the macroporous supports still contain surface defects. Deposition of an intermediate layer will fill up and cover these defects if they are not too large. The intermediate layer also helps to regulate the pressure drop across a microporous top layer during operation (Vercauteren et al.,1998).

CHAPTER IV

CHARACTERIZATION OF INORGANIC MEMBRANES

A better understanding of membrane microstructure and its role in the mechanisms of different separation processes is important in the development of new and more complex types of membranes. This understanding is particularly significant in the case of inorganic membranes because the permeation and separation properties are determined by the pore network properties of this microstructure such as, pore size and its distribution, pore shape, porosity and tortuosity, which in turn is controlled by the synthesis route. The description of many porous solids, such as membranes, is complicated by the existence of (a) different shapes of pores in the same material, (b) connections between pores and (c) a distribution in the size of the pores. In order to interpret the results obtained by different characterisation techniques, it is usual to assume an idealised geometrical model to describe the pore network. The most frequently used models are based on cylindrical, slit and sphere pores (Ramsay, 1999).

Some commercial inorganic membranes have a symmetric or homogenous microstructure. However, the majority of the commercially important inorganic membranes are asymmetric and composite in nature. They usually consist of a thin fine pore film responsible for separating components and a support or substrate with single or multiple layers having larger pores for improving the required mechanical strength to the composite membranes.

The basic idea behind the composite and asymmetric structure is to minimise the overall hydraulic resistance of the permeate flow path through the membrane structure. The permeate flux through a given layer is inversely proportional to some power of the pore size of the porous layer.

The final properties of ceramics, their microstructure and also their most important mechanical, thermal, electrical, chemical properties strongly depend on the physical and chemical properties of the starting powders. The most important physical properties of ceramic powders are specific surface area, primary particle size, agglomerate size, the microstructure of the unfired compact, and the morphology of the particles. The chemical composition and the nature of the phases are also very important. This section will cover the pore size determination and thermal

morphological characterisation techniques briefly since these are very important for ceramic membrane performance.

FTIR and XRD can be used for the determination of structural properties, TGA, DTA, DSC can be used to determine thermal properties, gravimetric or volumetric adsorption system can be used for the determination of adsorption related properties

4.1. Characterization of Pore Structures

The following classification is commonly accepted about the types of pores present in porous materials. Pores with diameters larger than 50 nm are called as macropores, mesopores have diameters between 2-50 nm, and pores below a diameter of 2nm are called as micropores. This classification also fits to the pore size determination techniques commonly used. Optical microscopy is limited to relatively big macropores, Mercury porosimetry is limited with macropores and mesopores and low temperature gas adsorption and desorption are mainly limited to micropores and mesopores (Webb and Orr, 1997).

4.1.1. Gas Adsorption and Desorption Techniques

This technique can be considered as a standard method in the science of porous ceramics. Of particular importance is the application of physical adsorption for the determination of the surface area, pore size distribution and total pore volume in micro and mesoporous materials.

It is based on the principle that inside a small pore a gas can condense to a liquid at a relative pressure lower than unity; this introduces capillary condensation theory. The adsorption and desorption isotherms of an inert gas determined as a function of the relative pressure. N_2 is often used as adsorption gas, and the experiments are carried out at the boiling liquid nitrogen temperature. The adsorption isotherm is determined by measuring the quantity of N_2 adsorbed for each value of P_{rel}. Adsorption starts at a low relative pressure. At a certain minimum pressure, the smallest pores are filled with liquid nitrogen. As the pressure is increased further, larger pores are filled, and near the saturation pressure, all the pores are filled. The total pore volume is determined by the quantity of gas adsorbed near the saturation pressure. Desorption occurs when the pressure is decreased from the saturation pressure. Many mesoporous systems exhibit distinct adsorption-desorption behaviours, which lead to a characteristic hysteresis loop. The curve shape is linked to different geometrical factors that rule the

adsorption and desorption processes. The reason for this hysteresis is that capillary condensation occurs differently in adsorption and desorption.

N_2 adsorption is the most common type of adsorption analysis used, however for porous structures with very small pores, N_2 molecule is too big to penetrate the pores. Consequently N_2 isotherms of porous materials with very small pores often indicate that the material is non-porous. To determine whether such a sample is porous CO_2 adsorption is used since the CO_2 molecule is smaller than N_2 and can fit into the smaller pores.

4.1.1.1. Surface Area

B.E.T and Langmuir adsorption methods are most widely used procedures for the determination of the surface area of finely divided porous materials.

The Brunauer-Emmett-Teller (BET) isotherm is a widely used, well-behaved method for extracting effective surface areas and adsorption energies from isotherm data. The method is based on a model of multilayer adsorption that satisfies several conditions;

  i. adsorption occurs on adsorbing sites and on top of adsorbed molecules,

  ii. the number of adsorbing sites per layer is constant,

  iii. the energy of the first-layer adsorbing sites is uniform, and

  iv. molecules in all layers above the first behave as if in a bulk liquid.

Given these conditions, the statistical mechanical problem may be solved by a variety of methods to yield the fundamental equation:

$$\frac{P/P^o}{n(1-P/P^o)} = \frac{1}{n_m c} + \frac{c-1}{n_m c}(P/P^o) \qquad\qquad (1)$$

where P/P^o is the relative pressure, n is the amount adsorbed (per unit mass of adsorbent), n_m is the BET monolayer capacity, and c is usually related to the net heat of adsorption by $c = \exp(q_{st}-q_L)/RT$, where q_{st} is the isosteric heat of adsorption in the monolayer and q_L is the heat of condensation. Conventionally, adsorption data are plotted as $(P/P^o) / n*(1-P/P^o)$ vs P/P^o, and the n_m and c parameters are determined from the slope and intercept of the resulting line.

The monolayer capacity n_m is often divided by some predetermined monolayer density to obtain the BET surface area of the system. The monolayer density is usually taken from adsorption studies of a nonporous material where the surface area can be calculated independently.

Classically, this equation is used for Type II (non-porous or macroporous) and IV (mesopores) isotherms only, but it may also be used for Type I (microporous) data, depending upon the c constant.

Langmuir was the first to propose a theoretical equation relating the quantity of adsorbed gas to the equilibrium pressure of the gas. The Langmuir model was originally developed to represent chemisorption on a set of a distinct localized adsorption sites. The basic assumptions on which the model is based on are as follows;

 i. The solid surface is made up of a uniform array of energetically identical adsorption sites,
 ii. A maximum of one monolayer (one adsorbate molecule per site) can be adsorbed,
 iii. There are no interactions between the adsorbed molecules.

$$\frac{P}{V} = \frac{1}{bVm} + \frac{P}{Vm} \tag{2}$$

where; P is the pressure, Po is the saturation pressure, Va is the quantity of gas adsorbed at pressure P, Vm is the quantity of gas adsorbed at monolayer, b is an empirical constant.

4.1.1.2. Characterization of Micropores : Pore Size Distribution

In microporous systems, various methods have been developed for the determination of micropore volume and pore size distribution, but the validity of pore sizes is often ambiguous. MP, Dubinin-Radushkevich, Dubinin-Astakhov and Horvath-Kawazoe methods are the evaluated mathematical models for pore size distribution determination.

Mikhail et al. proposed a method for constructing pore size distribution from the t-plot. The t-plot is a plot of t, the statistical thickness, versus the relative pressure, P/Po. The t-plot employs a composite t-curve obtained from the data on a number of nonporous adsorbents with BET equation C constants similar to those of the microporous sample being tested. The standard t-curve is expressed by the empirical de Boer equation .

The second means of determining PSDs of microporous materials from gas adsorption measurements is based on the theory of volume filling of micropores. The theory of filling of micropores (TVFM) is applied most widely for describing the physical adsorption of gases and vapours in micropores. This theory is based on the assumption that the characterization adsorption equation express the distribution of the degree of filling of the adsorption space.

The Horvath–Kawazoe method was developed to determine the effective pore diameters of microporous solids (solids with pore diameters smaller than 20 A). The method is based on the 10:4 potential functions of Lennard-Jones. Using Lennard-Jones functions and Gibbs free energy of adsorption, Horwath-Kawazoe derived an expression that correlates the effective pore diameter of a micropore to the adsorption isotherm:

$$RTLn\left[\frac{P}{Po}\right] = K\left[\frac{(N_a A_a + N_A A_A)}{\sigma(l-d)}\right] * \left[\frac{\sigma^4}{3\left(l-\frac{d}{2}\right)^3} - \frac{\sigma^{10}}{9\left(l-\frac{d}{2}\right)^9} - \frac{\sigma^4}{3\left(\frac{d}{2}\right)^3} + \frac{\sigma^{10}}{9\left(\frac{d}{2}\right)^9}\right] \tag{3}$$

where; N_a the number of atoms per unit area of adsorbent, N_A the number of the molecules per unit area of adsorbate, A_a & A_A are constants in Lennard-Jones potential for adsorbent & adsorbate, σ is the distance between a gas atom and the nuclei of the surface at zero interaction energy.

4.1.1.3. Characterization of Macro-Mesopores

The Kelvin equation, BJH adsorption and desorption method are used in the characterization of the mesoporous and macroporous materials.

In porous adsorbent there is continuous progression from multilayer adsorption to capillary condensation in which the smaller pores become completely filled with liquid sorbate. This occurs because the saturation vapor pressure in a small pore is reduced by the effect of surface tension . The mesopore size is usually calculated with the aid of the Kelvin equation in the form.

$$Ln\frac{P^*}{Po} = -\left[\frac{2\gamma * vCos\theta}{RTr_m}\right] \qquad (4)$$

where; P^* is the critical condensation pressure, γ is the liquid surface tension, θ is the contact angle between the solid and the condensed phase, r_m the mean radius of the curvature of liquid meniscus.

BJH (Barrett, Joyner and Halenda) method uses the Kelvin Equation for calculating the pore size distribution. This method involves an imaginary emptying of condensed adsorptive in the pores in a stepwise manner as relative pressure is likewise decreased.   The mathematics of the technique is equally applicable whether following the adsorption branch of the isotherm from high to low pressure or the desorption branch.

4.2. Chemical Thermal and Microstructural Characterization

Vibrational spectroscopy or as commonly known infra red spectroscopy (IR) gives information about the chemical composition of the materials, and in many cases can give information about the chain structure, degree of branching, stereoregularity, geometric isomerism, conformation, crystallinity and type of group present in the material. In IR spectroscopy IR radiation is passed through to a sample and certain frequencies are absorbed by the molecule that causes to vibrational changes in the molecule. There may be many IR bonds observed. Since each molecule has individual sets of energy levels, the absorption spectrum is characteristic of the functional groups that are in the molecule. IR spectroscopy could be useful for obtaining valuable information on the quality and relative quantity of the inorganic phases of materials.

Among the various spectroscopic methods Si NMR is particularly effective because numerous chemical environments of the Si nucleus can be identified (Brinker, Scherer 1990). In the terminology of NMR, Q_n represents a silicon atom bonded through oxygen to n other silicon atoms.

Studies based on nuclear magnetic resonance indicate that the condensation in silica gels continue long after gelation, because of the large concentration of hydroxyl groups. NMR analysis has shown that at gelation substantial amounts of Q_2 exist at the gel point, but the proportions of Q_3 and Q_4 increase with time after gelation (Brinker, Scherer 1990). The Q_n distribution can also be used to determine whether the gel system is weakly or highly branched. A Q_n distribution dominated by incompletely condensed Q_2 and Q_3 species represents a weakly branched structure. While a highly branched silica system is indicated by a greater portion of Q_4 Si species in the NMR spectrum.

The absence of measurable porosity or surface area in a xerogel or film by using NMR analysis is explained as follows:

i. Weakly branched precursors combined with limited condensation during film formation allows the precursors to interpenetrate in response to the decreasing solvent concentration, promoting dense packing and low pore volume,

ii. The weakly branched, compliant precursors are collapsed by the decreasing quality and by the high capillary pressures attained at the final stages of drying.

Thermogravimetric analysis (TGA) and Differential Thermal Analysis (DTA) can best study the thermal stability of ceramic precursors and membrane materials. The decrease or increase in the weight of a sample is followed as the temperature is slowly increased up to 1000 ºC in TGA. The information can be very valuable in the determination of the optimum calcination temperature. The optimum heat treatment conditions further should be determined by using pore size distribution information and SEM pictures. The microstructures of ceramic membranes may drastically change due to sintering above certain temperatures.

Scanning Electron Microscopy (SEM) and Optical Microscopy can be used for the morphological-microstructure characterization of ceramic membranes. SEM is a versatile technique in which 5-50 keV electron beam scans the specimen surface. The resulting secondary electrons, X-rays and backscattered electrons are detected and analysed to form images. The morphology of the ceramic particles making up the membrane, their packing, and the resulting pore structure can be analysed. With their improved resolution, SEM's have become basic surface and microstructural characterisation tools in membrane characterization.

CHAPTER V

GAS SEPARATION MECHANISMS

The history of porous ceramic membranes dates back to about 50 years ago when these membranes were developed for uranium enrichment (de Lange et al., 1995b). To apply uranium as a nuclear fuel it was necessary to increase the U^{235} – isotope concentration in a U^{238} /U^{235} mixture from 0.7 % (natural Uranium) to about 3.5 %. One of the possibilities of enrichment is gaseous diffusion according to the Knudsen diffusion mechanism. This process uses UF_6, which is the most practical volatile compound of uranium. Separation according to the Knudsen diffusion mechanism is based on differences in molecular mass (or molecular velocity). The lighter $^{235}UF_6$ molecule flows a little bit faster than the $^{238}UF_6$ molecule. The ideal Knudsen diffusion separation factor $\alpha_{B/A}$, for two components A and B, is equal to $(M_A/M_B)^{1/2}$. For the separation of $^{235}UF_6$ and $^{238}UF_6$ molecules, this ideal separation factor is 1.0043. In practice, this value is lower, about 1.0020–1.0025. Much is dependent on the process conditions and on the structure of the membrane. For instance, the pressure ratio of the process, P_r (=$P_{permeate}$ / P_{feed}), should be as small as possible. The separation factor of the total process ($\alpha_{process}$) is defined as;

$$\alpha_{process} = 1 + \frac{(1 - P_r)(\alpha - 1)}{1 + P_r(1 - y)(\alpha - 1)} \tag{1}$$

with y the molar fraction of the faster permeating component in the permeate (U^{235}). Pressure ratios cannot be too small because the amount of permeate then becomes too low.
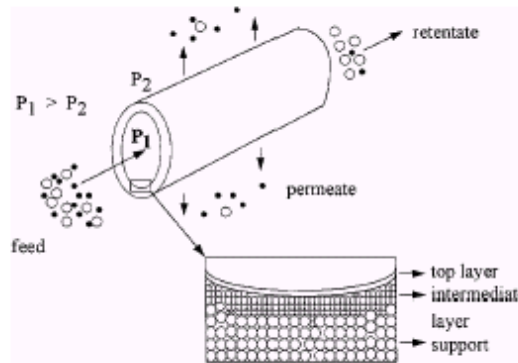

Figure 5.1. Schematic representation of a tubular, porous and asymmetric composite membrane (Vercauteren et al.,1998).

The Knudsen separation factor also decreases if there is momentum exchange between the molecules in the membrane itself. This decrease depends on the mean free path λ of the UF_6 molecules in comparison with the pore width d_p of the membrane. The ratio between these two numbers (λ/d_p) should be at least larger than 10 (Vercauteren et al.,1998).

A homogeneous and porous system of 2 mm thickness having these pore sizes transports far too less molecules because the permeance is not high enough. Therefore, a composite membrane has been developed as schematically presented in Fig.5.1. Most of the gas-flow resistance should be in the thin top layer, otherwise the pressure at the interface between top layer and support becomes too large and so the pressure ratio becomes too high. This is one of the most difficult points in designing the composite membrane structure.

The pioneering work on the development of such membranes was performed in the USA within the framework of the Manhattan project in the 1940s . Also in the former USSR, gaseous diffusion plants were constructed but very little is known about their developments. In France, the Commissariat a l'Energie Atomique (CEA) began research on these composite membranes in the 1950s. About 4,000,000 m^2 of membrane area were delivered for two enrichment factories (Pierrelatte and Eurodif), both located in the Rhone valley. This amount of membrane area was so large because for the enrichment from 0.7 to 3.5 % at least 1,000 separation stages are needed. The membrane and separation costs were about 10 % of the total cost for the electrical energy production. The enrichment capacity of Eurodif was enough for 90 nuclear reactors.

Although both enrichment plants started their production in the 1970s, still the original membranes are used. That is the reason why inorganic membrane production stopped at the end of the 1970s. The same holds for membrane manufacture in the USA and the former USSR. New applications were needed to use these inorganic membranes. In the first instance, they conquered a small part of the market in liquid filtration starting in the 1980s. Food, beverage, dairy and biotechnology markets and waste water treatment are examples of those applications.

In the 1980s also new developments started to provide membranes with more specific properties. The existing membranes were modified to obtain microporous or even dense membranes. Examples are microporous silica , zeolite , molecular sieve

carbon and dense Pd/Ag membranes. Preparation methods were based on sol-gel techniques, chemical vapour deposition or infiltration and plating techniques.

Microporous (r_{pore}<1nm) inorganic membranes are attracting much attention in the field of separation technology for applications in gas separation processes. This is mainly due to their high, molecular sieve like, selectivity and high stability at enhanced temperatures and in chemically aggressive atmosphere compared to polymeric membranes. Also membranes with catalytically active components, distributed in or on top of the membrane, were fabricated. These membranes can be applied in a high temperature membrane reactor for the selective removal of a product to improve the conversion or to increase the selectivity (de Lange et al., 1995a, de Lange et al., 1995c).

The mechanisms of gas permeation and separation for inorganic microporous membranes are different from polymeric membranes. It is generally recognised that gas transport mechanisms through polymeric membranes are intrinsic to a material and controlled by the solution and diffusion process of the permeating gases (Bhave, 1991). On the contrary, for inorganic porous membranes, gas transport is related to the membrane pore size relative to the permeate molecule size. It is thus important to control the pore size uniformly to nanometer scale without pinholes and cracks.

According to separation mechanisms we can divide the inorganic membranes into two groups. These are porous inorganic membranes and nonporous inorganic membranes. Alumina, silica, zirconia, zeolite membranes are good examples of porous inorganic membranes; metal, liquid immobilized membranes are the examples for nonporous inorganic membranes. Knudsen diffusion (gas phase transport), surface diffusion (surface transport, multilayer diffusion) and capillary condensation are the significant transport and separation mechanisms of the porous membranes. In nonporous membranes the transport is by solution diffusion mechanism of the gas molecules. Although the selectivity of most of these dense membranes can be very high, the permeability is quite low. Good separation membranes should be selective and have high permeability. Microporous top layers supply high selectivity and permeability in ceramic membranes. In porous membranes gases can be separated due to differences in their molecular masses (Knudsen diffusion), due to interaction (surface diffusion, multilayer diffusion and capillary condensation) and due to their size (molecular sieving) (Bhave,1991).

The permeability is calculated according to Darcy's law. The material flux J, through a membrane is related to microstructure according to,

$$J = \frac{V_p r^2 dP}{8\eta dx}$$ (2)

where V_p is pore volume, r is pore size, dP is pressure drop, η is viscosity and dx is the membrane thickness. Written another way, the permeability Q is

$$Q = \frac{F}{A} \frac{dx}{dP}$$ (3)

where F is flow rate in cm^3/s and A is the membrane area.

Phenomenologically it has been found that the flux J ($mol/m^2 s$) through microporous materials such as zeolite, microporous carbon, glass and amorphous systems, increases as a function of temperature (de Lange et al., 1995b).

$$J \propto J_o \exp \frac{-E_{act}}{RT}$$ (4)

Membrane technology competes successfully in its own right in a number of areas, covering:

i.   Hydrogen recovery from ammonia purge gas,
ii. Hydrogen recovery from refinery and petrochemical plant off-gases,
iii. Enhanced oil recovery, bio gas and other CO_2 / C_nH_m separations,
iv. Helium recovery from diving gas or balloon gas,
v.   Inert gas generation from N_n / O_2 ,
vi. LPG recovery from refinery off-gases.

5.1. Knudsen Diffusion

Knudsen diffusion occurs if the pores of a porous medium are smaller than the mean free path of the gas molecules, with no or only a weak interaction with the membrane material. Gas separation according to Knudsen diffusion is based on differences in molecular velocity of different components in a mixture. This means that lighter gases permeated faster than heavy gases. For a single component, molecular

velocity will increase at higher temperature, although the Knudsen permeation for this component decrease at elevated temperature. Knudsen diffusion mechanism gives relative permeation rates, which are equal to the inverse square root ratio of the molecular weights of gases.

$$F_o^A / F_o^B = \alpha_{A,B,Knudsen} = (M_B / M_A)^{0.5} \qquad (5)$$

For gases which are similar in molecular weight, such as O_2 and N_2, Knudsen flow is ineffective. For any pair of gases, increases in temperature make Knudsen flow less effective. These facts are hardly encouraging.

$$F_{k,o} = \frac{2\varepsilon_p \mu r v}{3RTL} \qquad (6)$$

$$v = \sqrt{8RT / \pi M} \qquad (7)$$

$F_{k,o}$ = Knudsen Permeability (mol / m^2.s.Pa)

ε_p = Porosity

r = Modal pore radius (m)

v = Average molecular velocity (m / s)

R = Gas constant (J / mol.K)

L = Layer thickness (m)

M = Molecular mass (kg / mol)

$$\text{Separation factor} = a = \frac{y}{1-y}\frac{1-x}{x} \qquad (8)$$

x = Mole fraction of the faster permeating component in the feed

y = Mole fraction of the faster permeating component in the permeate
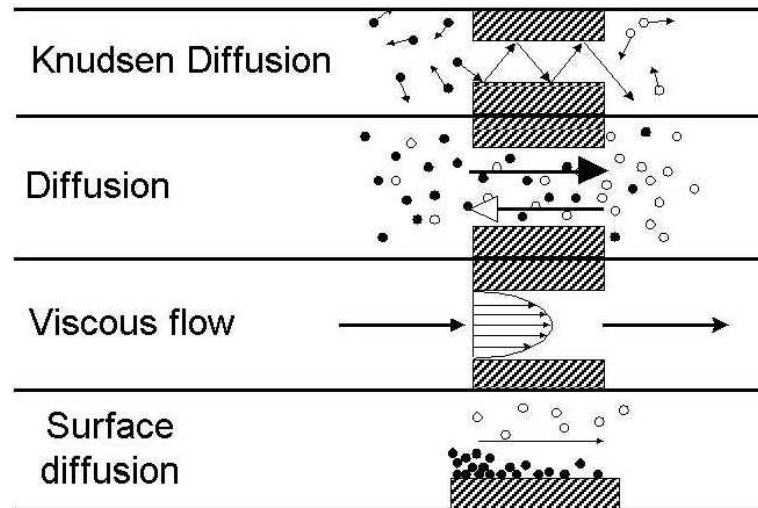
Figure 5.2. Schematic illustration of gas transport mechanisms.

5.2. Laminar Flow and Molecular Diffusion

Gas phase transport mechanisms can occur in three mechanisms. In one of these mechanisms due to molecule-wall collisions, the molecules loose momentum to the wall. If there is enough interaction between rebounded and adjacent molecules which means the molecules must statistically collide at least as much with each other as with the wall, the momentum loss is progressively and smoothly transferred to the bulk of the gas. This is so-called laminar flow regime. The other important mechanism is due to molecule-molecule collisions, taking place with conservation of the total amount of momentum. This is called molecular diffusion. It differs from the molecular diffusion by the fact that in laminar flow there is no segregation of species and there is a loss of momentum.

Of these mechanisms, ie, molecular diffusion, laminar flow and knudsen diffusion, only two are important in pressure driven separations. These are laminar flow and knudsen diffusion. If the molecules see each other much more than they see the pore wall (which means the mean free path of the molecules is much smaller than the pore radius), laminar flow and molecular diffusion are important. The laminar flow is much larger, however and the molecular flow can be neglected. If the molecules see the pore wall much more than they see each other, only Knudsen diffusion will occur. Thus, the molecular diffusion can be neglected in all circumstances (Bhave, 1991).

For pure gases, a good indication of which mechanism is dominant, Knudsen diffusion or laminar flow, is given by Knudsen number;

$$K_n = \frac{\lambda}{r} \quad \text{with} \quad \lambda = \frac{16\eta}{5\pi P_m}\sqrt{\frac{\pi RT}{2M}} \tag{9}$$

where λ is the mean free path, r is the pore radius, η is the gas viscosity, P_m is the mean pressure, R is the gas constant, T is the temperature and M is the molecular mass. Poiseuille flow through a porous medium, occurring for $K_n \ll 1$ is given by,

$$F_{p,o} = \frac{\varepsilon \mu_p r^2}{8RTL\eta} P_m \tag{10}$$

where $F_{p,o}$ = Poiseulille Permeabiliyy, (mol / m^2.s.Pa), ε is the porosity, μ_p is the reciprocal tortuosity, (-), η is the gas viscosity, (N.s / m^2), L is the membrane thickness (m), and P_m is the mean pressure , (Pa).
Knudsen diffusion occurring for $K_n \gg 1$ is given by,

$$F_{k,o} = \frac{2\varepsilon_p \mu r v}{3RTL} \quad \text{and} \quad v = \sqrt{\frac{8RT}{\pi M}} \tag{11}$$

where v is the mean molecular velocity, depending on the molecular mass. For $K_n \approx 1$ and pure gases, Poiseuille flow and Knudsen diffusion are assumed to be additive. As can be seen from equations (10) and (11), Poiseuille flow is nonseparative, while gas separation by Knudsen diffusion is possible.

For gas mixtures, description of transport becomes more difficult. If only Knudsen diffusion occurs, the molecules do not see each other and for binary mixtures equation (5) is valid. In the case of combined laminar flow and Knudsen diffusion, the gases interact.

In literature, several authors have described gas phase transport through various membranes, for pure gases as well as for mixtures. Okubo et al. (1990), reported the preparation of γ-Al_2O_3 porous membranes without pinholes and cracks by the sol gel process. Also they measured the He and N_2 permeabilities and their results implies that

gas permeation through pores in the membrane was mainly controlled by Knudsen flow mechanism.

Knudsen diffusion has been studied by Cho et al. (1995), γ-Al_2O_3 porous membranes have been produced by sol gel coating with boehmite sol. Permeation values of He, N_2 and CO_2 through the γ-Al_2O_3 with a pore diameter of 5 nm, were independent of the mean pressure and decreased with the square root of the temperature. Therefore these results imply the main mechanism of gas transport through the membrane was Knudsen diffusion.

In summary, it can be stated that the separation by gas phase transport (Knudsen diffusion) has a limited selectivity, depending on the molecular masses of the gases. The theoretical separation factor is decreased by effects like concentration-polarisation and backdiffusion. However, fluxes through the membrane are high and this separation mechanism can be applied in harsh chemical and thermal environments with currently available membranes.

5.3. Surface Diffusion

Separation of gases by Knudsen diffusion is limited by the differences in molecular masses of the gases and is therefore only of practical importance for the separation of light gases from heavier ones. For other mixtures, other separation mechanisms should be employed in order to obtain higher separation factors.

One of the alternatives is surface diffusion, that using differences in chemical and/or physical properties of the molecules to be separated. The surface of the separating (or active) part of the membrane is modified in such a manner that one type of molecule is transported much more rapidly than the other as a result of a difference in surface diffusion. Modification can also give rise to pore size reduction, resulting in an increasing importance of surface diffusion as a transport mechanism. However, the insight into the mechanism of surface diffusion is still poor, so that it is difficult to make appropriate use of differences in chemical and/or physical properties.

In the case of surface diffusion, gas molecules can interact with the surface, adsorb on surface sites and be mobile on the surface. If a pressure gradient exists, a difference in surface occupation will occur. Therefore, a surface composition gradient is created and transport along the surface will occur, if the molecules are mobile. The gradient in surface diffusion is thus a surface concentration gradient. It must be

considered that additional gas transport exist as a surface flow in the direction of decreasing surface concentration. The presence of surface flow is detected as a deviation of the total permeability from the gas phase permeability. The concentration of adsorbed phase is a function of three parameters: the pressure, the temperature and the nature of the surface.

$$J_{s,o} = -\rho_{app}D_s\mu_s\frac{d\rho}{dl}$$ (12)

where; $J_{s,o}$ = Surface diffusion flux (mol / m^2s)

ρ_{app} = Apparent density (kg / m^3), is defined as ($1-\varepsilon_p$)ρ_{cryst}

μ_s = Reciprocal tortuosity (-)

D_s = Surface diffusion coefficient (m^2 / s)

$\frac{d\rho}{dl}$ = Surface concentration gradient (mol / kg.m)

However, there is a contradiction, since the more the molecules are absorbed (the higher the heat of adsorption) the less the probability of their being mobile. When the surface of the γ-alumina membrane was modified with magnesia, the amount of CO_2 adsorbed on the surface increased. The heat of adsorption also increased however and thus the mobility decreased. Due to this lower mobility, effectively less CO_2 was transport through the membrane, although more adsorption occurred. It was claimed that the introduction of MgO gave strong basic sites and the more strongly bonded CO_2 was less mobile (Keizer, 1988).

Surface diffusion has been studied by Cho et al (1995). MgO impregnated γ-Al_2O_3 membranes has been prepared by introducing an interaction between CO_2 gas molecules and the pore wall, to improve the separation factor by surface diffusion. They concluded that if the metal oxide gives weak basic sites, surface diffusion occurs but the contribution to total transport is very small. When the membrane surface is modified by the metal oxide that provides strong basic sites, the surface diffusion does not occur because strongly adsorbed gas molecules are less mobile.

There is another way to increase the contribution of the surface diffusion to total transport, in addition to altering the amount adsorbed and/or the surface mobility. This is through a pore size decreasing. For cylindrical pores the following equation is

commonly used to describe the relation between surface permeability and the structure of the porous medium:

$$F_{o,s} \approx \mu_s \varepsilon / r \tag{13}$$

For a single gas, if gas phase transport and surface transport are assumed to be additive, the following is valid, if it is assumed that $\mu_p = \mu_k = \mu_s$:

$$F_o \approx F_{o,p} + F_{o,Kn} + F_{o,s} \approx \varepsilon \mu_k (r^2 + r + 1/r) \tag{14}$$

From equation (14), it is immediately clear, that by decreasing the pore size, only the surface diffusion contribution is increased (third term on the right hand size of equation (14)), due to increased surface area. It should be noted here that the additive nature of surface permeability and gas phase permeability is still a matter of debate, since it is very difficult to determine the surface permeability alone. The experimentally measured surface permeability will always include a contribution due to gas phase permeability.

Several models were developed in literature to describe surface transport. These can be divided into three categories (Choi et al., 2001);

1) The hydrodynamic model: In this model the adsorbed gas is considered as a liquid film, which can "glide" along the surface under the influence of a pressure gradient.

2) The hopping model: This model assumes that molecules can hop over the surface. Mean hopping distance and the velocity, with which the molecules leave their site, calculate the surface flux.

3) The random walk model: This is the most frequently used model in literature. It is based on the two-dimensional form of Ficks law. The surface diffusion coefficient has been the subject of many jump from one site to another. This is an activated process and the energy of activation is a fraction of the heat of adsorption. This means that strongly adsorbed species are less mobile than weakly absorbed species. If the activation energy is larger than 0.5 times the heat of adsorption, desorption occurs instead of surface diffusion.

Therefore, it can be concluded that in order to employ surface diffusion as an effective separation mechanism, the pores should be very small (radius<3nm) and the temperature should be kept low (T < 300 ^{o}C), due to the necessary physical adsorption of the gas.

5.4. Micropore Diffusion (Activated Transport)

For microporous membranes that have a pore size that is nearly equal to the diameter of permeating molecules, a molecular sieving like separation, the origin of which is the differences in molecular shape and size, might be expected. In these small pores there is a serious interaction between gas molecules and pore walls, because of overlapping adsorption force fields of the pore walls. The molecules therefore need sufficient energy to diffuse and consequently increased permeation is observed at higher temperature. Ideally, micropore diffusion mechanism enables gas molecules to separate , while the separation of those gas molecules is difficult if their diameter sizes are similar as in the CO_2 (3.3 ^{o}A)-N_2 (3.64 ^{o}A) system. This is because accurate pore size control is needed at the sub-nanometer scale. Moreover, the flux of the permeating molecule tends to be rather small for such pores. Kinetic diameters of some small molecules are tabulated in Table 5.1.

For molecules diffusing exclusively in the adsorption force fields of the pore walls, a pore size/molecule size ratio below 1.5 is necessary. This is the case for the silica membrane with pores of about 0.5 nm. For small gas molecules like He and H_2, the transport mechanism is then activated diffusion. CO_2 is also a rather small molecule and it has a strong dipole moment. In these small pores it shows high permeation, probably because of a strong interaction with the membrane material.

Table 5.1. Kinetic diameter of some selected gases(de Lange et al.,1995c).

Gases	Kinetic Diameter σ (nm)	Gases	Kinetic Diameter σ (nm)
He	0.26	CH_4	0.38
H_2	0.289	C_2H_4	0.39
CO_2	0.33	C_3H_8	0.43
O_2	0.346	n-C_4H_{10}	0.43
N_2	0.364	iso-C_4H_{10}	0.5

The diffusion of molecules in microporous materials is modelled as an activated process according to an Arhenius relation:

$$D = D_o \exp(\frac{-E_m}{RT}) \qquad (15)$$

where D_o is a temperature independent proportionality constant and E_m is the mobility energy or the activation energy for diffusion ($Jmol^{-1}$), R the gas constant ($Jmol^{-1}K^{-1}$) and T the absolute temperature (K). Gas adsorption on silica films are in the low coverage of Henry's regime except that CO_2 shows non linearity at 295-323 ^{o}C (de Lange et al.,1995b). Hence, Henry's law is generally obeyed:

$$c = Kp \qquad (16)$$

where p is the pressure (Pa) and the K the Henry's constant as a function of temperature according to van't Hoff relation:

$$K = K_o \exp(\frac{Q_{st}}{RT}) \qquad (17)$$

where K_o is a temperature independent proportionality constant, Q_{st} the isosteric heat of adsorption. De Vos Verweij (1998), proposed that the isosteric heat of adsorption for microporous silica films approaches those of silicalite as the average pore size if silica materials and silicalite are quite similar coupled with the fact that both materials are silica sol-gel process derived. Q_{st} values found in the literature for silica and silicalite are shown in Table 5.2.

Table 5.2. Typical isosteric heat of adsorption (Q_{st}) values (kJ mol^{-1}) (da Costa et a.,2002).

Material	CO_2	CH_4	H_2	N_2	O_2
Silica	22	10	6		
Silicalite	24	18,6	6	15	
Silicalite	20	28	6		
Silicalite	24	20	6	18	16
Silica	22	20	6	17	16

Subsituting equations (15)-(17) into Fick's law which is $J = -D\dfrac{dc}{dx}$, gives a temperature dependent flux equation (18) in the Henry regime.

$$J_x = -D_o K_o \exp(\frac{Q_{st} - E_m}{RT})\frac{dp}{dx} \qquad (18)$$

In this model, microporous diffusion which is essentially activated transport if pore sizes are of molecular sieve dimension, is assumed to be rate limiting. For pore sizes larger than molecular sieve dimensions, but still microporous the transport may coupled with Knudsen diffusion which is non activated. Based on the microporous model proposed by de Lange et al.(1995b) have demonstrated that in the case of gases complying with Henry's law in silica membrane diffusion, the mobility energy can be calculated as a function of the sorption energy in the micropores (Q_{st}) and the activation energy:

$$E_a = E_m - Q_{st} \qquad (19)$$

Depending on micropore size and gas molecule size, activation energies ranging from around 2 to 40 kj/mol have been reported. This activation energy, however, is an apparent one, since it can be regarded to consist of a contribution of the activation energy for micropore diffusion and contribution of the heat of adsorption of the gas molecules on the membrane surfaces. An extensive model description, which was among others based on the theoretical model for gas transport in microporous zeolite crystals, with a fixed pore size, was proposed by Barrer (de Lange et al.,1995b).

Discussion of permeance and permselectivity should also include activation energy as an important parameter of membrane quality. The activation energy for H_2 permeance gives a good correlation with the separation factor and is used as a measure of quality.

Various research groups produced microporous silica membrane with relatively high fluxes and separation factor. The best results have been reported by de Vos and Verweij (1998) with a permeance of (4.7-17.7) * 10^{-7} mol m^{-2}s^{-1}Pa^{-1} (H_2) and (2-3.2) * 10^{-7} mol m^{-2}s^{-1}Pa^{-1} (CO_2). The H_2 / CO_2 permselectivity ranged between 2.5-7.5 for the membrane calcined at 400 ^{o}C while for those calcined at 600 ^{o}C permselectivity range

increased to values 18-130 with a half reduction in H_2 permeance. And, they reported the activation energy for H_2 as 8 kJ mol^{-1}. They were able to produce 30 nm thick high quality silica film with a pore diameter of 0.5 nm.

Da Costa et al. (2002), synthesised molecular sieve silica membranes by two step and one step acid catalysed hydrolysis of TEOS. The transport of diffusing gases in these membranes was activated because the permeance increased with temperature. Although the permeance of He for both membranes were similar for the two step membranes He/CO_2 permselectivity were one to two orders of magnitude higher than the single step membrane. Also the two step membranes had high activation energy for He and H_2 permeance in excess of 16 kj mol^{-1}. And they reported that, although two step membranes had a pore diameter of 0.3 nm, single step membrane had slightly larger pores.

Nair et al. (1997a) demonstrated that H_2 permeation through silica membranes was comparable to He permeation under identical conditions. For a similar membrane at room temperature He and H_2 permeations were measured as $4*10^{-9}$ mol m^{-2}s^{-1}Pa^{-1} and $4.5*10^{-9}$ mol m^{-2}s^{-1}Pa^{-1} respectively. At 303 K hydrocarbon permeation was about two times higher than N_2 or O_2. He permeation in order of 10^{-7}-10^{-8} mol m^{-2}s^{-1}Pa^{-1} were reported in the temperature range of 303-460 K.

CHAPTER VI

EXPERIMENTAL

6.1. Materials

Alumina sols were prepared by using Aluminium-Isopropoxide, nitric acid, hydrochloric acid and water. In predetermined ratios, Tetraethylorthosilicate (TEOS), ethanol, water and HNO_3 were used to prepare silica sols. The properties of these materials used in this work are tabulated in Table 6.1. Two types of membrane supports were prepared by using an α-Al_2O_3 powder with PVA as a binder and partially stabilized zirconia powder, respectively.

Table 6.1. Specifications of the Materials.

Materials	Specifications
Aluminium Isopropoxide $[(CH_3)_2)CHO]_3Al$	98%, M=204.2, d=1.035 (Aldrich)
TEOS $Si(OC_2H_5)_4$	98%, M=208.33, d=0.934 (Aldrich)
Ethylalcohol C_2H_5OH	99,8%, M=46.07, d=0.79 (Riedel)
Nitric Acid HNO_3	65%, M=63.01, d=1.4 (Merck)
Hydrochloric Acid (HCl)	37 %, M=36.46 d=1.19 (Merck)
Alumina Powder α-Al_2O_3	99.99%,BET =12.3 m^2/g Sumitomo,(AKP-53)
Zirconia Powder	TOSOH TZ-3Y, BET=16m^2/g
Polyvinyl Alcohol (PVA)	80%,M=9000-10000 (Aldrich)

6.2. Sol Preparation

6.2.1. Alumina Sols

Alumina sols were prepared by the hydrolysis of aluminium isopropoxide at a temperature of 80 ^{o}C for 3 hours. The hydroxide precipitate was peptised with appropriate amounts of nitric acid to form a stable colloidal suspension and was kept at about 80 ^{o}C under vigorous stirring. The compositions and the codes of the alumina sols are given in Table 6.2 and membrane formation procedure from alumina sols is shown in Figure 6.1.

Table 6.2. Acid/Alkoxide and Water/Alkoxide ratios for Alumina Sols.

Codes	H$^+$ / Alkoxide	H$_2$O / Alkoxide
A00	0.07	100
A01[*]	0.1	100
A02[*]	0.15	100
A03[*]	0.2	100
A04	0.1	100
A05	0.2	100
A06	0.3	100
A07	0.4	100
A08	0.25	100
A09	0.25	120
A10	0.25	140
A11	0.25	160
A12	0.25	180

[×] HCl was used as the acid

Al-isopropoxide + H$_2$O

Stirring 3h at 80 ^{o}C

Dilute HNO$_3$

Stirring 2h at 80 ^{o}C

α-Al$_2$O$_3$ Support disk

Alumina Sol

Drying at 50 ^{o}C in petri dish

Dip Coating

Unsupported γ-Al$_2$O$_3$

Drying

Calcination at 500 ^{o}C / 550 ^{o}C / 600 ^{o}C
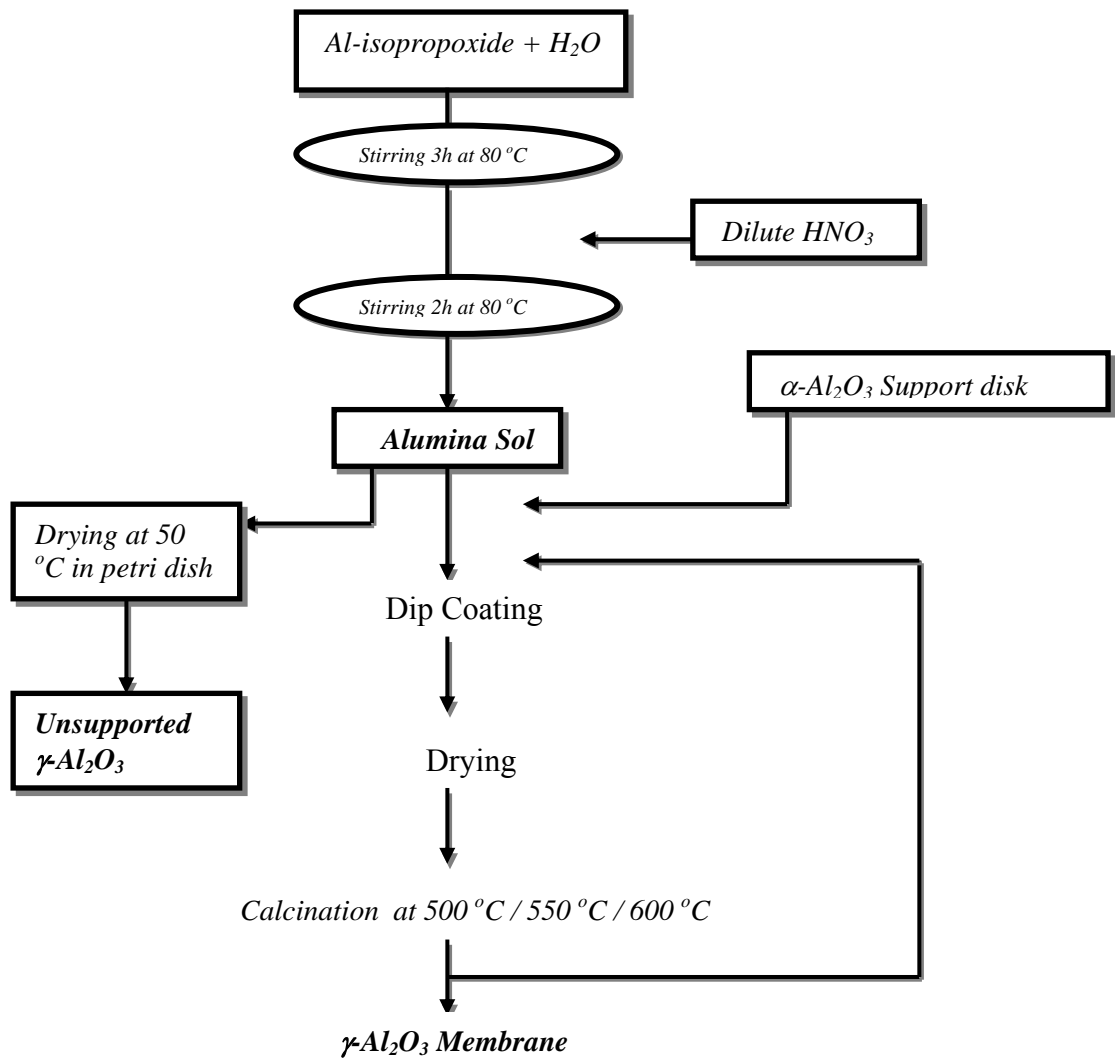
γ-Al$_2$O$_3$ Membrane

Figure 6.1. γ-Al$_2$O$_3$ Membrane preparation procedure.

6.2.2. Silica Sols

In this study, silica sols were synthesised by acid catalysed hydrolysis and condensation of tetraethylorthosilicate (TEOS) in ethanol. Predetermined water and acid was added drop-wise to TEOS/ethanol mixture with constant stirring. During the addition of the acid-water mixture, the reaction mixture was placed in an ice bath to avoid partial hydrolysis as suggested by de Vos and Verweij (1998). After the addition was complete the reaction mixture was heated of 60 ^{o}C for 3h under constant stirring. The compositions and the codes of the silica sols are given in Table 6.3. SiD was prepared by co-polymerization of methyltriethoxysilane and TEOS using a two step acid catalyzed process.

Table 6.3. Synthesis compositions of silica sols.

	TEOS	HNO$_3$	WATER	EtOH	MTES
SiA	1	0.05	6.4	3.8	-
SiB	1	0.085	6.4	3.8	-
SiC	1	0.17	6.4	3.8	-
SiD	0.9	0.056	5.1	3.8	0.1

All silica and alumina sols were prepared in pyrex shott bottles with open caps. Silica sols were stored in a refrigerator after preparation.

6.3. Sol Particle Size Characterization

Dynamic light scattering provides information about the dynamics of particles in a sol through measurement of the temporal fluctuation in scattered intensity associated with the Brownian motion of the particles. The information obtained by varying experimental methods can include average values for dynamic size and size distribution. In this work the measurements of the average particle size and size distribution by intensity, by volume and by number, in boehmite sols were analysed by using ZetaSizer 3000HS. Measurements for each sample were repeated 3 times. The wavelength of the laser light employed in the instrument was 633 nm, which could detect a minimal particle size of 2 nm.

6.4. Unsupported Ceramic Membrane Preparation

Unsupported membranes were prepared for characterization experiments. All silica and alumina sols have been dried in petri dishes. About 15 ml alumina sol samples were dried at 50 °C for one day and calcined at 500 °C, 550 °C, 600 °C, with a 4 °C/min heating and cooling rate for 3 hours. Silica sols (5 ml) were dried at 50 °C for one day and calcined at 400 °C for 3 hours with a 3 °C/min heating and cooling rate. Heat treatment were performed by a Carbolite RH 1600 programmable furnace.

6.5. Characterization of Unsupported Membranes

The pore size distributions and surface area determinations were performed in a volumetric adsorption-desorption analyzer (Micromeritics–ASAP 2010). Selected samples from alumina unsupported membranes were characterized by Nitrogen adsorption-desorption experiments. About 0.1g alumina unsupported membrane samples were degassed for 1 hour at 90 °C and 4 hours at 350 °C prior to N_2 adsorption. Pore size determinations were performed according to cylindrical geometry and by using BJH method for Alumina unsupported membranes.

Thermo Gravimetric Analyzer (TGA-51/51H, Shimadzu Co.) was used to perform the thermal behaviour analysis. The samples were heated at a rate of 10 °C per minute to 1000 °C. A plot of the percent weight loss with increasing temperature was produced as TGA curves.

FTIR spectroscopy was carried out to determine the molecular functional groups embedded in the membrane. FTIR Spectrum was obtained by Fourier Transform Infrared Spectroscopy (FTIR-1600, Shimadzu Co.). The samples were prepared by pressing the ground samples with dried crystalline KBr. Every five minutes scans, consisting of the accumulation of 20 spectra, were performed from 4000 to 600 cm^{-1}.

The microstructure of the silica and alumina membranes deposited on zirconia supports were examined by SEM (Philips XL30S SFEG). Phase structure characterization of the alumina membranes was performed by X-ray diffraction (Philips X'pert Pro) by using CuK$_\alpha$ radiation.

6.6. Support Preparation

Alumina support discs were prepared from Sumitomo AKP-53 powder.100 grams of powder was mixed with PVA solution (3 grams PVA in 50 ml water), and then dried until 3-4% relative humidity. Pellets (~8 gram) with dimensions 4,5 cm in diameter and 2 mm in thickness were uniaxially pressed and heat treated at 1100 ^{o}C for 3 hours.

Zirconia support discs were prepared from partially stabilised Tosoh TZ-3Y zirconia powder using slip casting technique. The average diameter of the powder measured by Particle Size Analyzer (Sedigraph) was 1.059μm. To obtain a 15 vol% stable suspension a polyelectrolyte (poly-acrylic acid) was used and pH was adjusted with NH_4OH solution. The slip-cast support discs with dimensions of 4,5 cm in diameter and 2 mm in thickness were prepared by pouring 11 ml stable suspension into plastic tubes and were cast on plaster of pairs molds. Cast supports were sintered at 1150 ^{o}C for 3h with a heating rate of 10 ^{o}C/min.

6.7. Membrane Preparation

γ-Al_2O_3 membranes were prepared by dip coating the sintered ZrO_2 supports into   diluted (1:3) boehmite (γ-AlOOH) sol (A08) followed by drying and calcination. The dipping time was fixed at 10 seconds. After the dipping procedure, the membranes were dried at room temperature for 15 minutes, calcined for 3 hours at 500 ^{o}C, 550 ^{o}C, and 600 ^{o}C. The whole process of dipping, drying and calcination was repeated up to three times to repair any defects in the first γ-Al_2O_3 layer.

Silica membranes were prepared by dipping a ZrO_2 support into silica dip solutions with different compositions. Dipping time was varied from 5s to 20s. Membranes were heat treated from 50 ^{o}C to 400 ^{o}C with heating a rate of 3 ^{o}C/min. Also aging of the sol was studied for SiB sol up to 16h. Membranes were coded as a SiB-5, SiB-10, SiB-15 and SiB-20 with respect to the dipping time.

6.8. Membrane Test System

Membrane gas permeance was carried out on pressure controlled dead-end mode membrane test system as shown in Figure 6.2. The system consisted of two pressure transducers, teflon membrane module, gas tube (O_2, N_2 and CO_2) and expansion chamber. The permeate pressure was varied from 2.5 bar to atmospheric pressure.

In the dead-end mode, the feeding pressure p_H is constant at all time while the pressure in the second expansion chamber p_L changes from an initial condition close to zero pressure to a final condition. Pressure data from both feed and permeate transducers were recorded to calculate the pure gas permeance.
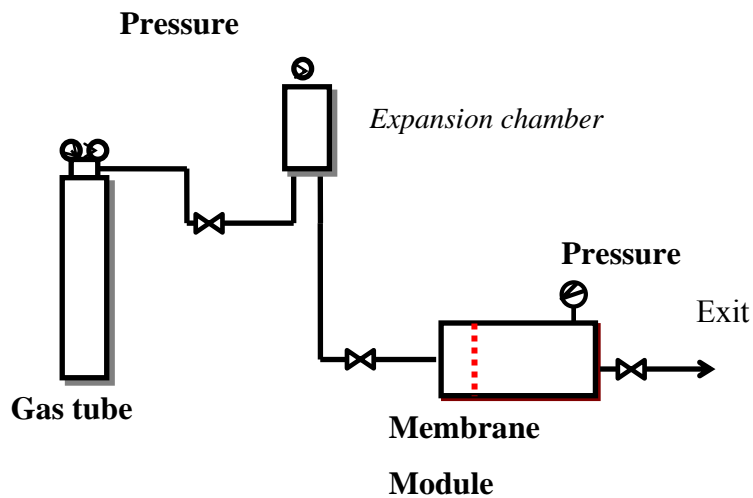
Figure 6.2. Schematic diagram of the experimental setup for gas permeation.

6.8.1. Gas Permeation Modelling

As discussed in Section 5.4 a temperature dependent flux equation (1) in the Henry regime is:

$$J_x = -D_o K_o \exp(\frac{Q_{st} - E_m}{RT}) \frac{dp}{dx} \qquad (1)$$

In the permeation system shown in Figure 6.2, the flux of gases through a membrane of effective area, A, 12.5 cm^2 into permeate reservoir of volume V, (100cm^3) can be derived from the ideal gas law:

$$J(t) = -\frac{V}{ART}\frac{dp}{dt} \tag{2}$$

As the flux through the membrane is the same as the flux into the expansion chamber, equations (1) and (2) are equal and can be integrated as a function of time and pressure to give the following relationship:

$$\ln(\frac{p_H - p_o}{p_H - p(t)}) = \frac{D_o K_o}{l} \exp(\frac{E_m - Q_{st}}{RT})\frac{ART}{V}t \tag{3}$$

where p_o is the initial permeate pressure and generally is equal to zero, l is the membrane thickness, p_H refers to the high or feed pressure in the retentate side while p(t) is permeate side pressure at time=t. The permeance of gases (P/l) may be defined as an activated transport normalised pressure flux (mol m^{-2} s^{-1} Pa^{-1}) as follows (da Costa et al., 2002):

$$\frac{P}{l} = \frac{D_o K_o}{l} \exp(\frac{E_m - Q_{st}}{RT}) \tag{4}$$

$$\ln(\frac{p_H - p_o}{p_H - p(t)}) = \frac{P}{l}\frac{ART}{V}t \tag{5}$$

Using equation 5, the slope of the natural logarithm of the pressure versus time plots yield the normalised pressure flux or permeance (P/l) as A (12.5 cm^2), R, T, and V (100 cm^3) are known constant.

CHAPTER VII

RESULTS AND DISCUSSION

7.1. Sol Characterization

7.1.1. Particle Size Distributions of Alumina Sols

The preparation, characterization and pure gas permeation of sol-gel derived alumina and silica membranes were investigated in this work. The effects of water/alkoxide, acid/alkoxide ratios on the properties of unsupported membranes were examined. The effects of water/acid contents, and the acid type on particle size were also analysed in alumina sols.

In sol-gel derived structures, the size of the smallest pore is closely related to the average particle size in the sol. One of the factors affecting the size of the sol particle is the type of the acid used. Table 7.1 gives the peptising effects of two types acids which were HNO_3 and HCl, at 0.1 H^+/Alkoxide and 0.2 H^+/Alkoxide mole ratio.

Table 7.1. Effect of acid type on the mean sol particle size.

Acids	H^+ / Alkoxide	Particle Size Distribution	Hydrodynamic Diameter (nm)
HCl	0.1	Narrow	68
HCl	0.2	Narrow	49
HNO_3	0.1	Broad	73
HNO_3	0.2	Broad	51

The type of peptizing acid had a slight effect on sol particle size where HCl use resulted in the formation of smaller sol particles as shown in Table 7.1. Yoldas (1975) studied effects of various acids on sol formation and he concluded that the acid type affects the particle size in the order of HCl > HNO_3 > Formic acid > Acetic acid. An inorganic acid favours the formation of smaller particles but larger particles were favoured by organic acids.

Variation of particle size of the alumina sols with different concentrations of HNO_3 with constant water/alkoxide mole ratio (100) is depicted in Figure 7.1. Clear sols were obtained when the H^+/Alkoxide mole ratio were in the range of 0.07 to 0.4 but

sol with the lowest acid content (below 0.07), remained unpeptised and the dense cake formation occurred at the bottom of the bottle. Particle size in the same H^+/Alkoxide
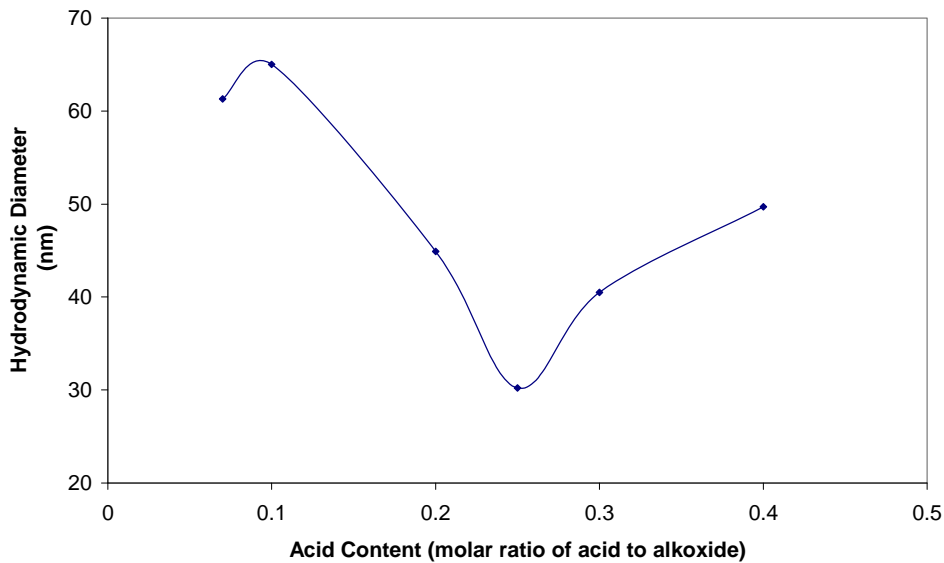
Figure 7. 1. Effects of acid amount on the mean particle size.

mole ratio range, had an optimum value at 0.25 giving the minimum particle size. Peptisation requires a critical amount of acid to stabilise the sol. These results also indicates that the amount of acid in relation to aluminium must not be higher than a certain value which may cause the formation of the large sol particles.

The other factor that affects the size of the sol is water/alkoxide mole ratio. Figure 7.2 shows the effect of water content on the alumina sol particle size.
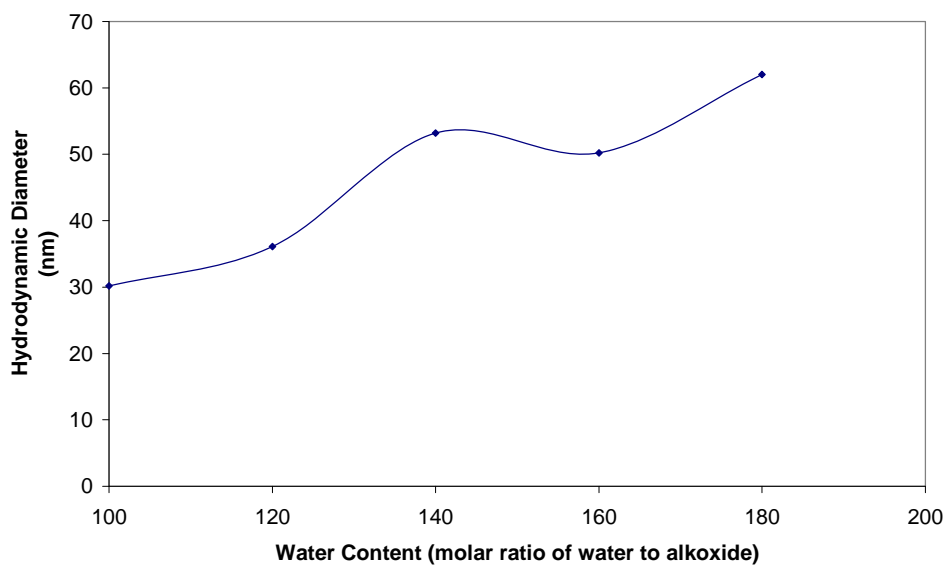
Figure 7.2. Effect of water content on the mean sol particle size.

As shown in Figure 7.2 as the water content increases, the mean particle size of the alumina sols increase. Therefore the minimum water content has been chosen as a optimum water/alkoxide mole ratio (100) the in preparation of alumina sols.
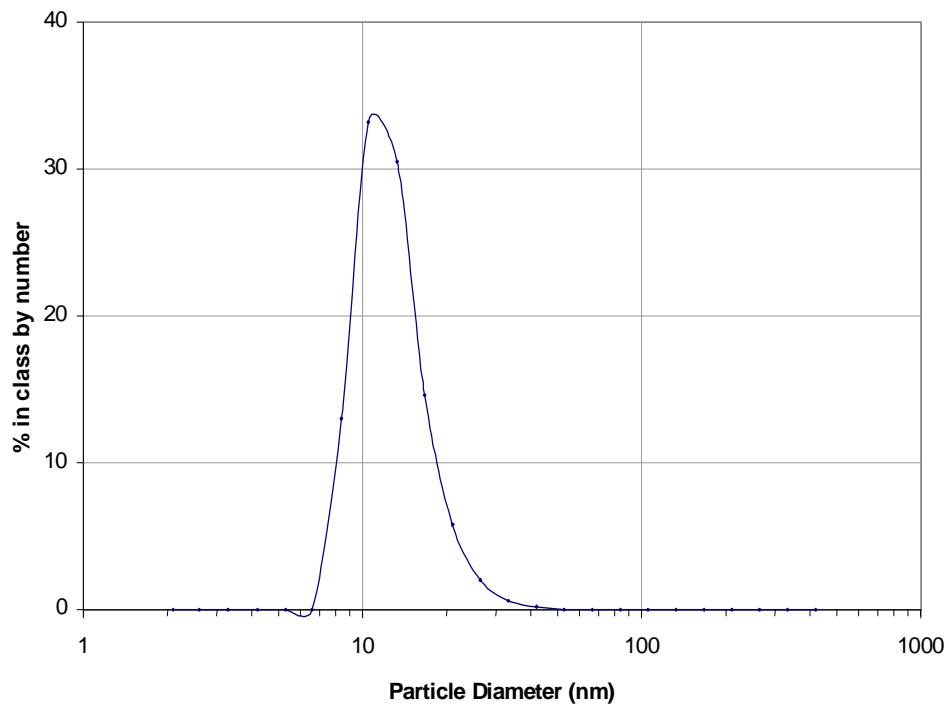
Figure 7.3. Number based particle size distribution for A08 sol.
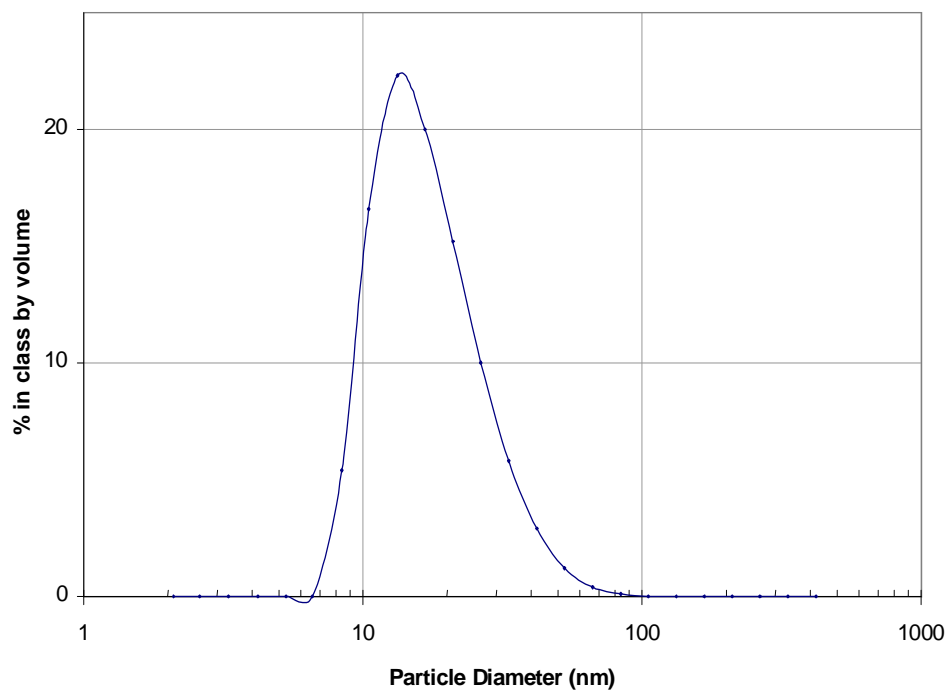
Figure 7.4. Volume based particle size distribution for A08 sol.
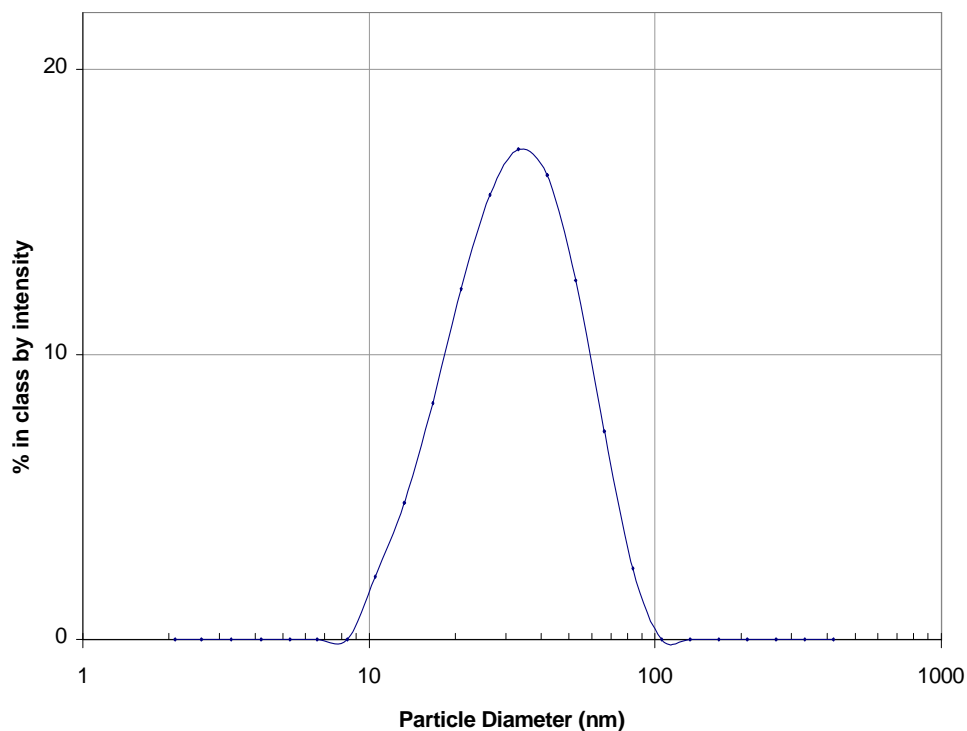
Figure 7.5. Intensity based particle size distribution for A08 sol.

Figure 7.3 to 7.5 shows the number, volume and intensity based particle size distributions in the 1/3 diluted A08 sol of concentration 0.2 mol Al/litre. The sol had a sharp peak around 13.1nm, 18.5nm and 35.5 nm at number, volume and intensity based distribution, respectively. Table 7.2 also summarise the mean particle size distribution in other sols prepared at different compositions.

Table 7.2. Mean sol particle size distribution.

	Hydrodynamic Diameter (nm)	Intensity Distribution Peak Means (nm)	Volume Distribution Peak Means (nm)	Number Distribution Peak Means (nm)
A00	61.3	97.1	19.5	12.8
A01		48.4 216.9	20.4	14.8
A02		160.8	29.8 589.3	20.4
A03	43.1	31.8 104.1	31.5 102.9	30.8
A04	65	55.4 365.6	19.7 473.7	13.8
A05	44.9	34.6 259.8	17.2 383.2	12.4
A06	40.5	52	25.8	19.5
A07	49.7	66.8	30.4	21.5
A08	30.2	35.5	18.5	13.1
A09	36.1	46.3	19.2	12.8
A10	53.2	36.8 199.6	24	18.1
A11	50.2	40.9 188.6	17.5	12.1
A12	62	20.5 81.8 406.4	16.4	12.9

7.1.2. XRD Characterization of Boehmite Films

The XRD pattern of 200 ^{o}C dried gel revealed the presence of boehmite as shown in Figure 7.6. The diffraction peaks of the sample is very broad. Because of these broad reflections only the (020), (120) and (031) reflections of boehmite can be used for the determination of the crystallite size by using Scherrer's equation and are tabulated in Table 7.3.
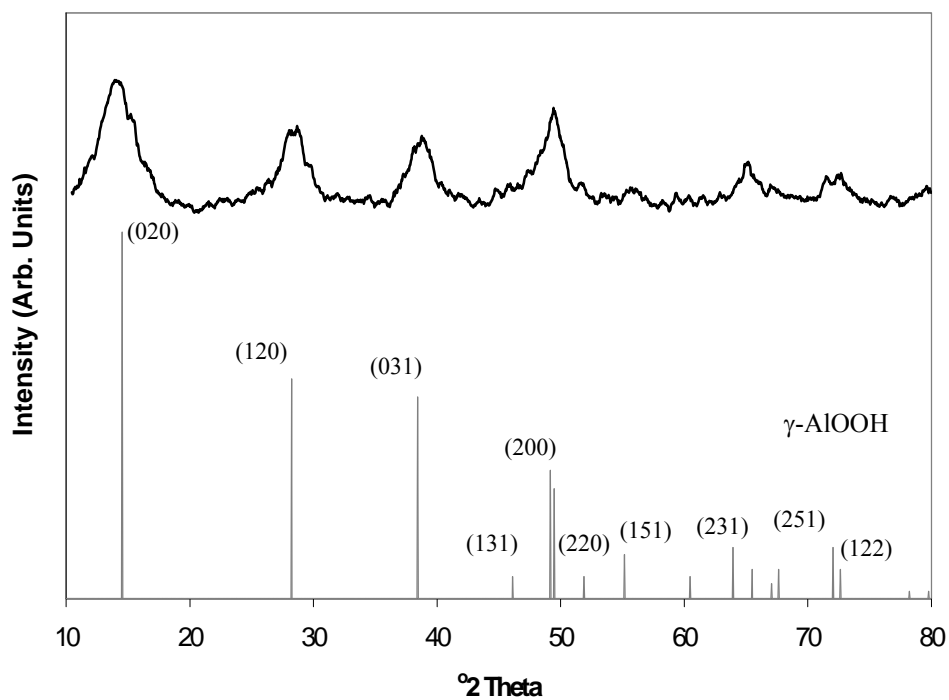
Figure 7.6. XRD Patterns of boehmite films dried at 200 ^{o}C

Table 7.3. Crystal size of boehmite film.

Temperature (^{o}C)	Phase	D^{*}_{hkl} (nm)
200	γ-AlOOH	D_{020} = 2.9
		D_{120} = 4.0
		D_{031} = 5.8

7.2. Unsupported Membrane Characterization

7.2.1. TGA Characterization

The results of the thermal analysis of some of the unsupported alumina membranes are give in Figures 7.7 to 7.16. Heating causes dehydration and rearrangement leading to a series of transitional aluminas and finally α-Al_2O_3. Almost all the weight loss occurred at temperatures lower than 500 ^{o}C and the weight stabilised to a constant value up to 1000 ^{o}C.
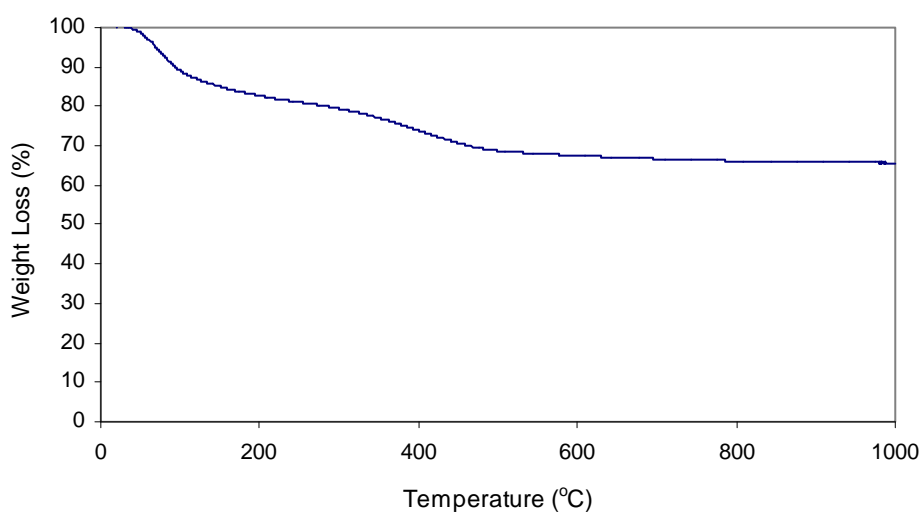
Figure 7.7. TGA curve of A01.
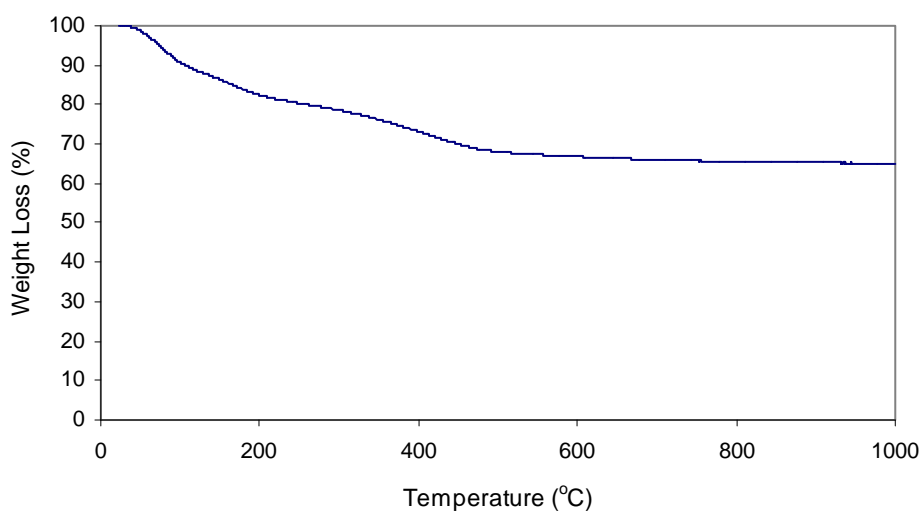
Figure 7.8. TGA curve of A02.
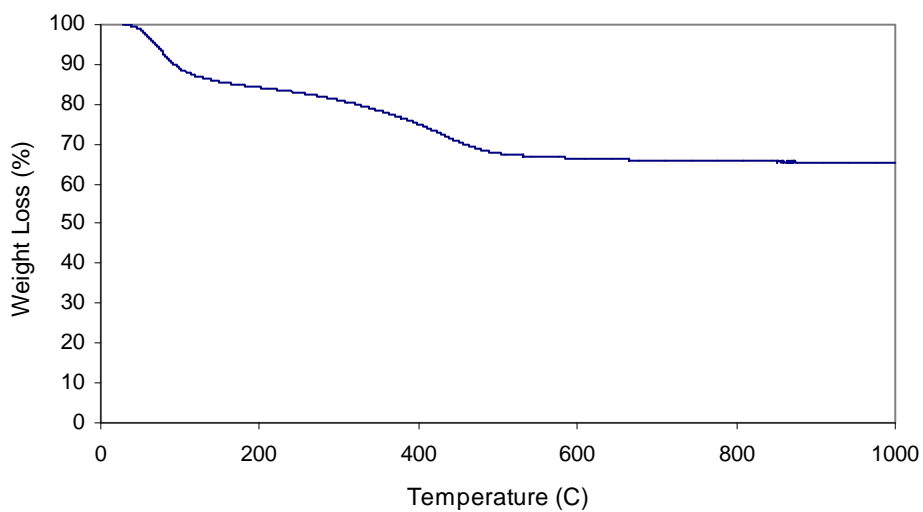
Figure 7.9. TGA curve of A04.
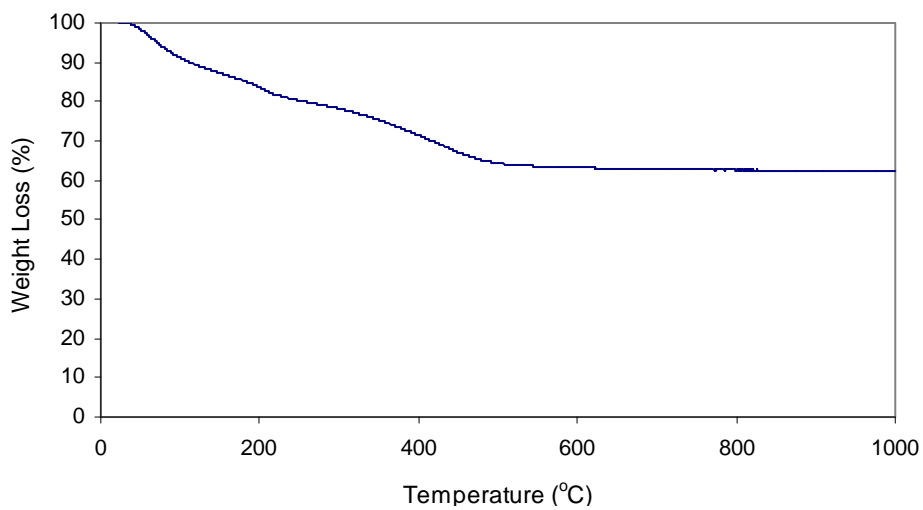
Figure 7.10. TGA curve of A05.
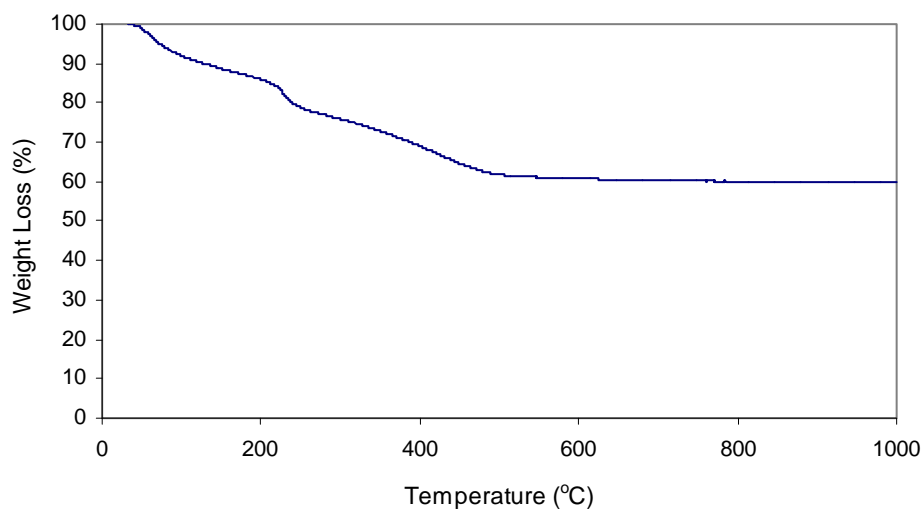
Figure 7.11. TGA curve of A06.
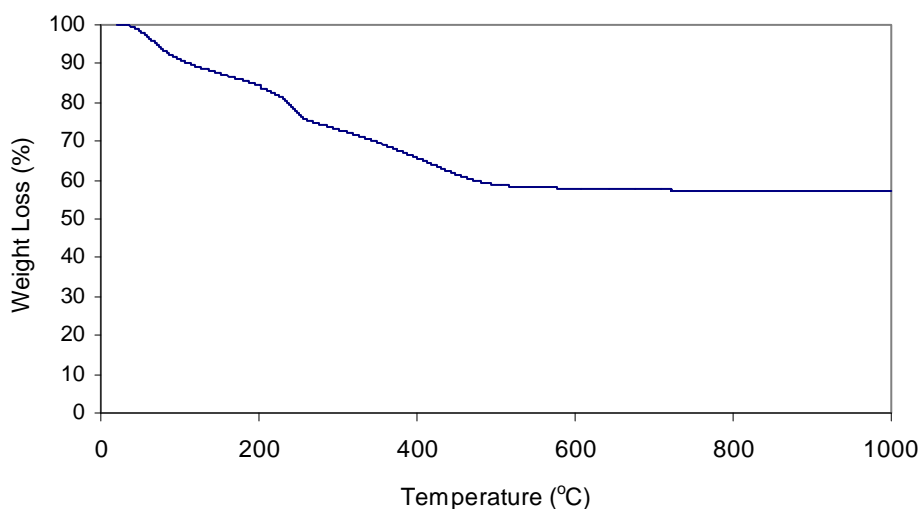
Figure 7.12. TGA curve of A07.

The initial loss of physically bound water occurred at about 80 $^\circ$ C. The weight loss from 80 to 270 $^\circ$ C may be due to the removal of chemically bond water and in the range of 340-380 $^\circ$ C present NO_3^- groups was removed from the membrane. The final weight loss at about 380 to 500 $^\circ$ C was due to the boehmite transformation to γ- Al_2O_3 with additional loss of water as a result of following reaction;

$$2AlOOH \rightarrow \gamma\text{- } Al_2O_3 + H_2O$$
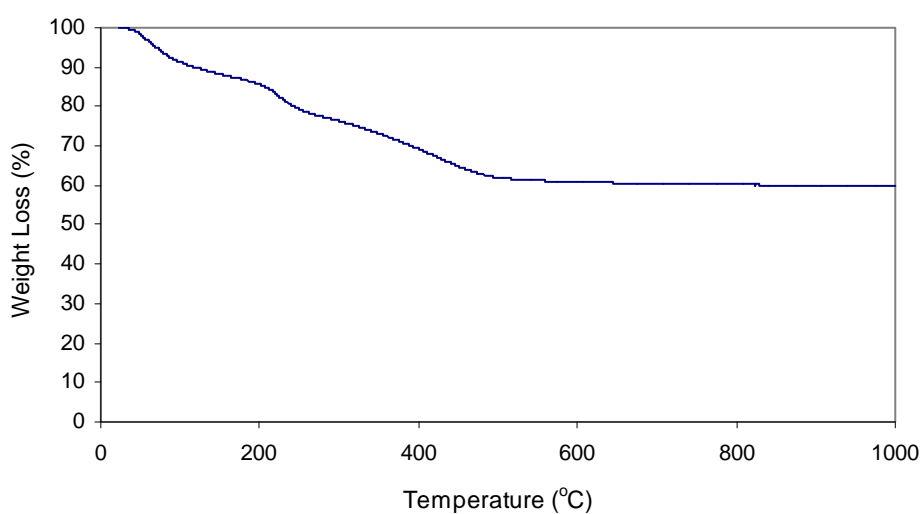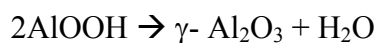
Figure 7.13 TGA curve of A08.
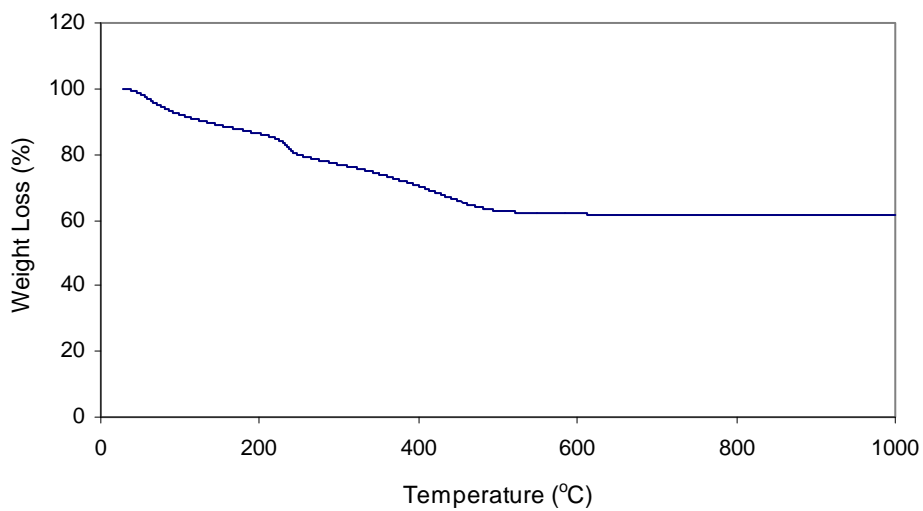
Figure 7.15. TGA curve of A09.
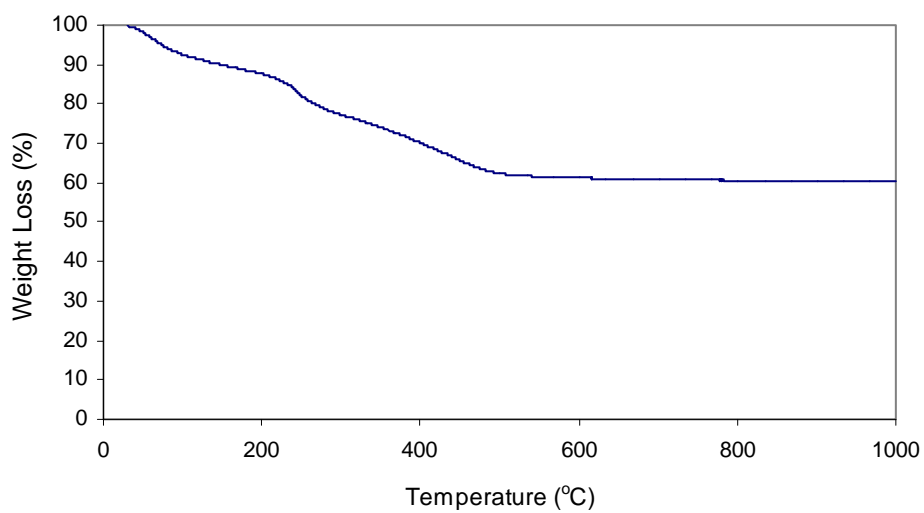
Figure 7.16. TGA curve of A11.

Figures 7.17 to 7.19 show the percent weight losses of uncalcined silica unsupported membrane with increase in temperature. The total weight loss of SiB is 15.15 % and SiC is 18.85 %. From room temperature to 120 ^{o}C the most of the weight losses were observed for all samples due to physical water removal. The weight loss which occurs betwen 100 to 400 ^{o}C is was at a lower level because at 100 ^{o}C most of the water has been expelled from the membrane pores and evaporated. In the final stage of weight loss a gradual weight loss was observed up to about 1000 ^{o}C and it was attributted to the removal of adsorbed chemically bound water.
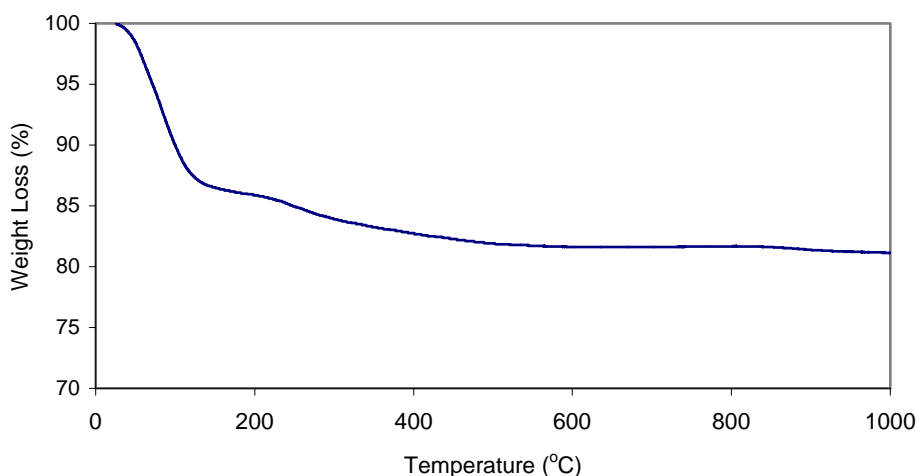
Figure 7.17. TGA curve of SiC.
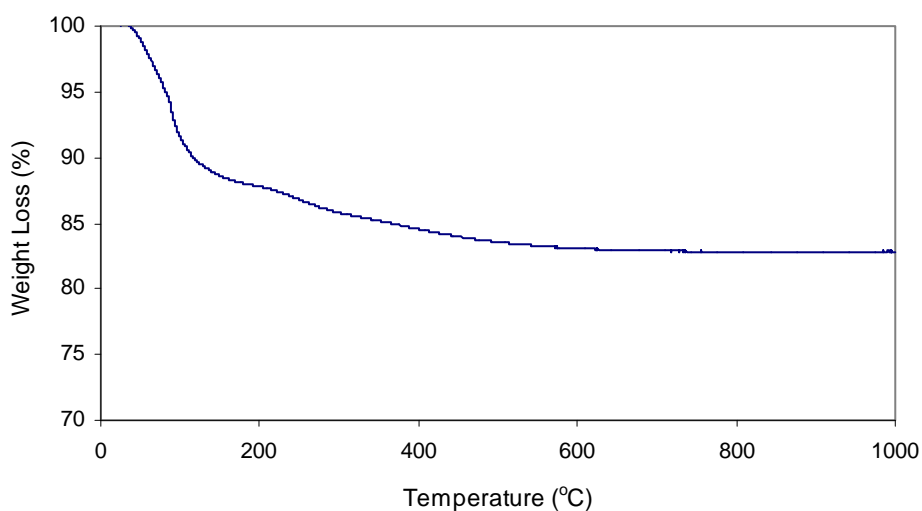
Figure 7.18. TGA curve of SiB.
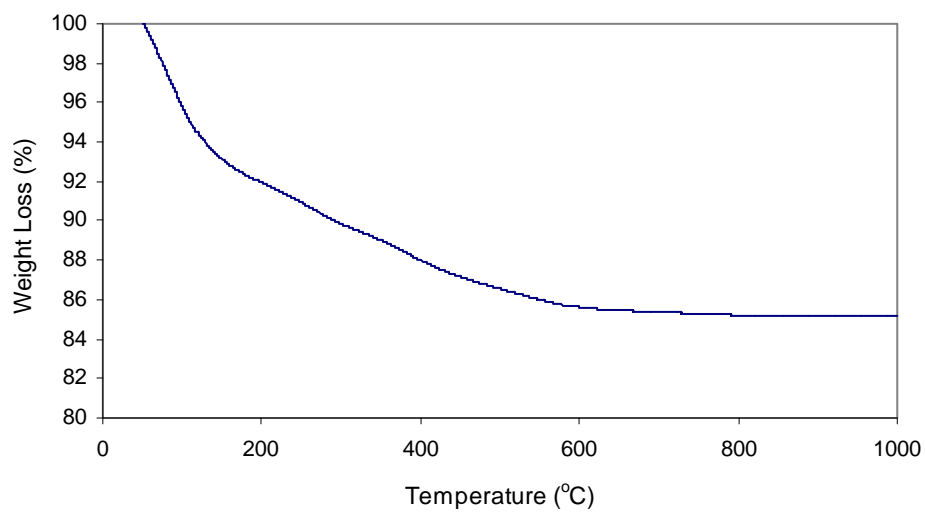
Figure 7.19. TGA curve of SiD.

7.2.2. FTIR Analysis

The FTIR spectra of uncalcined and calcined alumina unsupported membranes (A08) are given in Figure 7.20. Infrared absorption spectra for uncalcined alumina sample indicate NH^+ peak which is located at 1380 cm^{-1}. This peak disappeared in the calcined alumina sample. And also, all defined peak at 1070, 740, 470 cm^{-1} were found in spectra for uncalcined sample. This peaks were reported to be due to the Al-OH (boehmite) bending vibration (Chane-Ching and Klein, 1988). For calcined sample the region between 1000-400 cm^{-1} can be defined Al-O bending.

The spectra indicates the presence of water at 1650 cm^{-1} peak and broad peak at 3500 cm^{-1} for both calcined and uncalcined samples. Samples were not kept in a desiccator to prevent moisture adsorption therefore this is the result of water peaks at FTIR spectra (Chane-Ching and Klein, 1988). The peaks at 2325 cm^{-1} were reported as CO_2 peaks.
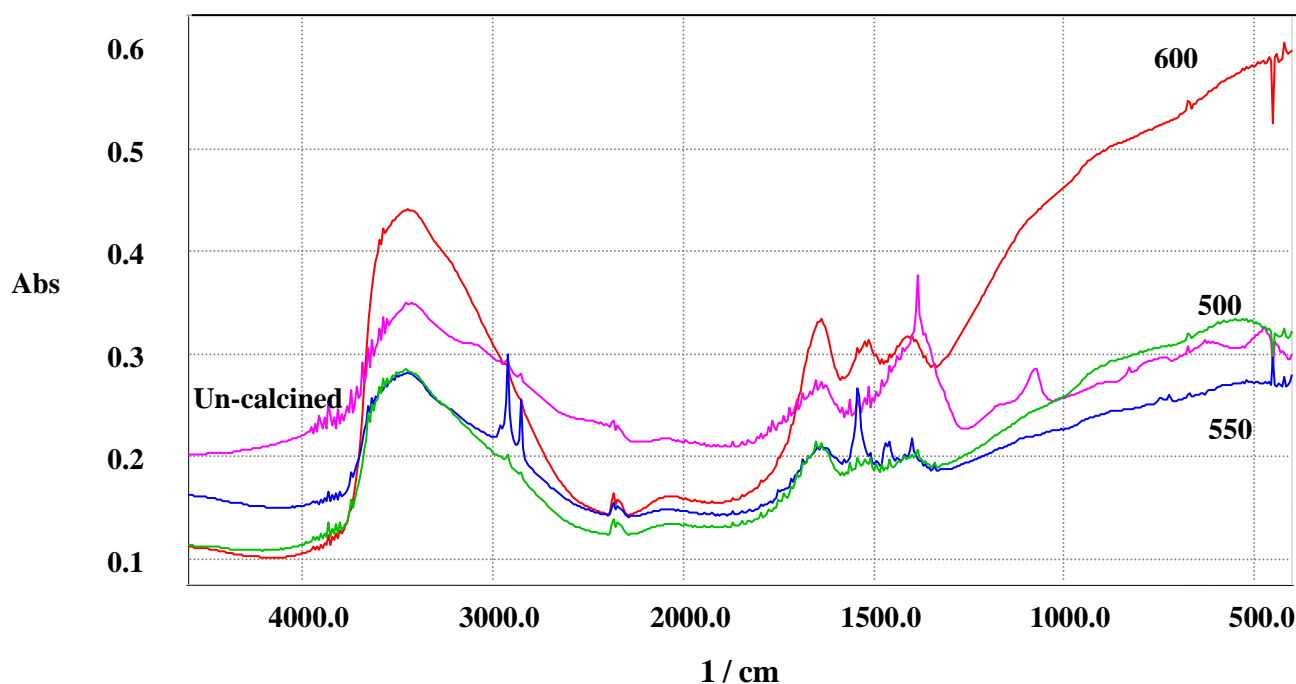
Figure 7.20. FTIR spectrum for uncalcined and calcined unsupported alumina membrane.

FTIR analysis was performed to provide structural information on the silica gelation process as well as information about structural changes of the uncalcined sample is given in Figure 7.21. Silanol and silicon alkoxide groups appear in the range from 1400 to 400 cm^{-1}. The band at 940 is attributed to the stretching modes of –Si-OH and Si-O. The peak observed at 1050 cm^{-1} that transverse Si-O-Si asymmetric stretching modes. The band at 3450 cm^{-1} is attributed to the stretching and deformation modes of hydroxyl groups and molecular water and also there is another water peak at 1650 cm^{-1}. The band at 800 is attributed to silicon oxides (Si-O-Si stretching). Another well known peak for silica samples at 460 cm^{-1} is attributed to vibrational modes of tetrahedral SiO_4. Silica unsupported membrane show a bond at 1380 cm^{-1} associated with the NH_3 and alcohol (da Costa et al.,2002).
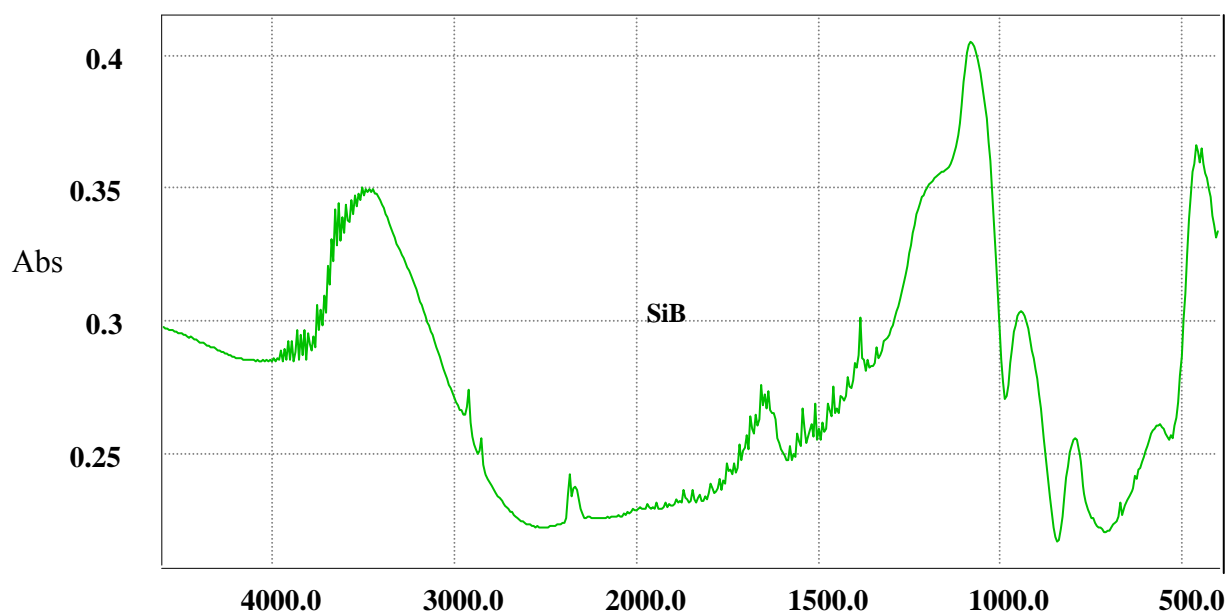
Figure 7.21. FTIR Spectrum of uncalcined silica (SiB) unsupported film.

7.2.3. N₂ Adsorption Analysis of Alumina Membranes

Adsorption-desorption isotherms for unsupported membranes which were heat treated at various temperatures are given in Figures 7.22 to 7.29. These isotherms are of Type IV typical of mesoporous and macroporous materials with H2 type hysterisis loops commonly observed for materials with interconnected pore networks with different size and shape (Webb and Orr, 1997).

These isotherms were used for the determination of cumulative pore volume and pore size distribution versus pore diameter plots by using BJH desorption data and these are shown in Figures 7.30 to 7.37.
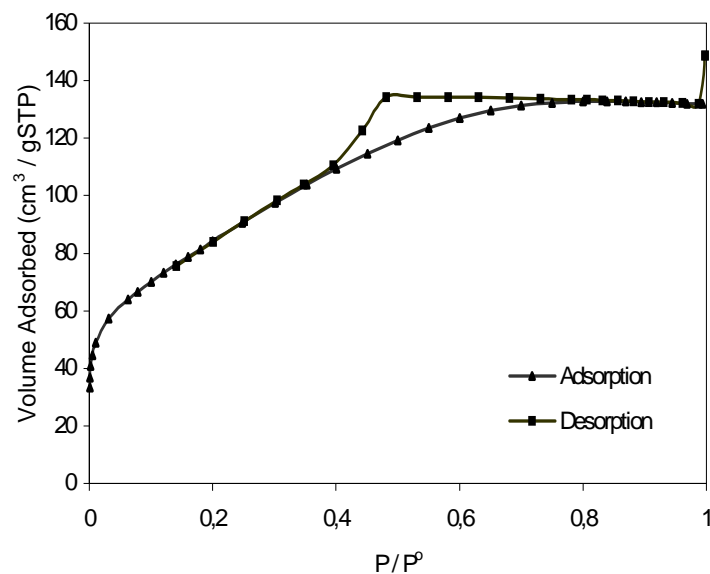
Figure 7.22. Nitrogen adsorption-desorption isotherms for A08 calcined at 500 °C.
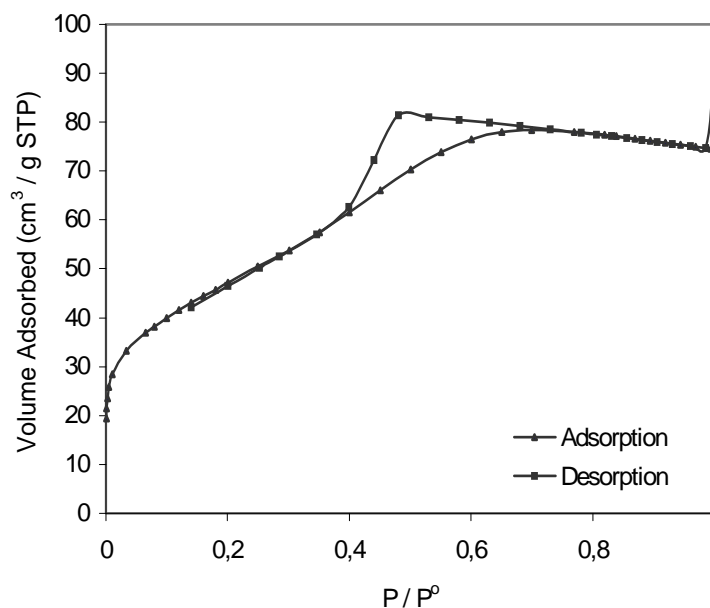
Figure 7.23. Nitrogen adsorption-desorption isotherms for A08 calcined at 550 °C.
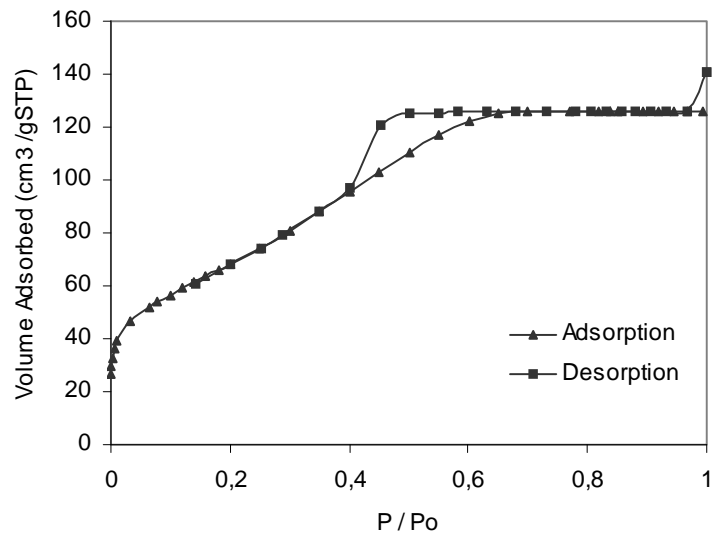
Figure 7.24. Nitrogen adsorption-desorption isotherms for A08 calcined at 600 ^{o}C.
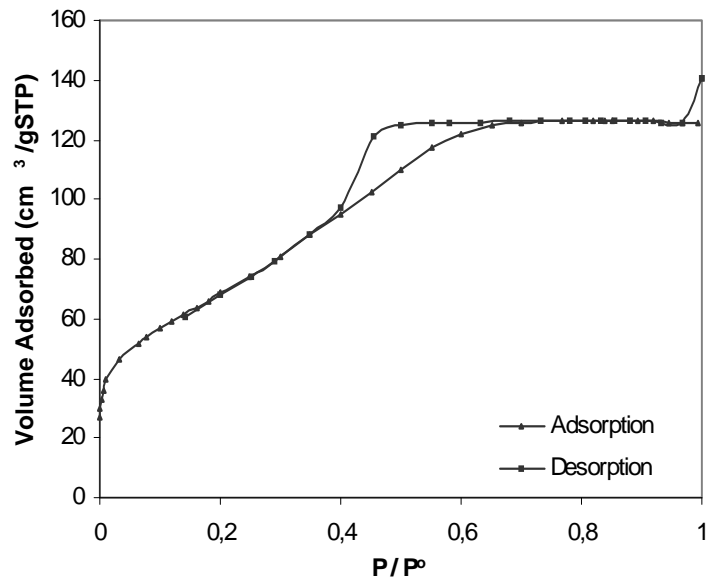
Figure 7.25. Nitrogen adsorption-desorption isotherms for A12 calcined at 550 ^{o}C.
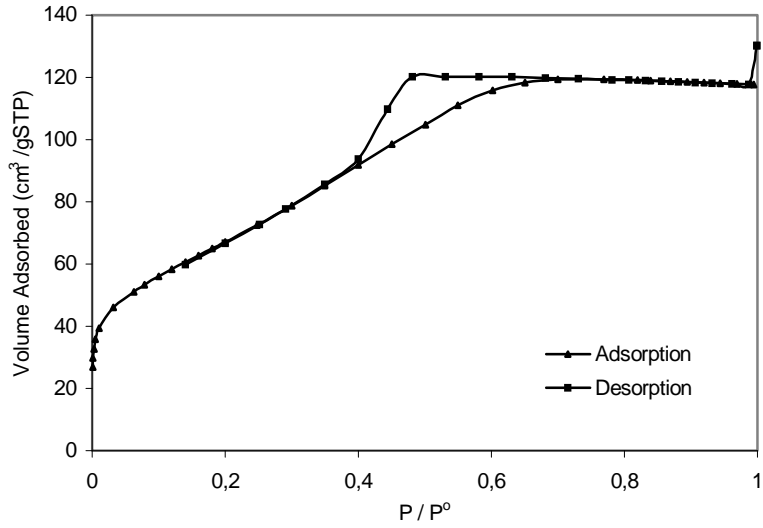
Figure 7.26. Nitrogen adsorption-desorption isotherms for A12 calcined at 600°C.
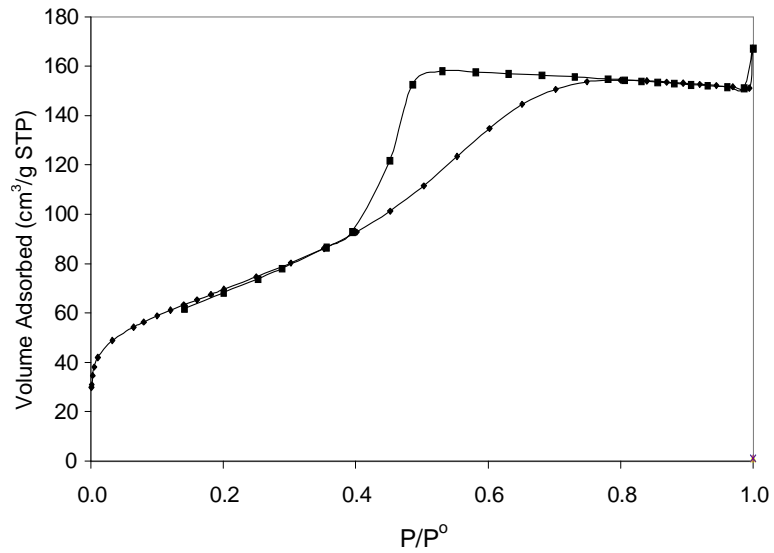
Figure 7.27. Nitrogen adsorption-desorption isotherms for A00 calcined at 600 ^{o}c.
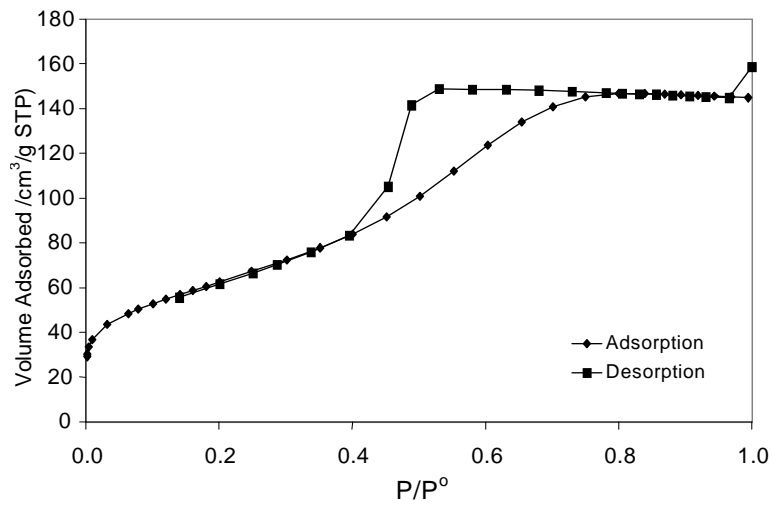
Figure 7.28. Nitrogen adsorption-desorption isotherms for A04 calcined at 600 ^{o}C.
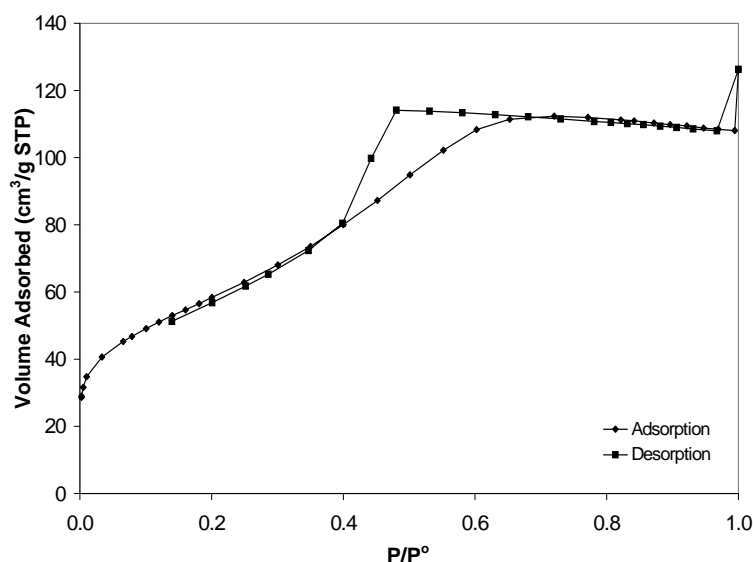
Figure 7.29. Nitrogen adsorption-desorption isotherms for A05 calcined at 600 ^{o}C.

Table 7.4. Surface areas and pore diameters of alumina unsupported membranes.

	Single Point Surface Area at p/p^{o}(m^{2}/g)	BET Surface Area (m^{2}/g)	Langmiur Surface Area (m^{2}/g)	Pore Diameter by BJH Adsorption (A^{o})	Pore Diameter by BJH Desorption (A^{o})
A08 (500)	297	305	434	26.95	28.15
A08 (550)	164	168	226	28.16	28.72
A08 (600)	246	254	357	29.02	29.90
A12 (550)	196	200	267	28.44	31.03
A12 (600)	240	245	345	28.32	30.19
A00 (600)	228	233	331	40.20	35.29
A04 (600)	220	225	319	36.32	32.64
A05 (600)	207	212	300	30.40	30.55

The surface areas and the pore sizes of the unsupported alumina membranes are tabulated in Table 7.4. The desorption curves steeply go down at about P/P^{o} $\cong$ 0.5 and the adsorption–desorption curves coincide at P/P^{o} $\cong$ 0.4. BET surface area varies in the range of 168 to 305 m^{2}/g. One of the advantages of the sol-gel processing for preparing

membranes is the increase in the pore size with heat treatment temperature allowing the choice of the calcination temperature for desired applications. A08 sample that has the smallest sol particle size (about 30 nm), leads to the largest BET surface area and the smallest pore size (2.8 nm) when calcined at 500 ^{o} C. The pore size was increased from 2.8 nm to 3 nm upon increasing the calcination temperature from 500 to 600 ^{o}C. As a result, surface area decreases and pore size increases with increasing temperature but the porosity remains nearly constant.

Besides the effect of calcination temperature on pore size, the boehmite concentration was also an important parameter. At the same calcination temperature, as the concentration is reduced (A08 to A12), pore size increased from 29.9 A^o to 30.2 A^o and the surface area decreases from 246 to 240 m^2/g. This differences may be due to the particle size of the A12 sols which had higher particle sizes than A08 sols.
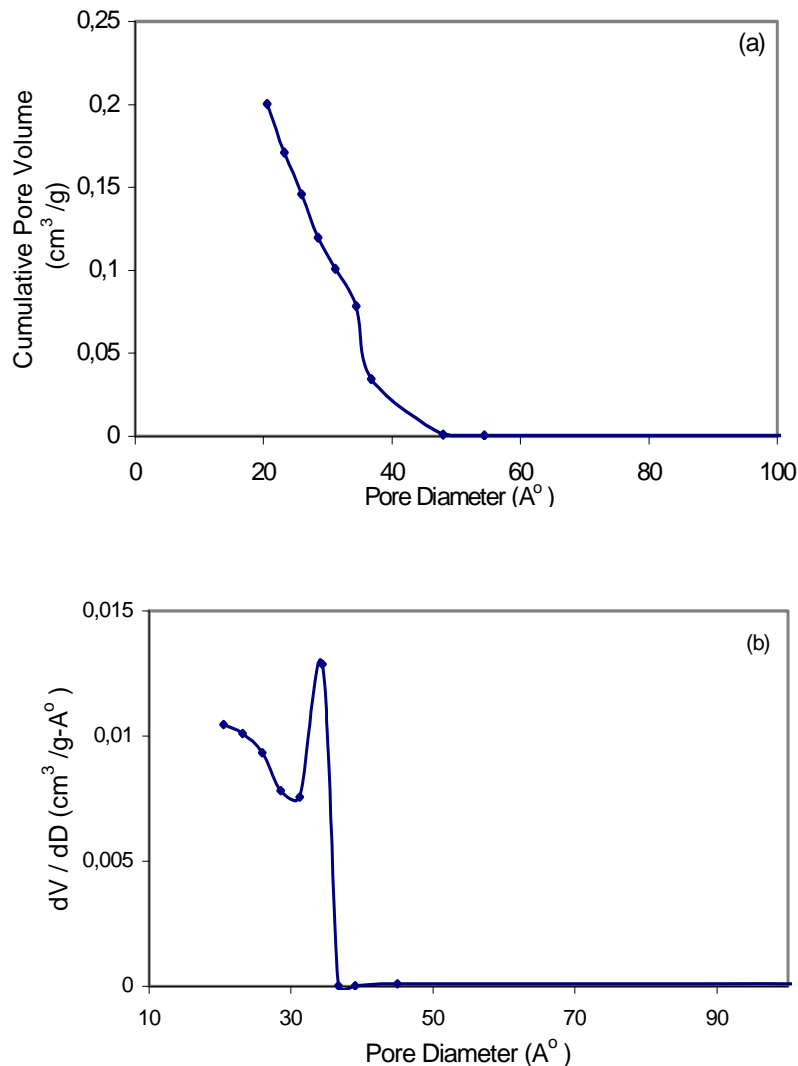

Figure 7.30. BJH cumulative pore volume (a) and pore size distribution (b) for A08 (500).
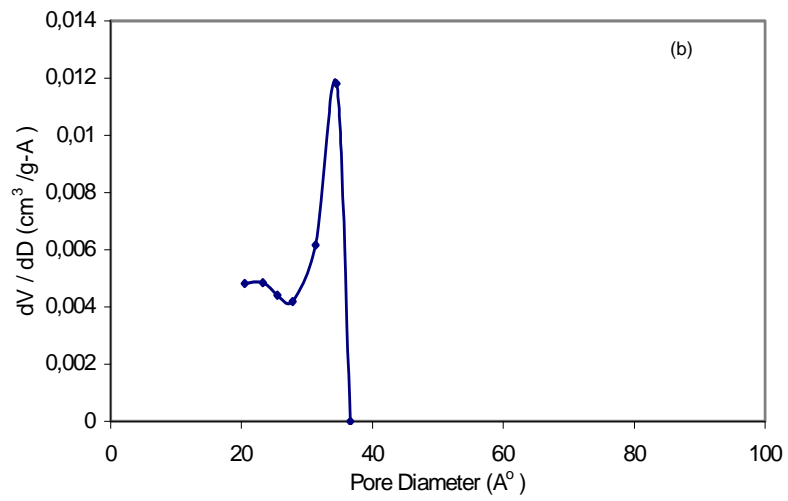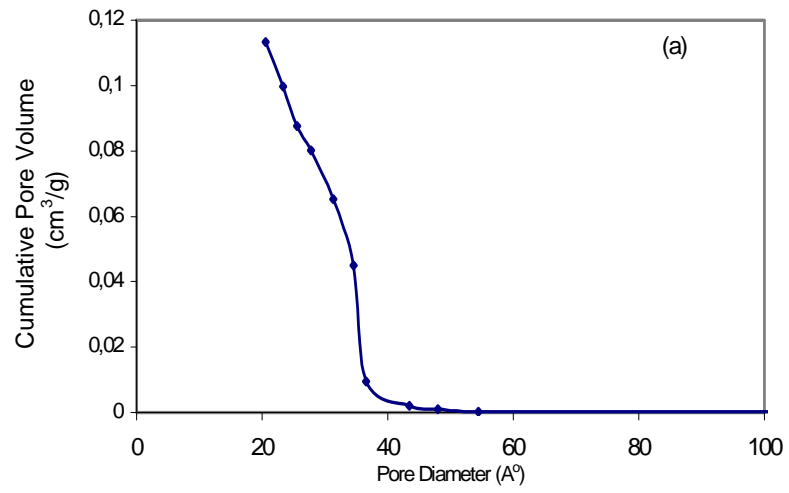
Figure 7.31. BJH cumulative pore volume (a) and pore size distribution (b) for A08 (550).
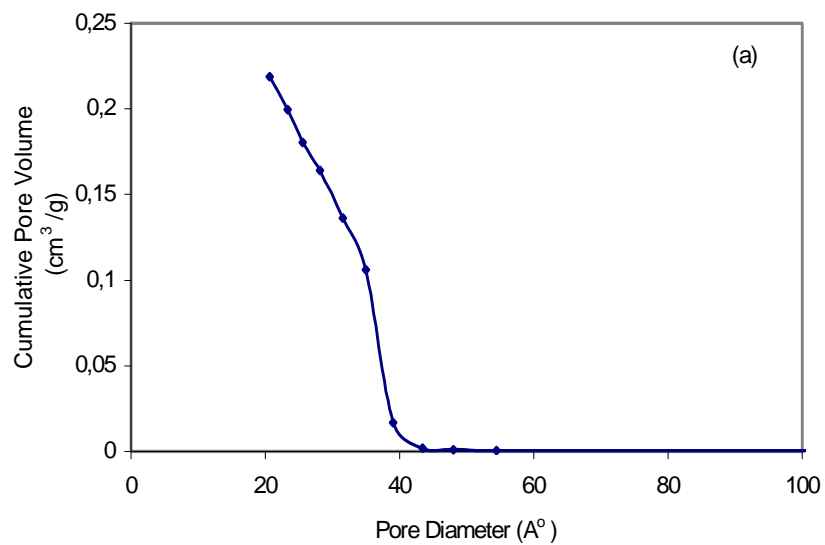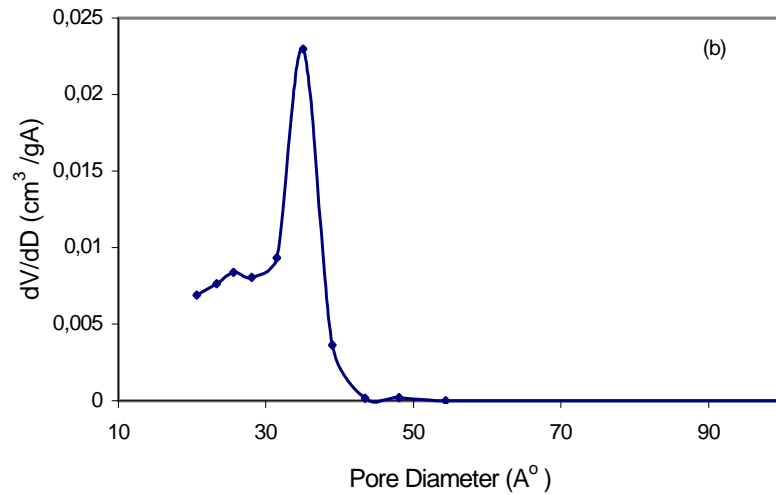
Figure 7.32. BJH cumulative pore volume (a) and pore size distribution (b) for A08(600).
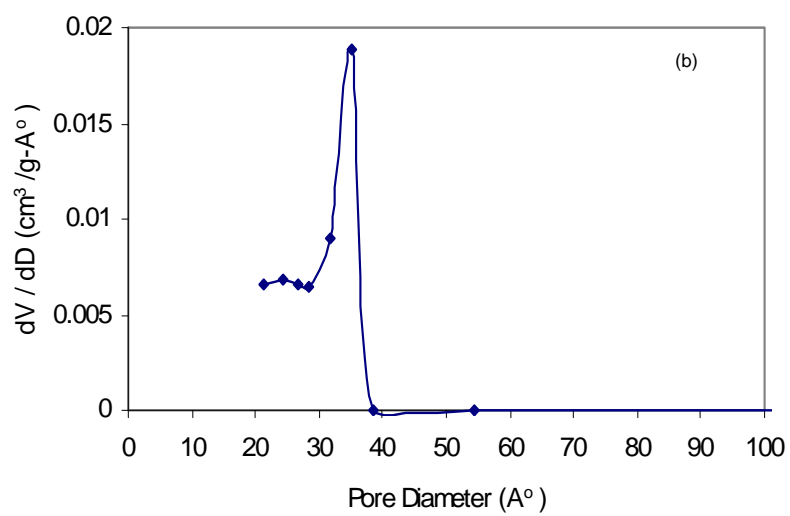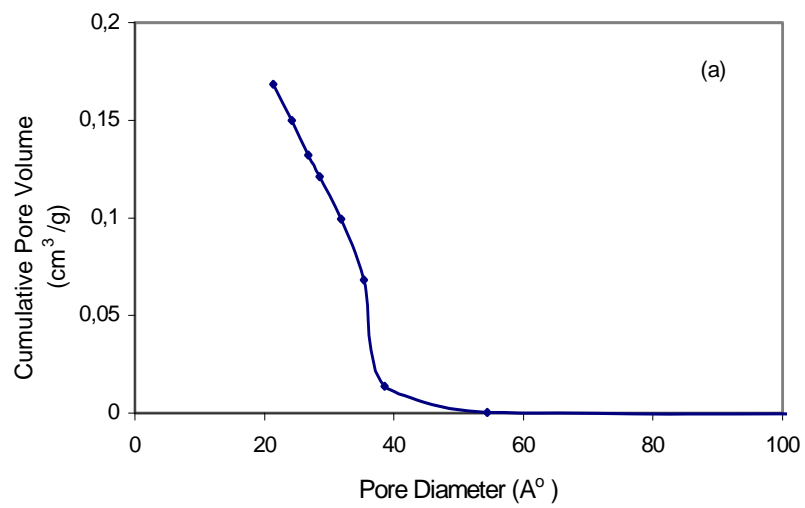
Figure 7.33.BJH cumulative pore volume (a) and pore size distribution (b) for A12(550).
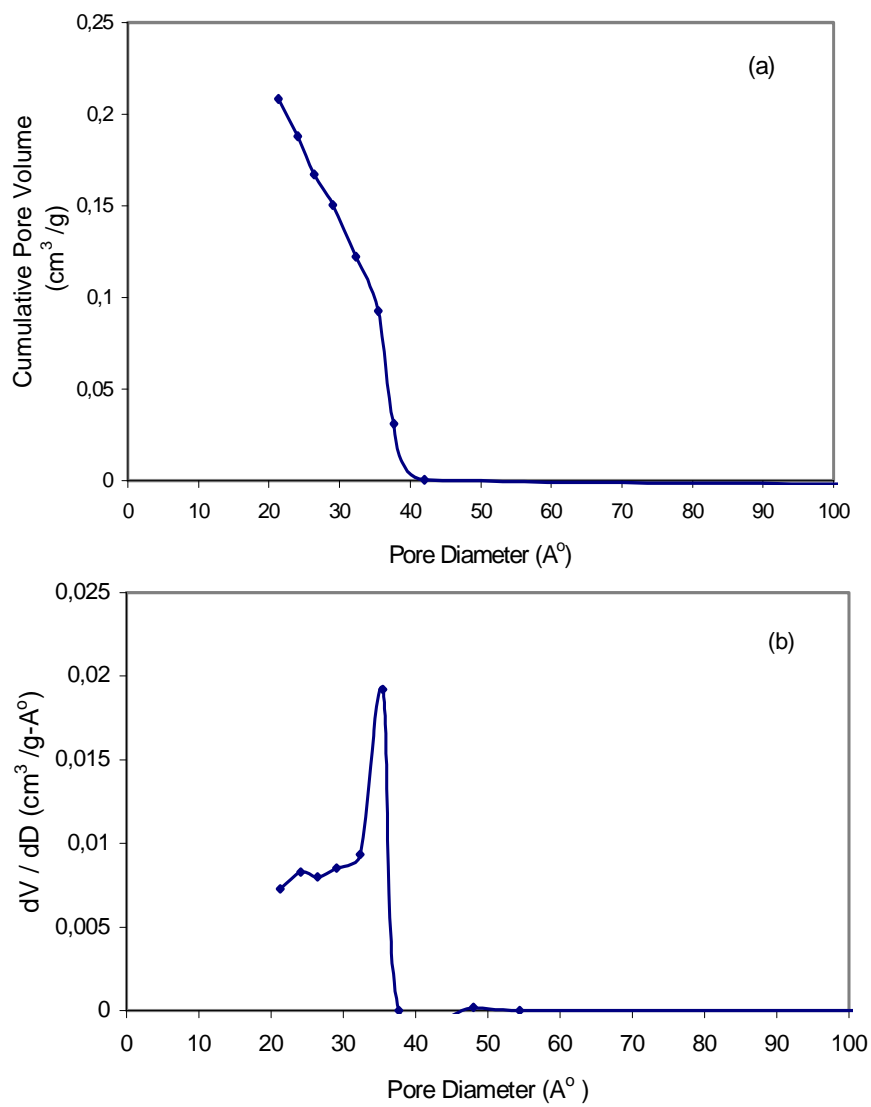
Figure 7.34. BJH cumulative pore volume (a) and pore size distribution (b) for A12(600).
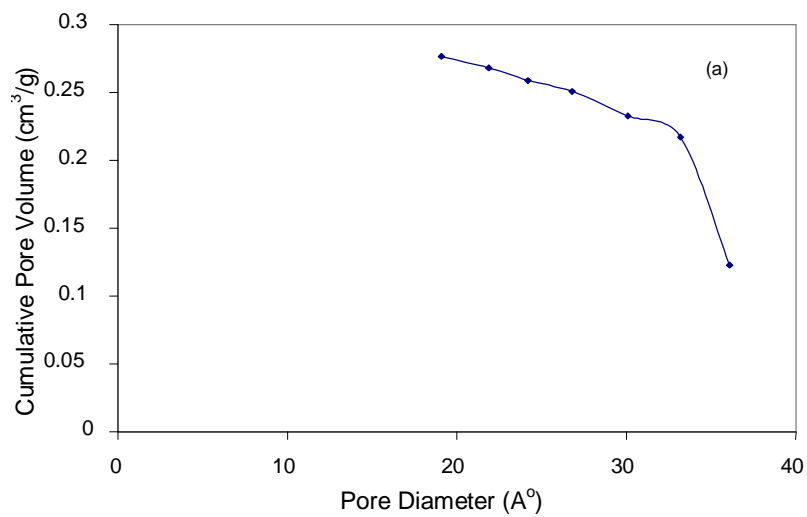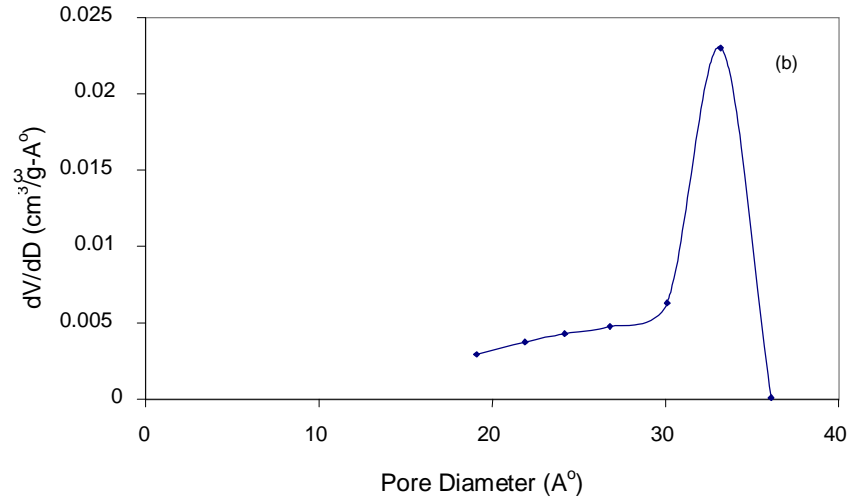
Figure 7.35. BJH cumulative pore volume (a) and pore size distribution (b) for A00 (600).
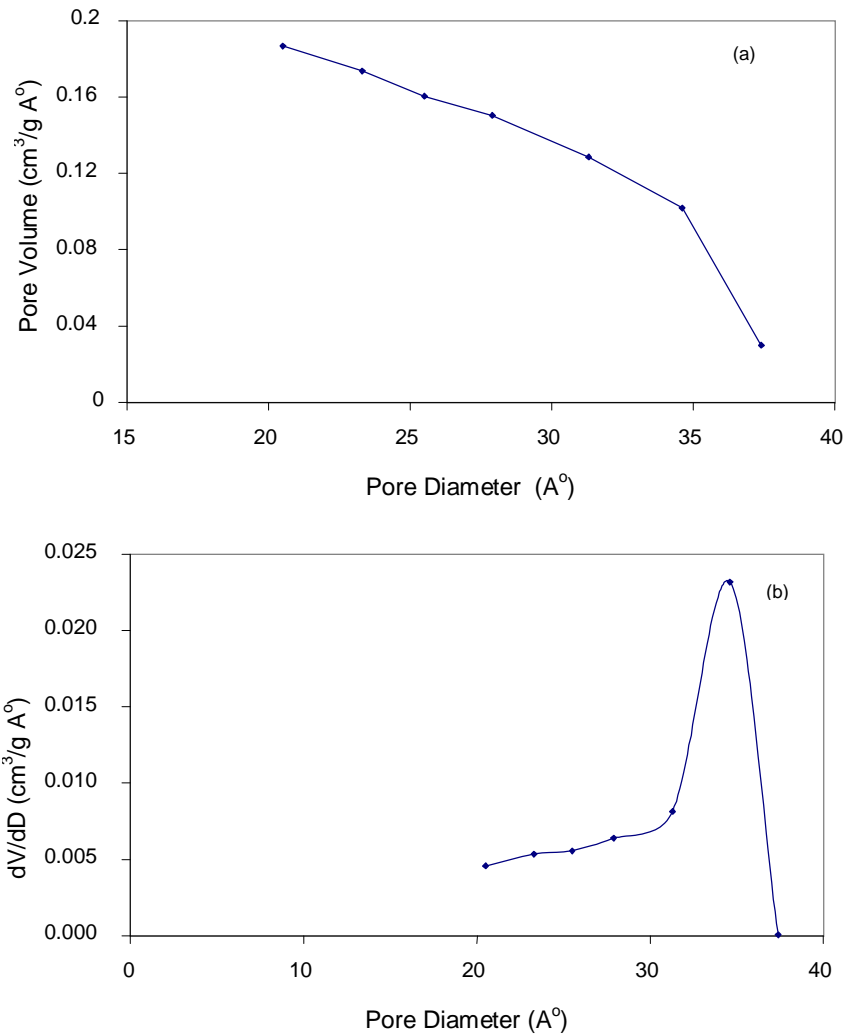
Figure 7.36. BJH cumulative pore volume (a) and pore size distribution (b) for A05 (600).
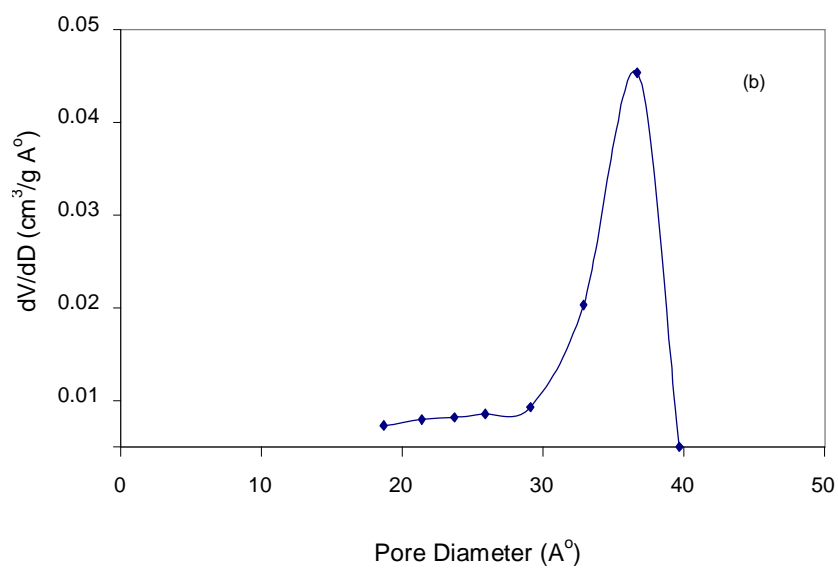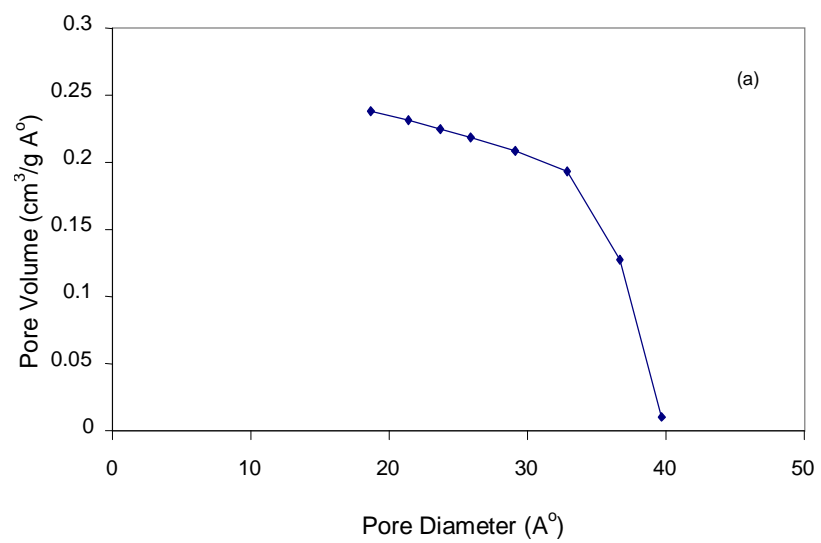
Figure 7.37. BJH cumulative pore volume (a) pore size distribution and (b) for A04 (600).

Table 7.5. Pore contents of alumina unsupported membranes.

	Single Point Cumulative Pore Volume (cm^3 / g)	BJH Adsorption Pore volume	BJH Desorption Pore Volume	Pore %
A08 (500)	0.204	0.139	0.200	0.395
A08 (550)	0.115	0.085	0.113	0.27
A08 (600)	0.194	0.151	0.219	0.384
A12 (550)	0.143	0.109	0.168	0.314
A12 (600)	0.182	0.142	0.208	0.368
A00 (600)	0.256	0.231	0.269	0.45
A04 (600)	0.223	0.200	0.238	0.417
A05 (600)	0.167	0.145	0.186	0.35

The total volume adsorbed and the monolayer volume vary in the range of 89 to 184 cm^3/g STP and 42 to 75 cm^3/g STP respectively for the alumina unsupported membrane and are tabulated in Table 7.4. The pore contents of alumina membranes varied in the 27-45 % of total volume, as calculated by using single point cumulative pore volumes is also given in Table 7.5. Calcined alumina membranes were about 55-65 % dense.
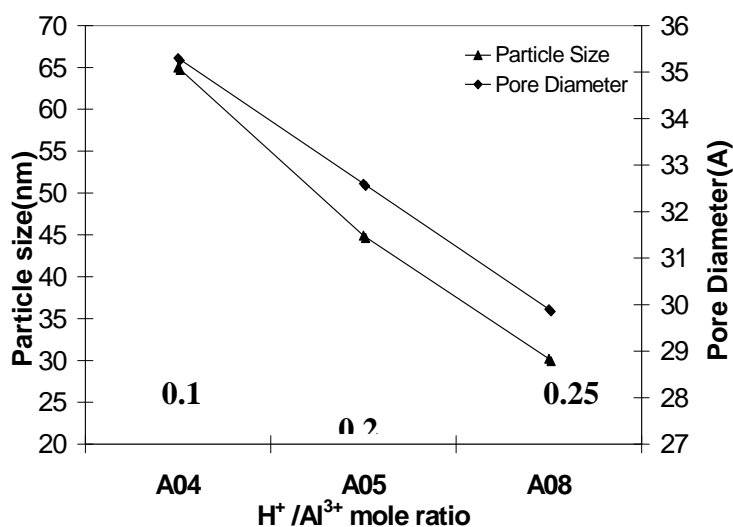
Figure 7.38. Effect of acid amount on the mean particle size of the alumina sols and the mean pore size of the alumina membrane.

The variation of the particle size of the alumina sols and the pore size of the alumina membranes that were calcined at 600 $^{\circ}$C with concentration of the inorganic acid is shown in Figure 7.38. The increase in the acid content of the sol caused almost proportional decreases in both sol particle size and the membrane pore diameter. This obviously indicates the fact that packing of smaller particles results in finer pore structures. The significant implication of this would be the ability of designing of the microstructure of the membrane.

7.2.4. XRD Analysis of Alumina Membranes

XRD patterns of the unsupported alumina membranes heated in the 200 to 1200 $^{\circ}$C range are shown in Figure 7.39 and Figure 7.40. The diffraction peaks of all samples other than the sample heated to 1200 $^{\circ}$C are very broad due to their low crystallinity. Slight difference was observed in the XRD patterns of the samples treated between 500 to 900 $^{\circ}$C. Because of that, no distinction was observed between poly-types (γ,δ,θ-Al_2O_3). Moreover, only the (400) and (440) reflections were used for the determination of the crystallite size by using Scherrer's Equation. As shown in Table 7.6, the crystallite size is nearly constant (5 nm) and exhibit no systematic change in the range of 500 to 900 $^{\circ}$C. These characterizations indicate that gamma phase is the dominant phase up to 900 $^{\circ}$C and pure α-Al_2O_3 phase was obtained upon heat treatment at 1200 $^{\circ}$C with a crystallite size of about 20nm.
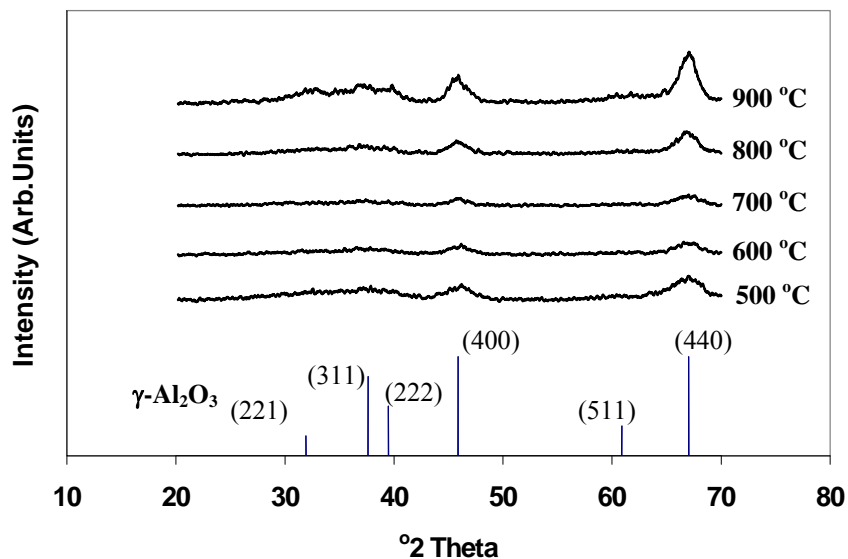

**Figure 7.39. XRD patterns of the membranes heat treated at various temperatures.**
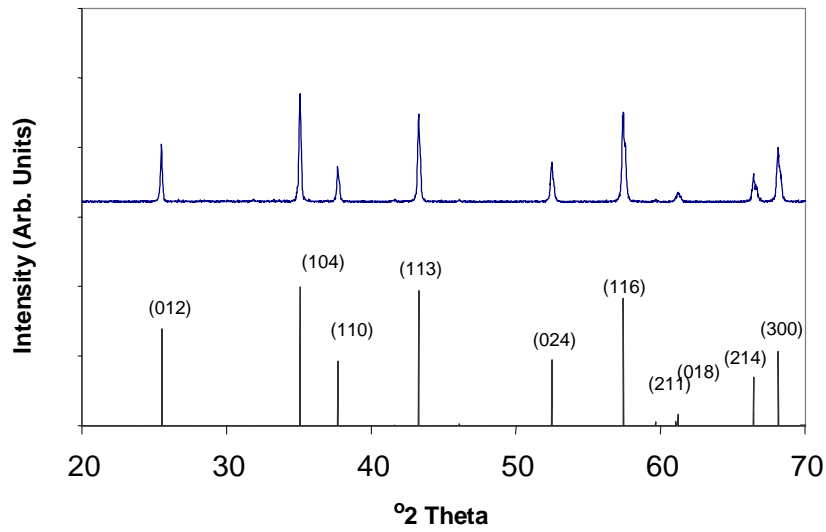
Figure 7.40. XRD patterns of the membranes heat treated at 1200°C.

Table 7.6. XRD crystallite sizes of the alumina membranes as a function of T.

Temperature (°C)	Phase	D^*_{hkl} (nm)
200	γ-AlOOH	$D_{020} = 2.9$ $D_{120} = 4$ $D_{031} = 5.8$
500	γ/δ-Al_2O_3	$D_{400} = 6$ $D_{440} = 4$
600	γ/δ-Al_2O_3	$D_{400} = 4.3$ $D_{440} = 4.1$
700	γ/δ-Al_2O_3	$D_{400} = 4.7$ $D_{440} = 3.2$
800	γ/δ-Al_2O_3	$D_{400} = 4.3$ $D_{440} = 4.8$
1200	α-Al_2O_3	$D_{012} = 22$ $D_{104} = 17.7$ $D_{110} = 22$ $D_{113} = 16.5$ $D_{024} = 18.7$ $D_{116} = 18.1$ $D_{122} = 23.6$ $D_{214} = 25.6$ $D_{300} = 21.7$

7.3. Support Characterization

7.3.1. Particle Size Distribution of Powders

Initial particle size of the powder and the size distribution have a strong influence on the pore size distribution of the fired support. Figure 7.41 and 7.42 show the graphical representation of the particle size distributions of alumina and ytria-stabilized zirconia powders used in support preparation. In these figures it may be noted that the zirconia powder contains a large percentage of fines (about 15 % below 0.1 μm) compared to the alumina powder (about 3.5 % below 0.1 μm) . Accordingly the D_{50} (median) particle sizes of zirconia and alumina were 0.262μm and 0.258μm, **respectively.**
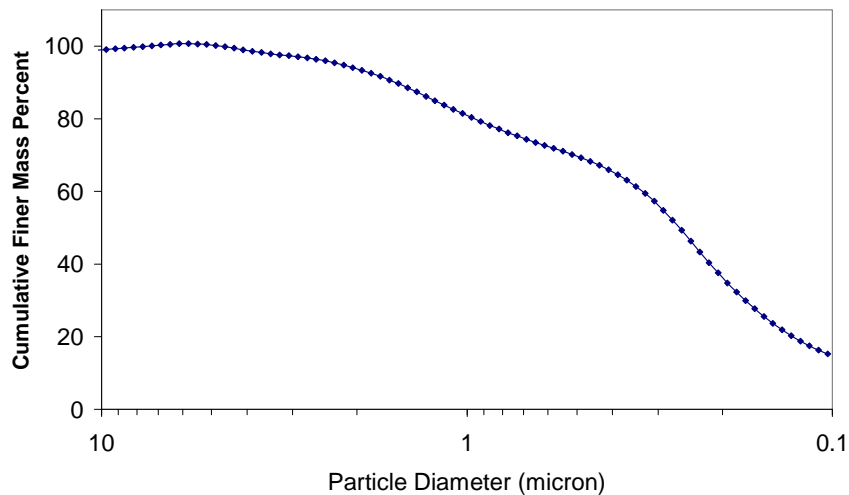
Figure 7.41. Particle size distribution of partially stabilized zirconia powder.
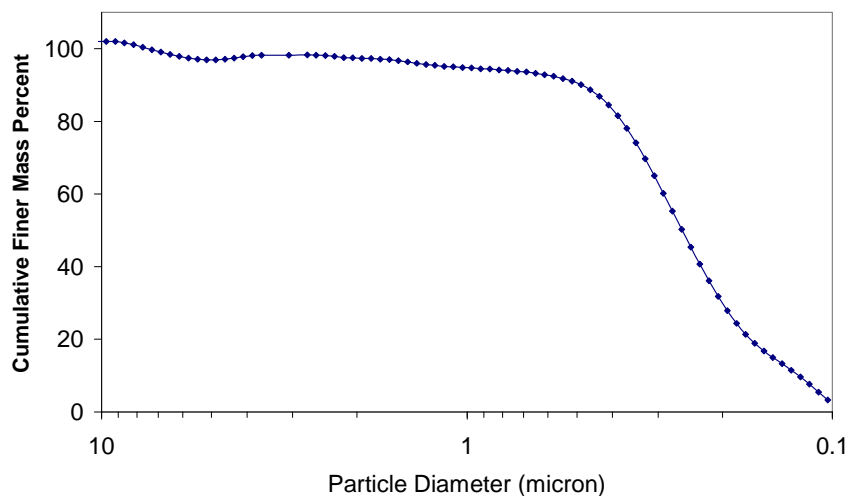
Figure 7.42. Particle size distribution of alumina (AKP-50) powder.

7.4. Microstructural Characterization of Alumina and Silica Membranes

SEM pictures of the top and the fracture surfaces of the 1150 $^{\circ}$C heat treated zirconia support are shown in Figure 7.43 and 7.44, respectively. The micrographs indicated the presence of 70-80 nm size particles in a uniform porous structure.
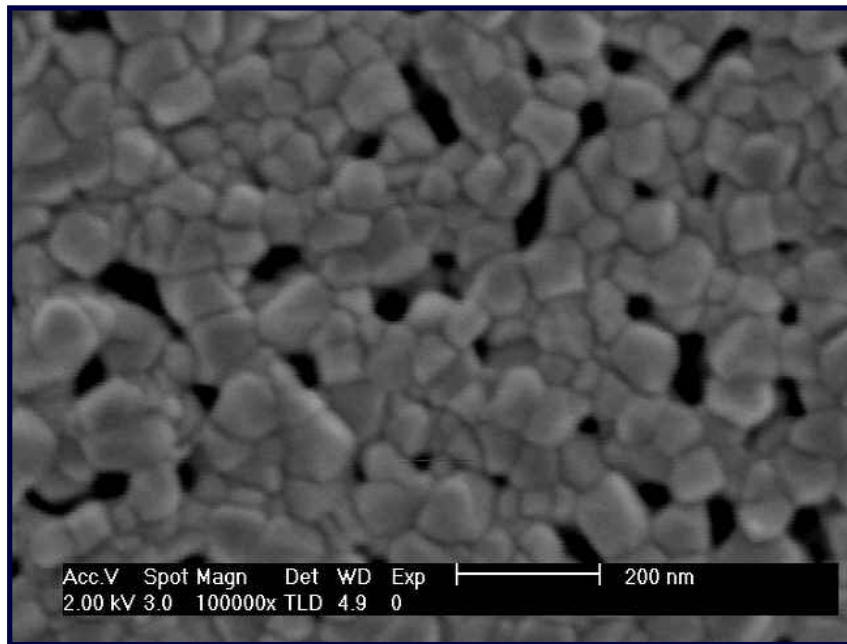

Figure 7.43. SEM micrograph of top surface of the1150 $^{\circ}$C heat treated Zirconia support.
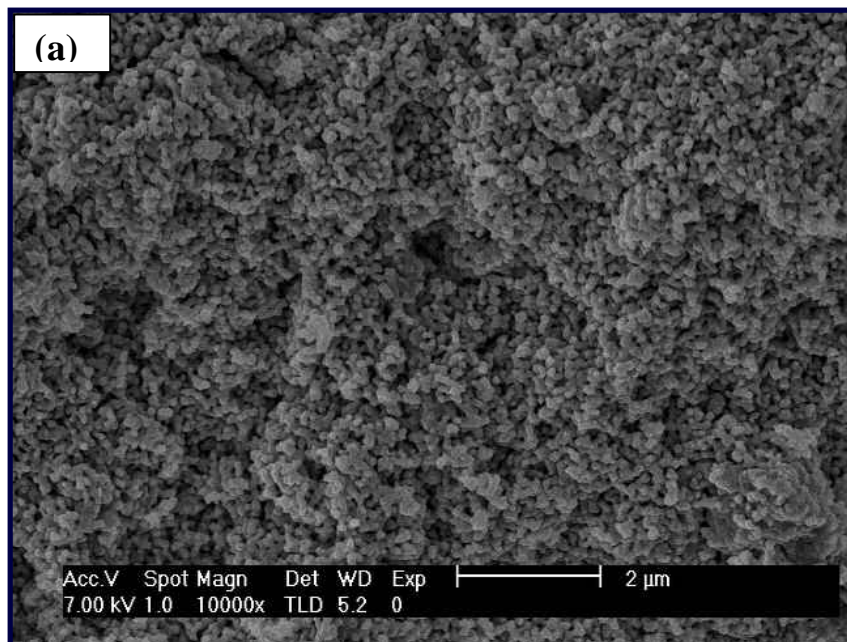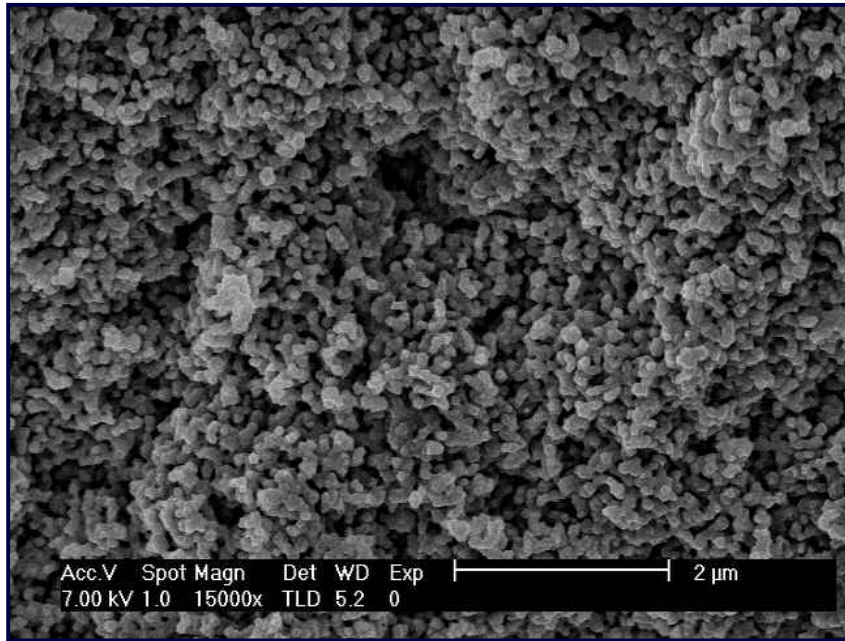
Figure 7.44. SEM micrographs of fracture surfaces of the 1150 ^{o}C heat treated Zirconia support : (a) ×10000 (b) ×15000.

Figure 7.45 shows the microstructure of the top surface of the two layer alumina membrane which was heat treated at 600 ^{o}C and 500 ^{o}C. The crack-free alumina membranes were obtained after two times dipping-drying-firing procedure when a dilute boehmite sol of 0.2 M was used.

(b)
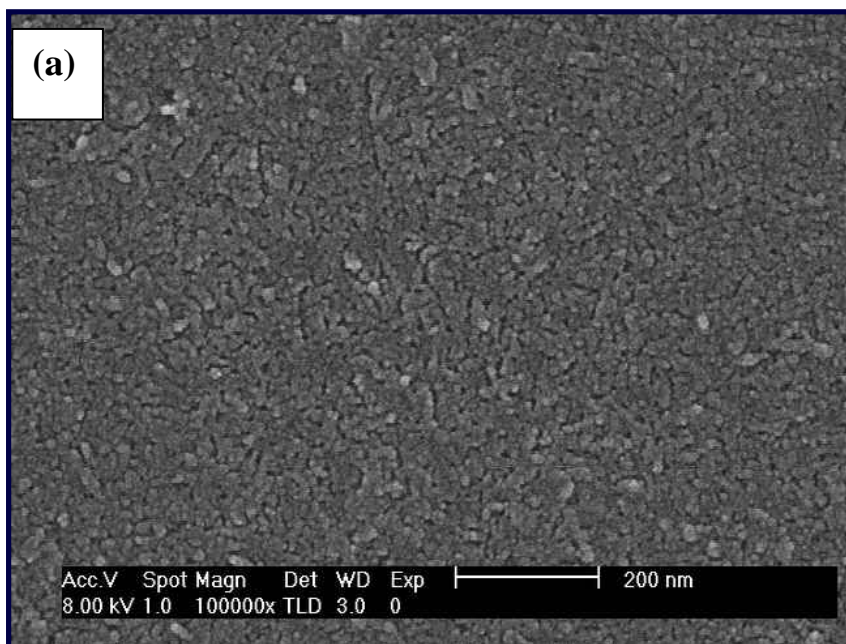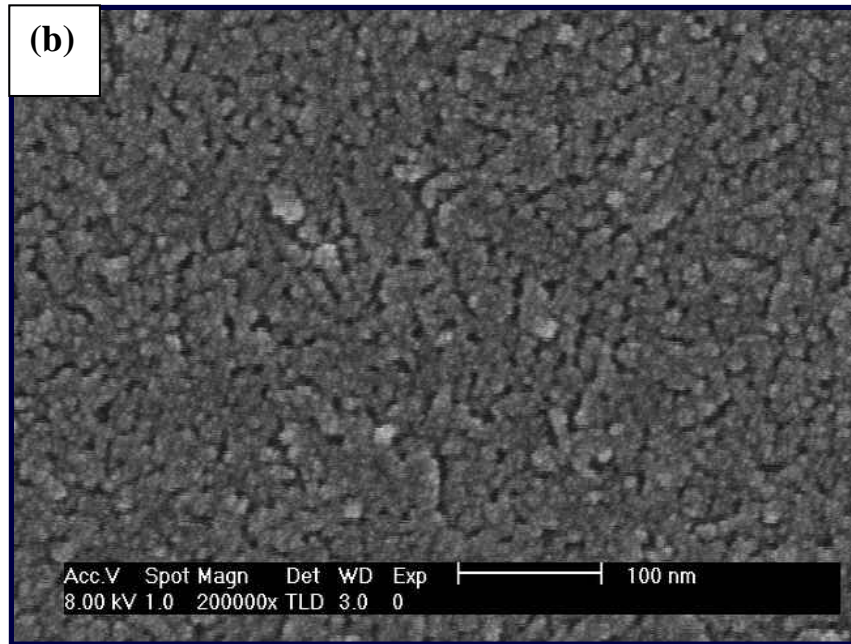
Figure 7.45. SEM micrographs of top surfaces of a two times dipped alumina membrane :
(a) ×100000 (b) ×200000.

The thickness of the membrane layer, its particle size and their change with calcination temperature are clarified at SEM micrograph of double layer alumina membrane fractured surface as shown in Figure 7.46. It was found that, γ-Al_2O_3 membrane thickness after 2 dipping procedure without significant penetration was about 3.2 μm. Heat treatment temperature reduction from 600 ^{o}C to 500 ^{o}C for the second layer causes a reduction in both particle size and pore size of the membranes.

(a)
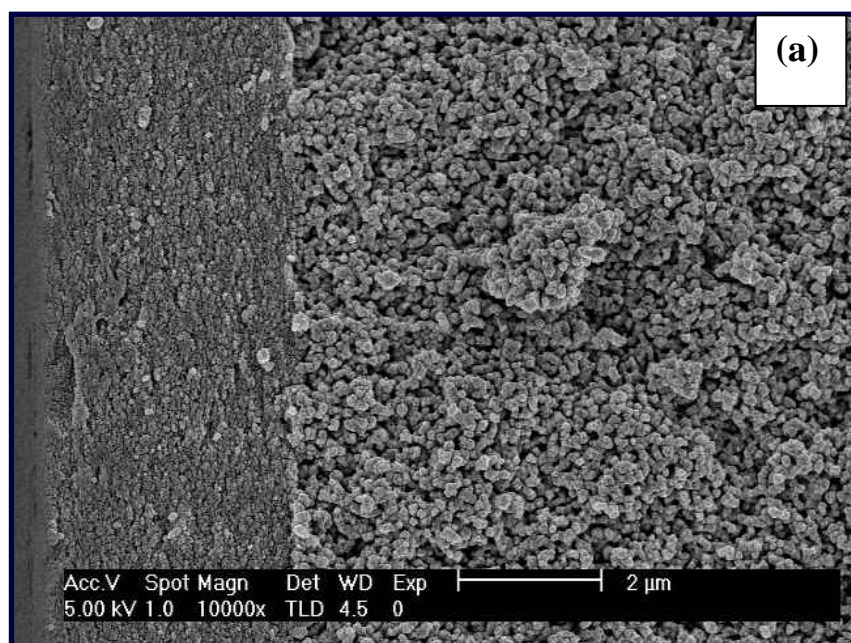
Also it can be seen from Figure 7.46 that no sol was penetrated into the support during dipping. This indicated that alumina layer was deposited on top of the support as a distinct separated layers.
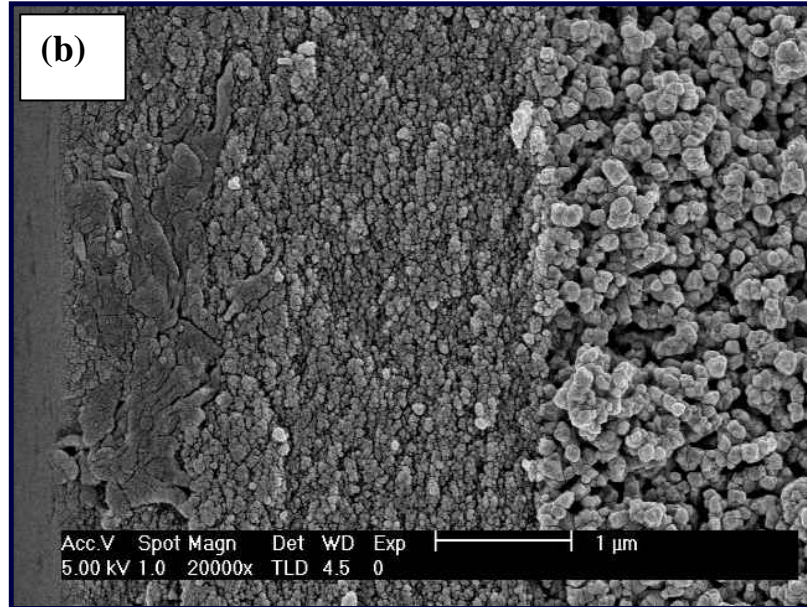

Figure 7.46. SEM micrographs of fracture surfaces of a 2 times dipped alumina membrane : (a) ×10000 (b) ×20000.

Figure 7.47 and 7.49 show the top surfaces of the 50 ^{o}C and 400 ^{o}C heat treated silica membranes. Support particles were coated with very fine particles.
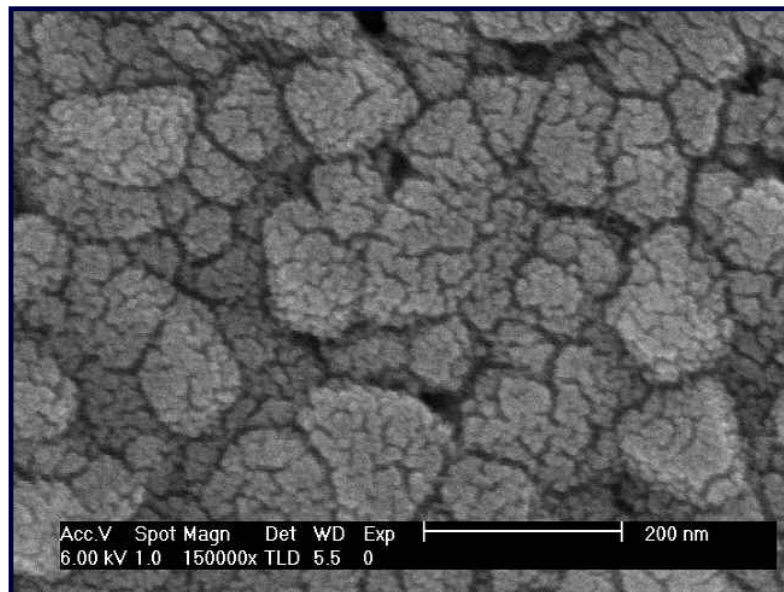

Figure 7.47. SEM micrograph of a top surface of the 1-layer 50 ^{o}C treated silica membrane.

SiO$_2$ membranes were elaborated to coat the ZrO$_2$ substrate with silica sols. However, the sol penetrated into the substrate and SEM examination of fractured cross-sections showed in Figure 7.48 and Figure 7.50 that discrete silica layers were not formed on the surface of the substrate. This penetration indicates that a good interaction (adherence) is present between the top layer and the support.

Also low permeability was exhibited by silica membranes without intermediate layers. This was attributed to the penetration of the sols into the substrate, which increased the effective thickness of the silica layers.
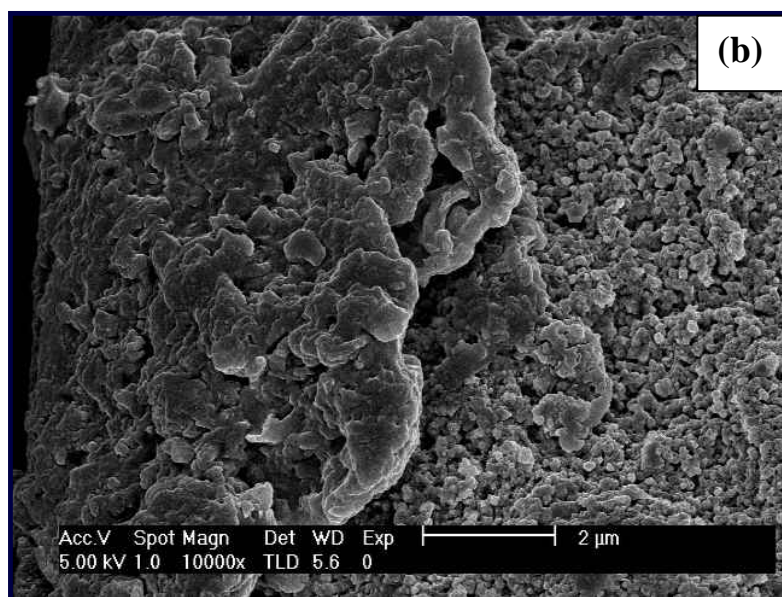

Figure 7.48. SEM micrograph of fracture surface of the 1-layer 50 °C treated silica membrane: (a) ×5000 (b) ×10000.
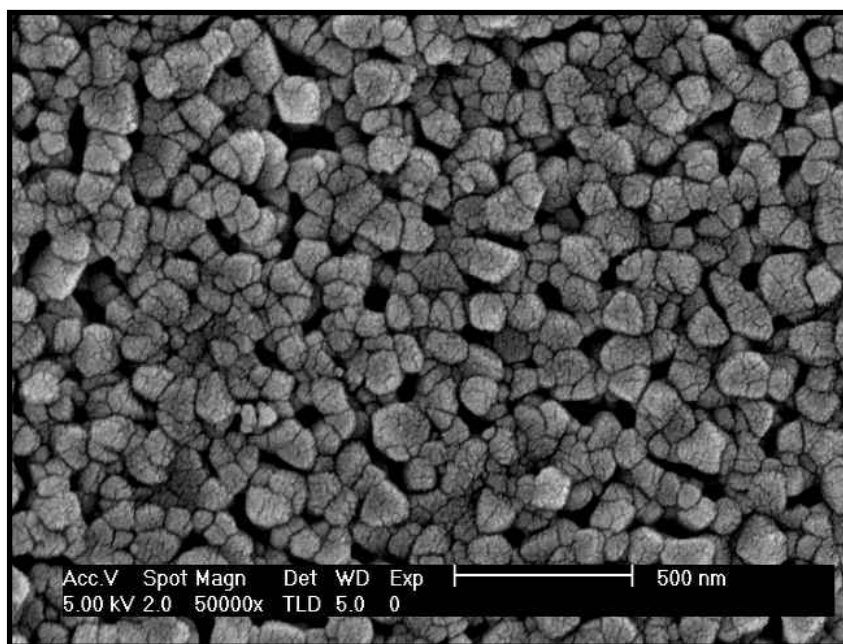
Figure 7.49. SEM micrograph of top surface of the 1-layer 400 ^{o}C treated silica membrane (×50000).
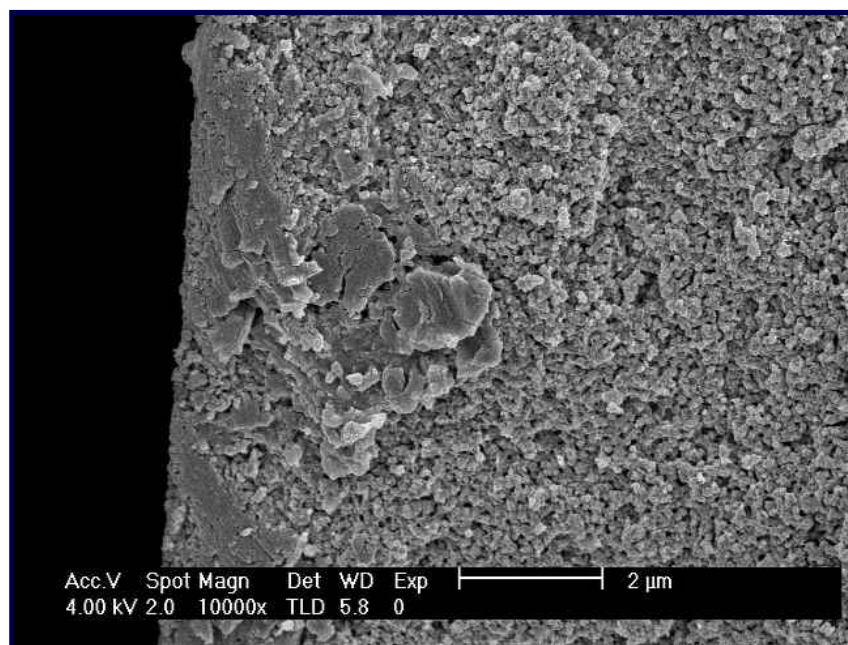

Figure 7.50. SEM micrograph of fracture surface of the 1-layer 400 ^{o}C treated silica membrane (×10000).

Top surface of a silica membrane is shown in Figure 7.51. The membrane was prepared by two times dipping procedure with SiB sol and heat treatment was conducted at 400 ^{o}C. for each layer. No defects (cracks and pinholes) were observed from pictures and silica layer was formed from very small particles on the support surface. Figure 7.52 shows the fractured surface of the same membrane and the penetration into the support is also clearly visible at this picture.
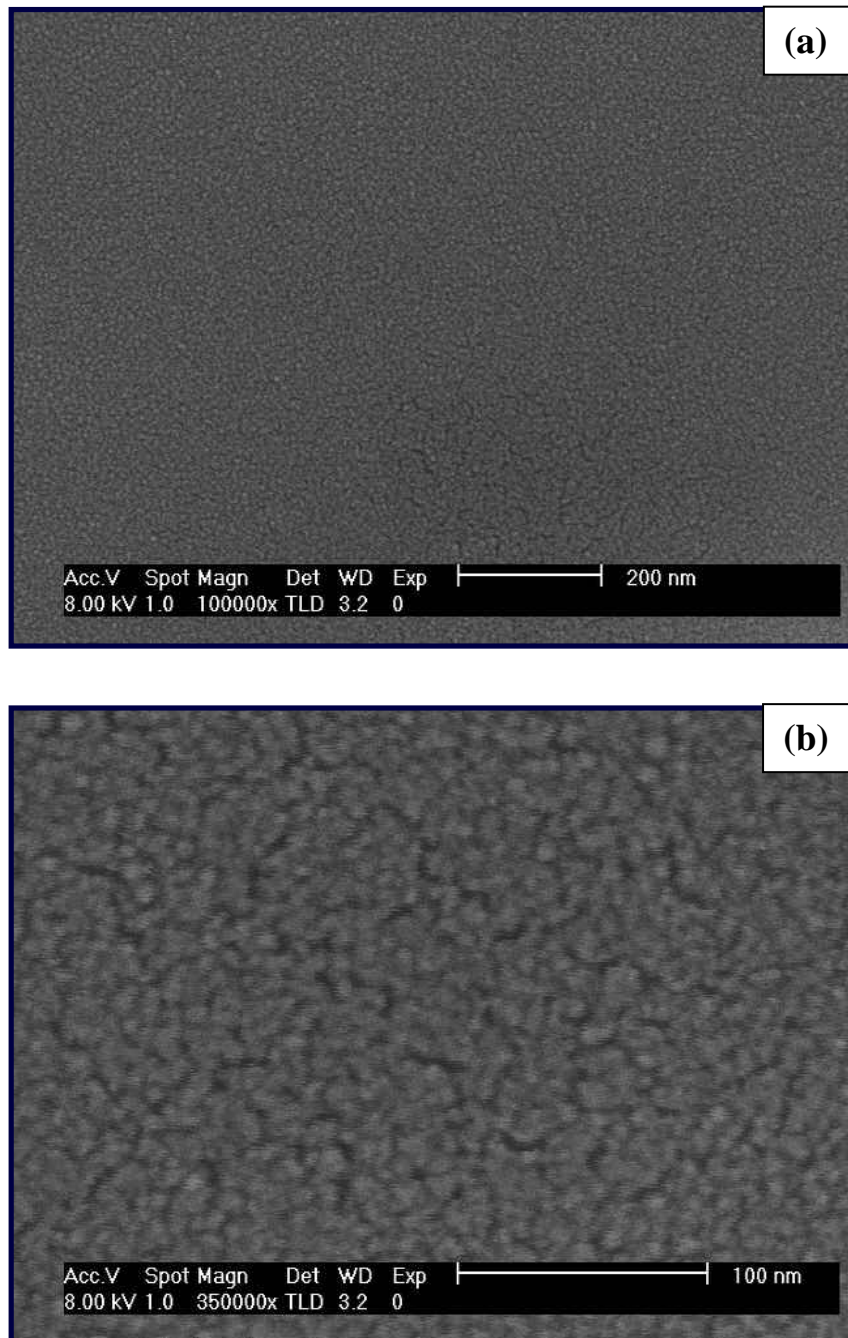

Figure 7.51. SEM micrograph of top surfaces of the 2-layer 400 ^{o}C treated silica membrane: (a) ×100000 (b) ×350000.
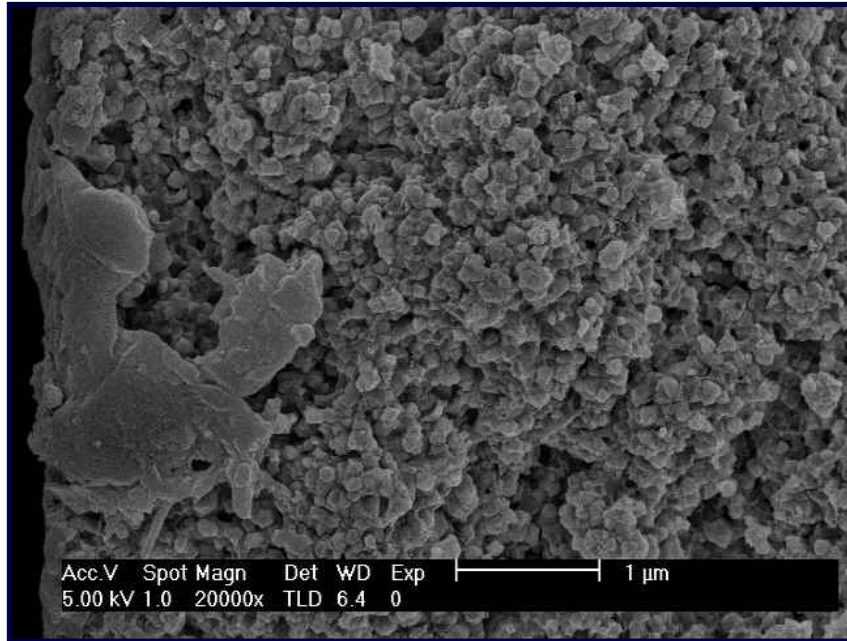
Figure 7.52. SEM micrograph of fracture surface of the 2-layer 400 °C treated silica membrane: ×20000.
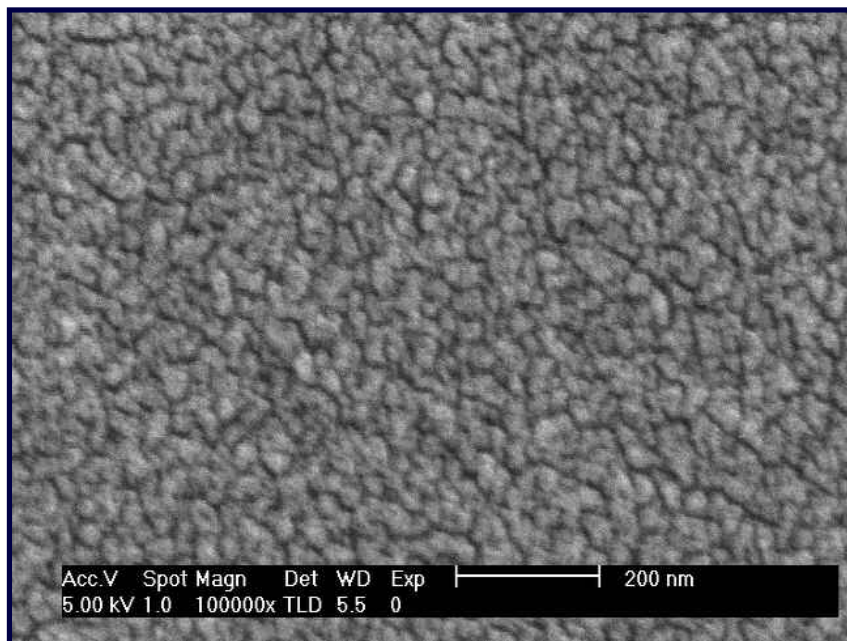

Figure 7.53. SEM micrograph of top surface of the 400 °C treated silica coated on 3-layer alumina membrane: ×100000
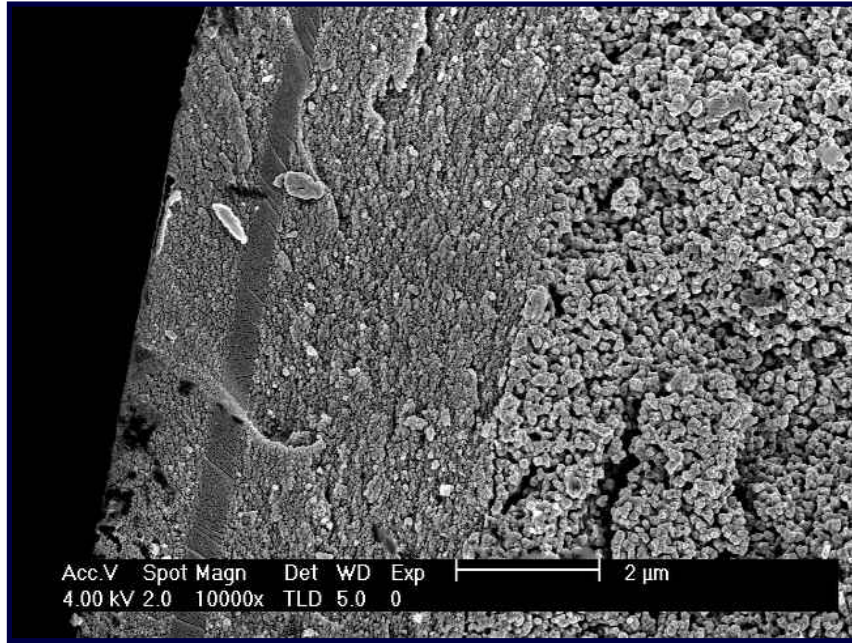
Figure 7.54. SEM micrograph of fracture surface of the 400 $^{\circ}$C treated silica coated 3-layer alumina membrane: ×10000.

7.5. Gas Permeation Results

7.5.1. Zirconia Support Permeation

It is necessary to determine the gas transport characteristics of the substrate so that its contribution to flow through the membrane without the thin top layers is known. The permeability of CO_2 and N_2 through the substrate as a function of front pressure is shown in Figure 7.55, and these values are further tabulated at Table 7.7. It can be easily seen that the permeability of the support increases linearly with pressure. This is an indication of viscous flow besides the Knudsen flow in the support.
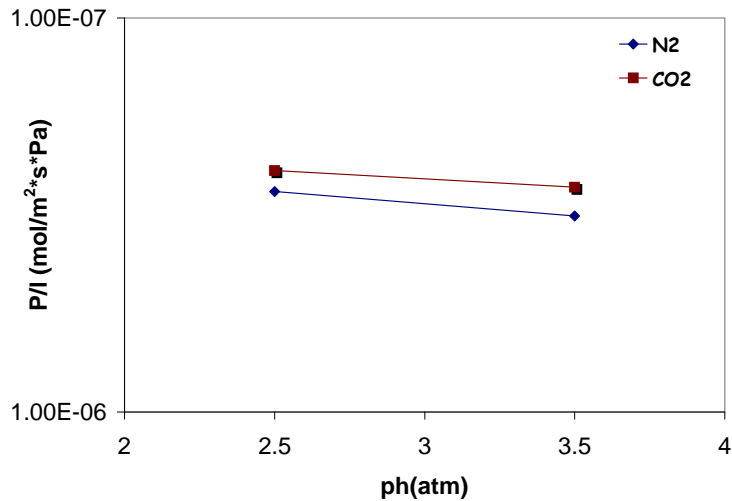

Figure 7.55. N_2 and CO_2 permeation of substrate as a function of pressure.

The N_2/CO_2 separation ratios at high side pressure equal to 2.5 and 3.5 atm are 1.13 (1.25) and 1.18 (1.25), respectively, which are consistent with the Knudsen diffusion mechanism (the ratios expected for a pure Knudsen flow are shown in brackets, which are equal to the inverse square root ratio of the molecular weights of gases). A small contribution from Viscous (laminar) flow that is an unselective mechanism can also be expected and would explain why selectivities with less than ideal Knudsen ratios were obtained.

Table 7.7. Permeability of gases through ZrO_2 substrate.

Gases	Front Pressure (atm)	Permeability (mol/m^2*s*Pa)
CO_2	2.5	$2.44*10^{-7}$
	3.5	$2.69*10^{-7}$
N_2	2.5	$2.76*10^{-7}$
	3.5	$3.18*10^{-7}$

7.5.2. Alumina Membrane Permeation

Permeability measurements with alumina membranes have been performed with N_2, O_2 and CO_2. The variation of the permeabilities of these gases through the one layer alumina membranes with calcination temperature are shown in Figures 7.56, 7.57 and 7.58. It can be seen that for all gases permeabilities of one layer alumina membranes which were calcined 500, 550 and 600 ^oC, increases slightly with pressure. This implies that transport takes places with combined Knudsen flow and Laminar flow.
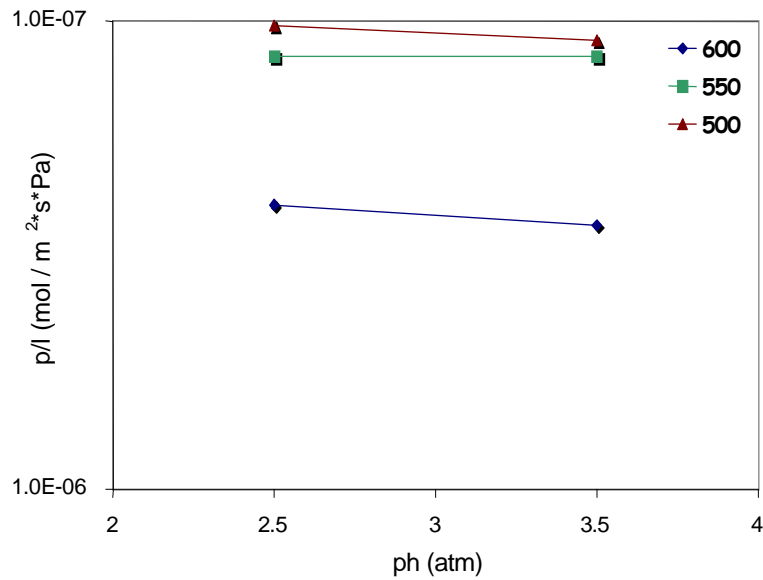

**Figure 7.56. Calcination temperature effect on N_2 permeation for A08-1.**
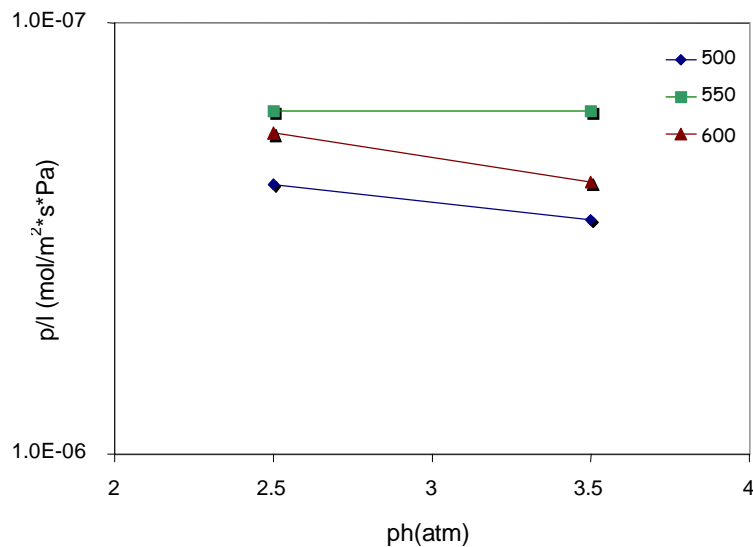
**Figure 7.57. Calcination temperature effect on CO_2 permeation through A08-1.**
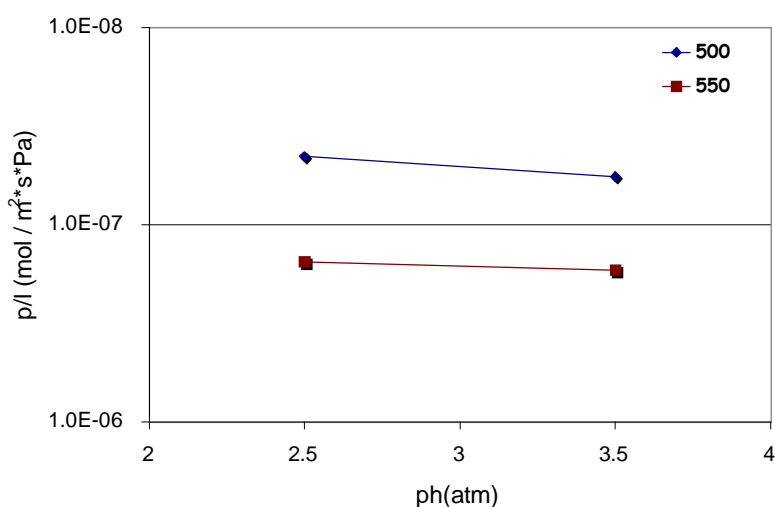
Figure 7.58. Calcination temperature effect on O_2 permeation through A08-1.

The increase in the heat treatment temperature from 500 to 600 ^{o}C increased the permeability of gases. This may be explained by changes in pore radius, porosity, tortuosity and membrane thickness. The first factor was examined by N_2 Adsorption-Desorption Analyzer and calculated pore diameter according to BJH Desorption model were tabulated in Table 7.4. Although 500 ^{o}C treated alumina membrane had a sharp pore size distribution with a mean pore diameter of 2.7 nm, 600 ^{o}C treated membrane had a relatively broad pore size distribution with a mean pore diameter of 2.9 nm. Therefore the change in the pore size resulted in increases in the gas permeability through the membrane. Table 7.8 shows the variations of CO_2, O_2 and N_2 permeabilities, CO_2/N_2 and CO_2/O_2 permselectivities through the one layer alumina membrane.

Table 7.8. Permeability and separation factor of one layer alumina membrane[1].

Heat Treatment T (^{o}C)	N_2 Permeabilities ($*10^{-7}$ mol/m^{2}sPa)	O_2 Permeabilities ($*10^{-7}$ mol/m^{2}sPa)	CO_2 Permeabilities ($*10^{-7}$ mol/m^{2}sPa)	CO_2 / N_2	CO_2 / O_2
500	1.02	0.45	2.37	2.32	5.26
550	1.19	1.54	1.6	1.34	1.04
600	2.47		1.8	0.73	

[1]These results were obtained using a front and back-pressure of 2.5 and 1 atm, respectively.

Separation efficiency of the membrane were also investigated at different heat treatment temperature is shown in Figure 7.59. The increase in heat treatment temperature caused decreases in permselectivities of these gases.
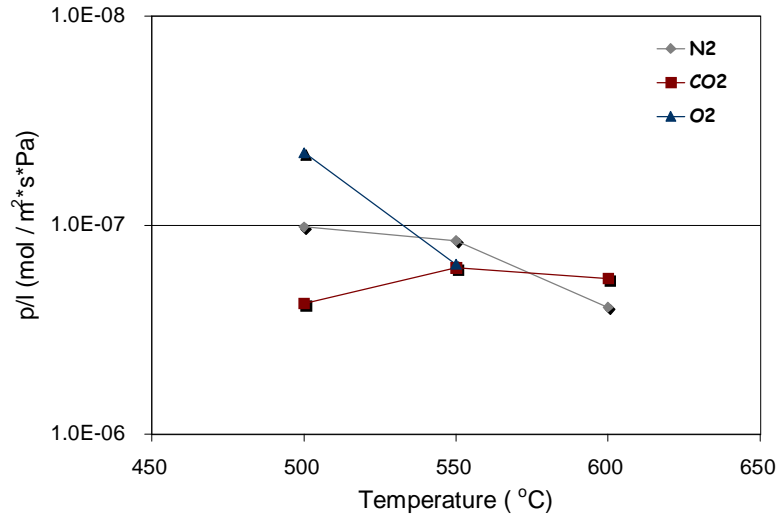
Figure 7.59. Permeances of different gases at different calcination temperatures.

Figure 7.60 and 7.61 illustrate the effects of repeating the dipping-drying-firing procedure on the permeabilities of N_2 and CO_2 through the alumina membrane, respectively. The permeabilities were decreased with the number of coating cycles due to the increase of the thickness of the alumina layer on the substrate. After the first dipping, as can be seen from Figures 7.60 and 7.61, the permeation level of two gases were constant at both pressures indicating that permeation was pressure independent.
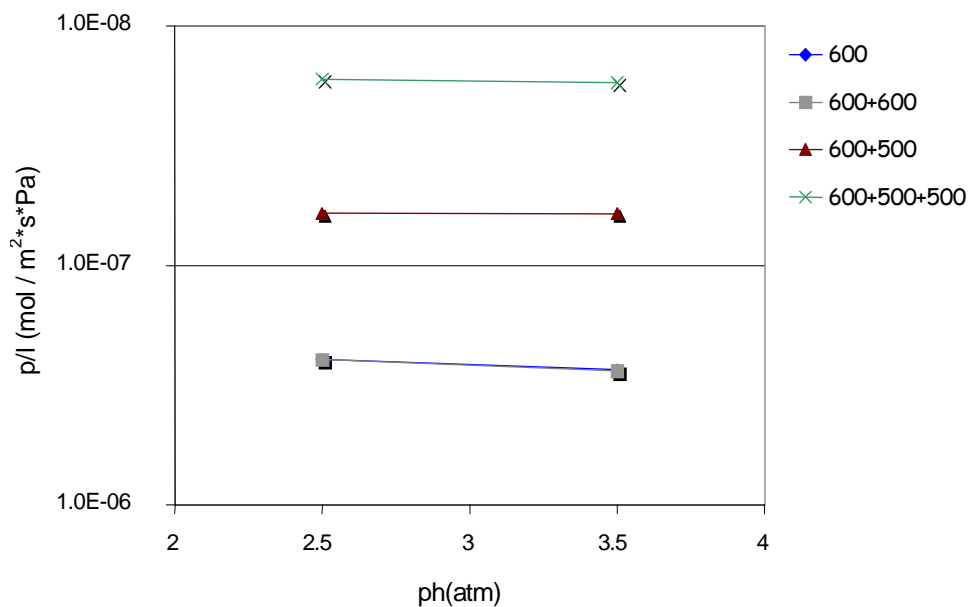
Figure 7.60. N_2 permeance variation with number of layers.

This implies that the dominant transport mechanism for the membranes is Knudsen diffusion as could be expected with a pore size in the 2.5-3 nm range. Also pinholes and cracks were eliminated after the first cycle of the multiple coating process and crack free membranes were prepared.
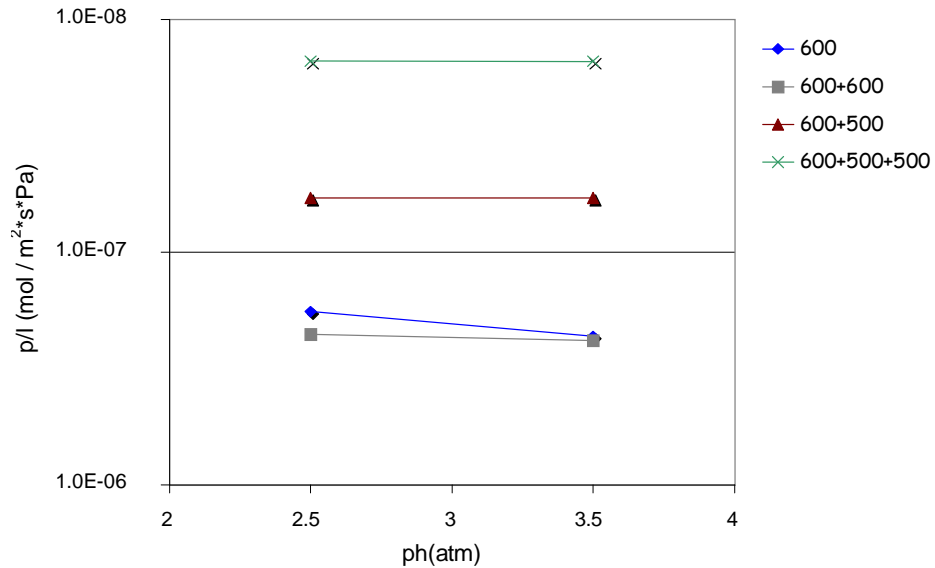
Figure 7.61. CO_2 permeance variation with number of layers.

CO_2 and N_2 permeation results of alumina membranes with respect to the number of dip coating are summarised in Figure 7.62. The permeation rates of both gases decreased with the number of coating cycles. Considering the permselectivity of these gases, one dip coating seems to give the best result.
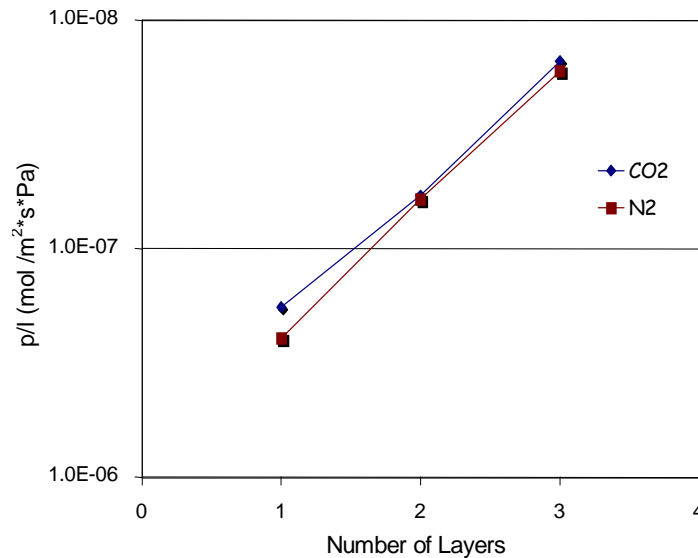
Figure 7.62. Permeance variation with number of layers.

The permeance of N_2 was reported (Okuba et al., 1990) at $2*10^{-6}$ mol m^{-2}s^{-1}Pa^{-1} for 3-layer alumina membranes but pressure independence on gas permeability were found after 6th coating.

7.5.3. Silica Membrane Permeation

The use of silica polymeric sols can make the design of pore networks possible for gas separation problems. The effects of processing parameters like acid amount utilised and the use of organic template during sol preparation, sol aging, heat treatment conditions, dipping time on the permeation of pure gases were investigated in this section.

The thermal stability of a ceramic membrane is one of the most important factors in gas separation applications. Permeability of $CO_2$, O_2 and N_2 was determined for heat treatment temperatures from 50 to 400 ^{o}C in order to investigate the thermal stability of silica membranes which were prepared at different conditions. Permeability increased with increasing heat treatment temperatures as shown in Figures 7.63 to 7.66. This is most likely due to partial sintering and microcrack formation during the shrinkage and densification of the membranes.
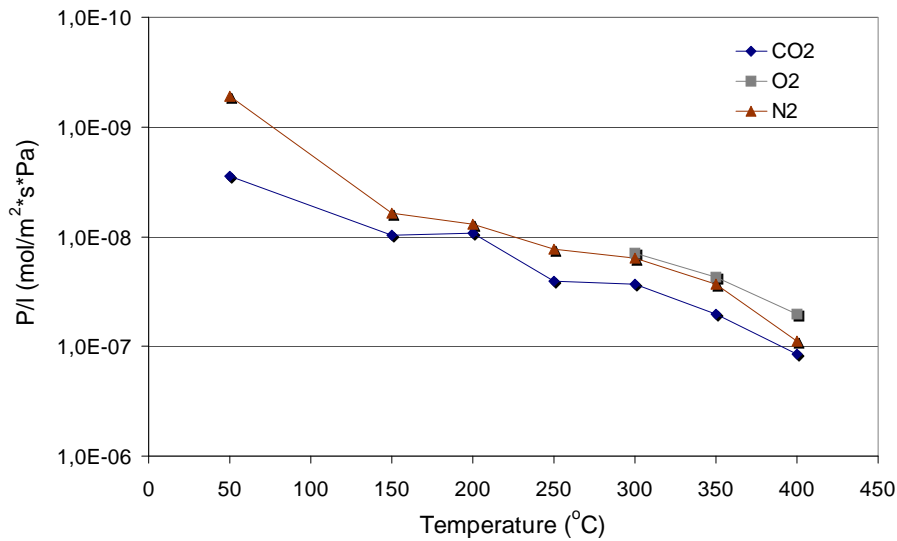
Figure 7.63. SiB-5 membrane permeability variation with heat treatment temperature.

The results have been reported by de Vos and Verweij (1998) with a permeance of (4.7-17.7) * 10^{-7} mol m^{-2}s^{-1}Pa^{-1} (H$_2$) , (2-3.2) * 10^{-7} mol m^{-2}s^{-1}Pa^{-1} (CO$_2$) and (0.09-0.27) * 10^{-7} mol m^{-2}s^{-1}Pa^{-1} (N$_2$) . The H$_2$/CO$_2$ permselectivity ranged between 2.3-7.5 for the membrane calcined at 400 ^{o}C . They were able to produce 30 nm thick high quality silica film with a pore diameter of 0.5 nm.
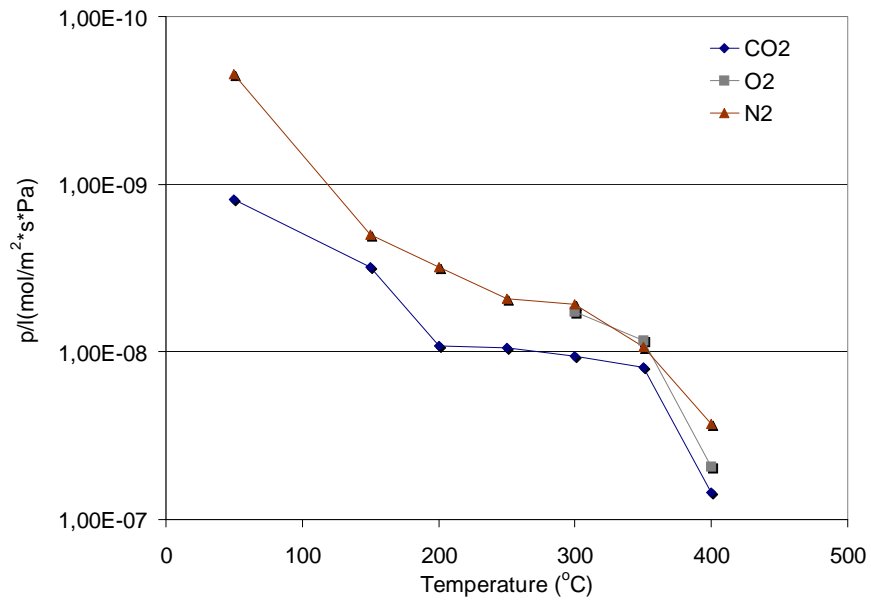
Figure 7.64. SiB-10 membrane permeability variation with heat treatment temperature.
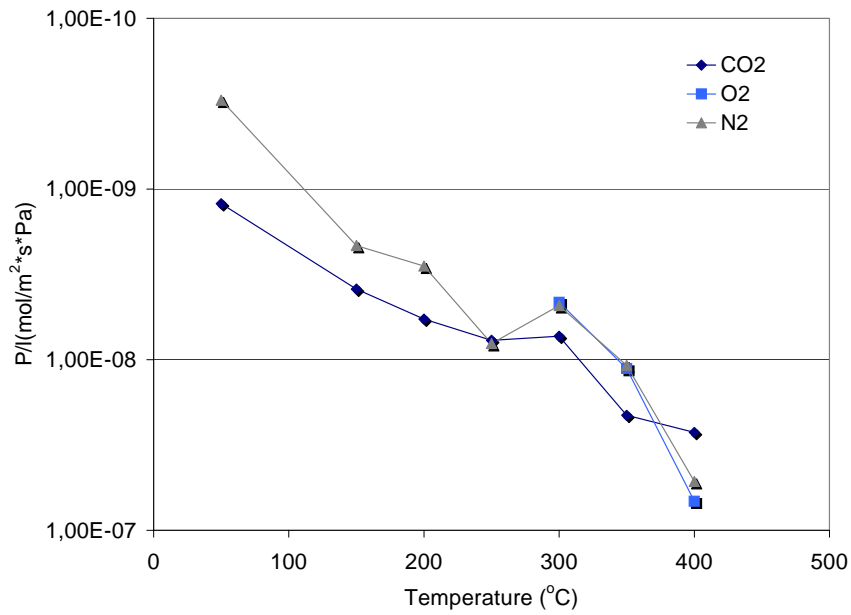
Figure 7.65. SiB-15 membrane permeability variation with heat treatment temperature.
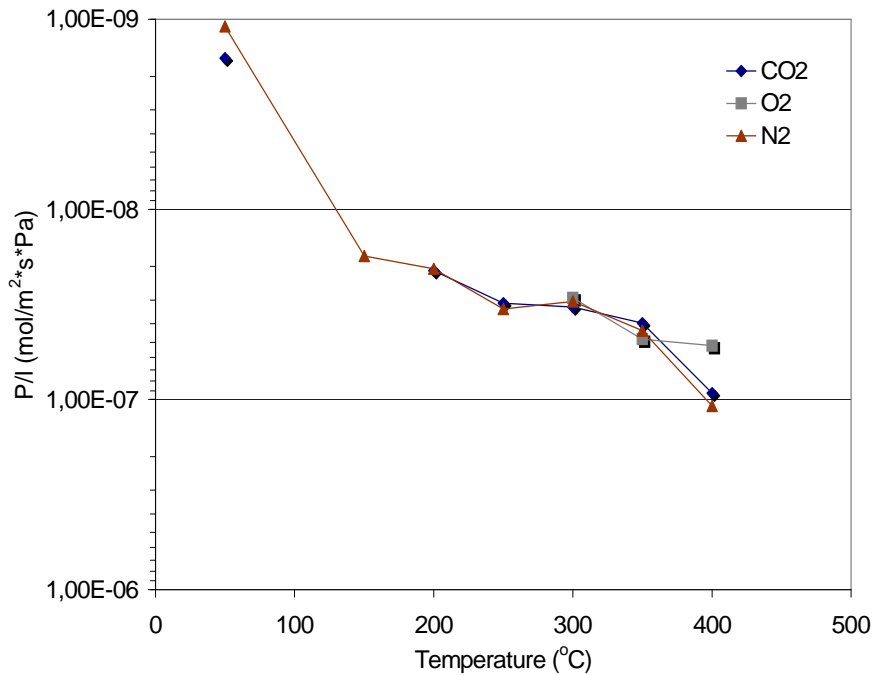
Figure 7.66. SiB-20 membrane permeability variation with heat treatment temperature.

Permeation results for silica membranes with different dipping times have been shown in Figures 7.67 to 7.69. The dipping time was varied from 5 to 20 seconds. N_2 permeability through membranes was lowest for 10 second dipping and the highest value for 20 second dipping for various heat treatment temperatures.
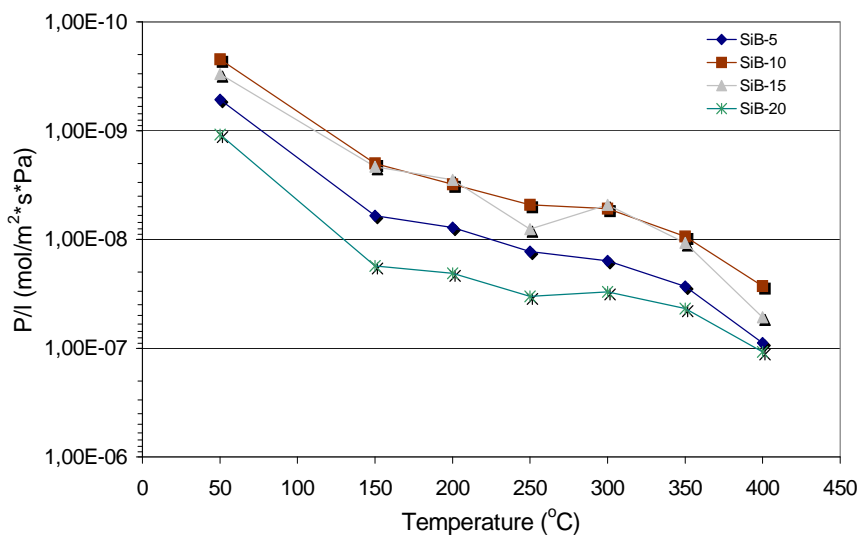
Figure 7.67. The change of N_2 permeability with dipping time as a function of heat treatment temperature.

For the CO_2 permeation, silica membranes had an optimum of 15 seconds dipping time with the lowest permeability and 5 seconds dipped membrane had greater permeance at all heat treatment temperatures. On the other hand, CO_2 permeability through 10 seconds dipped membrane did not show any variation from 150 to 350 ^oC.
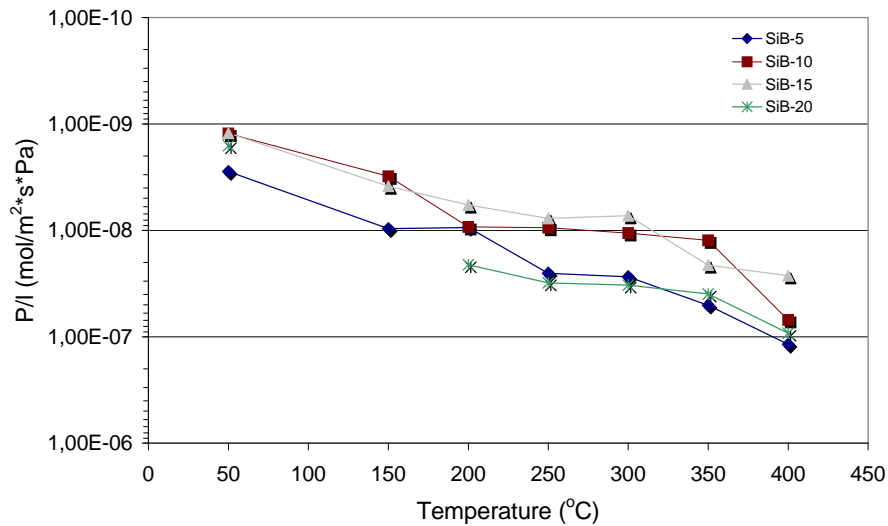
Figure 7.68.The change of CO_2 permeability with dipping time as a function of heat treatment temperature.
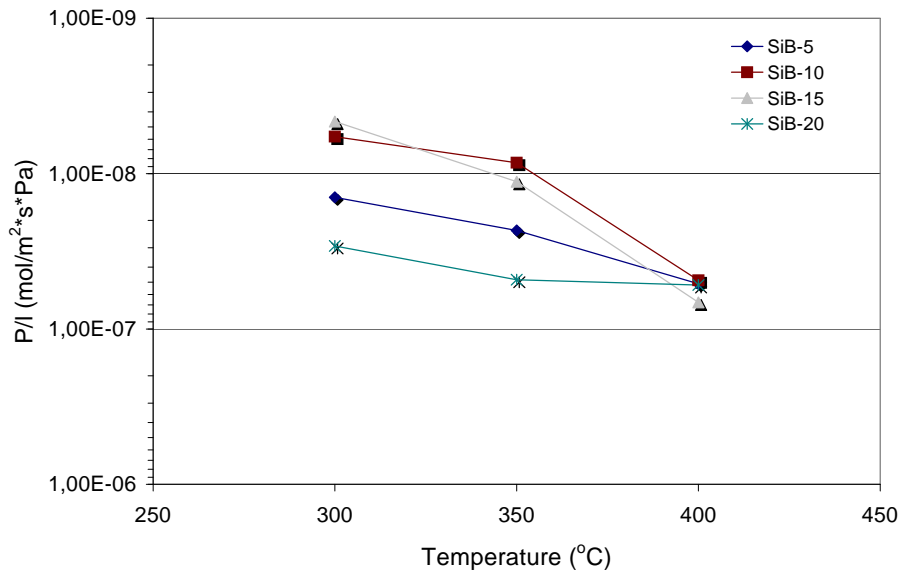
Figure 7.69.The change of O_2 permeability with dipping time as a function of heat treatment temperature.

Dipping time effect on O_2 permeation through silica membrane with changing heat treatment temperature was investigated from 300 to 400^oC as shown in Figure 7.69. It was observed that O_2 permeation rate through the membrane treated at 400^oC converge to the same value eventough the dipping times vary.

Figure 7.70 shows the gas permeation results of 50 ^oC treated silica membranes produced by sol dip coating at various dipping times. The results are summarised by plotting (i) permeation rates of CO_2 and N_2, and (ii) CO_2/N_2 permselectivity with respect to dipping time. The permeation rates of CO_2 and N_2 decreased as the dipping time was increased from 5 seconds to 10 seconds. For 15 seconds dipped membrane, CO_2 permeation rate was almost the same with the 10 seconds dipped silica membrane but N_2 permeability slightly increased. Although N_2 permeation rate increased from $3.02*10^{-10}$ to $10.9*10^{-10}$ mol/m^2*s*Pa as dipping time extended from 15 seconds to 20 seconds, CO_2 permeation rate slightly increased. From the viewpoint of CO_2/N_2 selectivity, 10 second dipping time seems to be the best (~5.6) of all. The theoretical CO_2/N_2 selectivity for the Knudsen diffusion regime is calculated as 0.8. These differences from the theoretical Knudsen CO_2/N_2 selectivity is most likely due to the effects of surface diffusion.
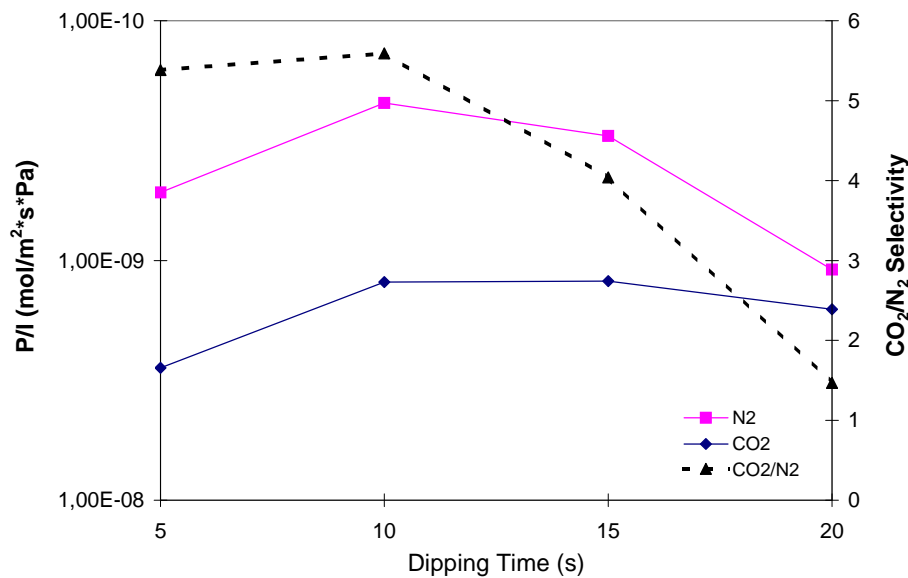
Figure 7.70. Variation of Permeance with dipping time through 1-layer silica membranes treated at 50^oC.

The influence of dipping time on permeance of gases through 400 ^{o}C treated silica membrane is shown in Figure 7.71. In contrast to O_2 permeation rate, CO_2 and N_2 permeation rates decreased significantly as dipping time was increased to 10 seconds. The optimum dipping time during processing was determined to be 10 seconds for N_2 and O_2 permeation, but 15 seconds dipping into sol seems to be best for CO_2 permeation through 400 ^{o}C treated silica membrane.
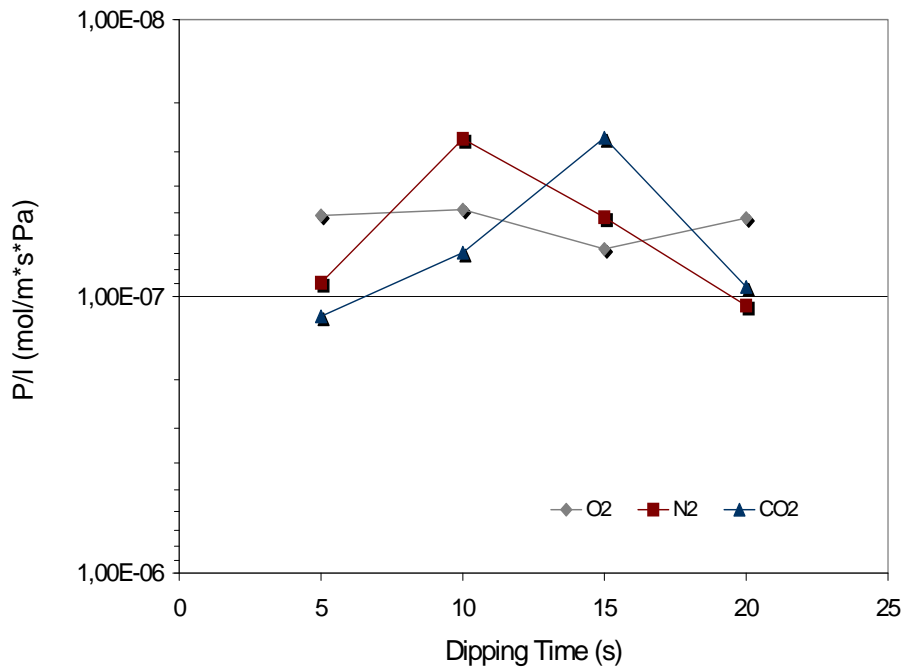
Figure 7.71.Variation of Permeance with dipping time through 1-layer silica membranes treated at 400°C.

It was also found that application of longer dipping time caused to the formation of a thick gel and resulted in cracking or peeling off during drying, since the thickness of the membrane is proportional to the square root of the dipping time. This is explained by the slip casting model. On the other hand, a shorter dipping time is not sufficient to form a gel during dipping. Therefore a certain dipping time at certain sol concentration is necessary to obtain a thin membrane layer without defects. The difference in the gas permeation performance might be attributed to this behavior of membranes.

The variation of the permeability of O_2, N_2 and CO_2 through two layer 50 ^{o}C treated silica membranes with aging time is shown in Figure 7.72. The increase in permeability may attributed to increase in porosity of the membrane with aging the sol prior to film formation. Aging of the sol may cause increased fractality of the constituent polymers of the membrane, hence increasing the pore size and the porosity of the dried gel. As can be seen in Figure 7.72, significant permeability increases with aging was observed up to 4 hours. Thereafter, permeability of gases did not show any variation up to 12 hours.
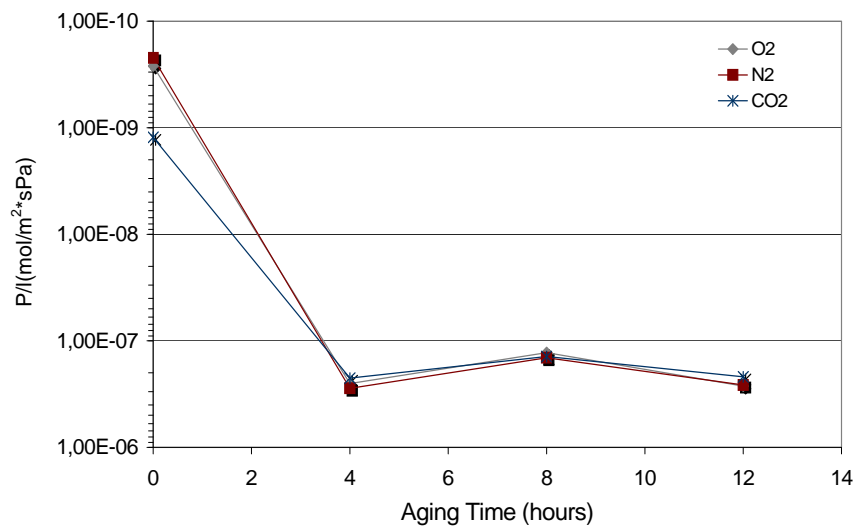
Figure 7.72. Aging time effect on permeability of 2-layer silica membrane treated at 50 ^{o}C.

Figure 7.73 summarizes O_2 permeation results for the two layer 50 and 400 ^{o}C treated silica membranes at various aging times. Similar to the case of 50 ^{o}C treated membrane, permeation rate of O_2 through 400 ^{o}C treated membrane increases significantly with an extremely same slope as the aging time was increased up to 4 hours. It can be understood from both figures that the pore microstructure of the silica membrane can be modified by aging of the sol prior to film deposition. Gas permeation performance of membranes varies significantly due to the changes in the pore structure of the membrane with increasing aging time.
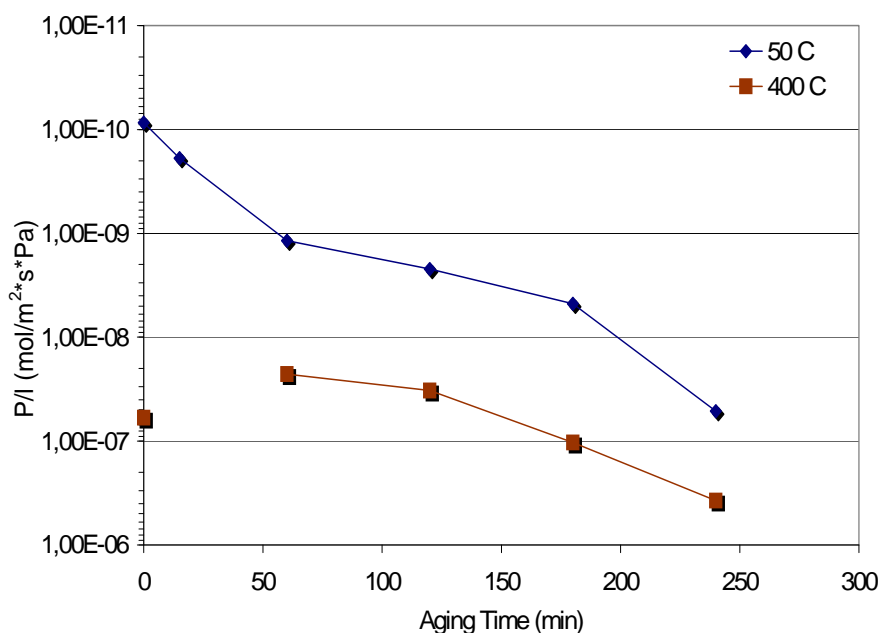
Figure 7.73. O$_2$ permeability variation through 2-layer silica membrane with aging time.

Synthesis composition of the reactants is an important factor in deciding the structure of the final membranes produced by sol-gel techniques. The synthesis parameters can influence the fractal behavior of the polymers and hence will affect the packing behavior. As can be expected an increase in the hydrolysis ratio (acid ratio) increased the porosity (shown by an increase in gas permeance) which consequently reduced the permselectivity of the gases as shown in Figures 7.74 to 7.77. This may be explained in terms of acceleration of the condensation reaction which leads to the formation of larger pores after drying and calcination of the membrane. If the catalyst concentration is low, almost no polymer are formed and also during the condensation rate is slow. This means packing can be dense. High permselectivity was obtained for SiA membranes which had the lowest acid concentration as shown in Figure 7.74. The details of the gas permeation behavior of the SiC membrane is shown in Figure 7.76. In contrast to other membranes, permeation of gases through SiC membrane did not show significant variation in the heat treatment temperature range 50 - 400 ^{o}C.
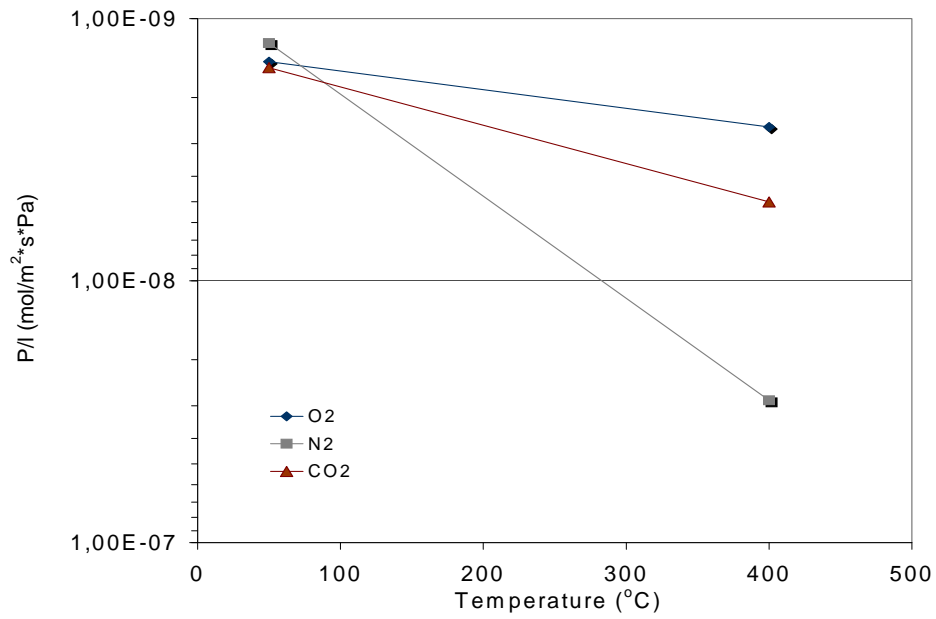
Figure 7.74.Permeance variation of silica (SiA-10) membrane with heat treatment temperature.
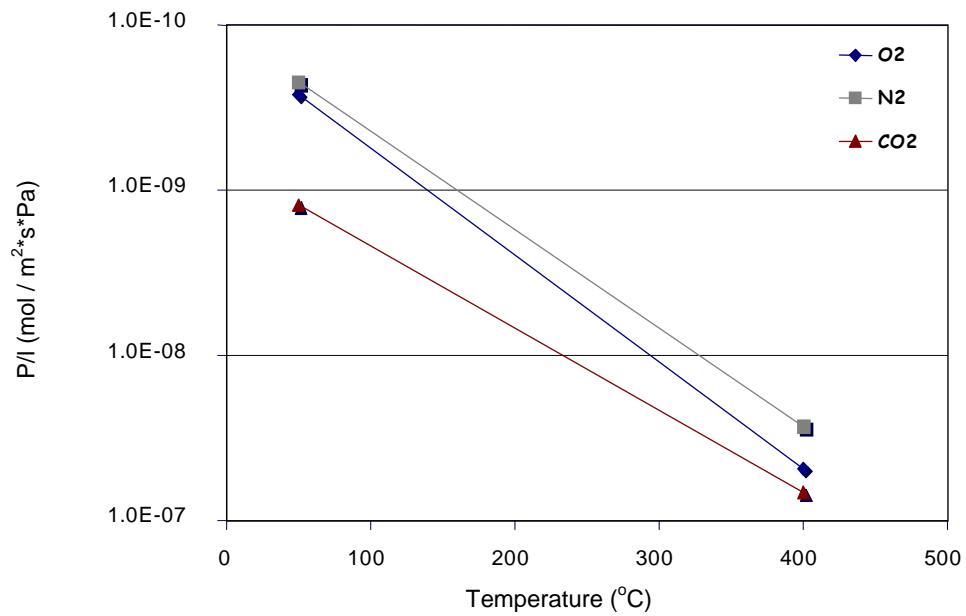
Figure 7.75. Permeance variation of silica (SiB-10) membrane with heat treatment temperature.
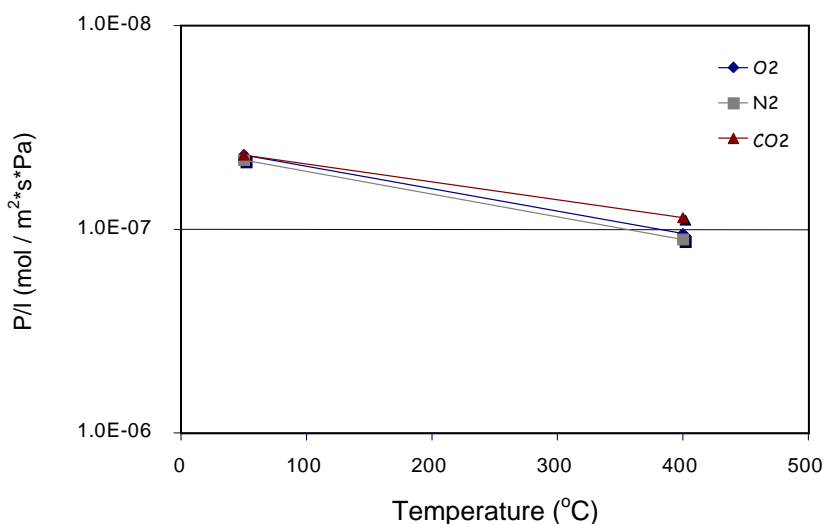
Figure 7.76. Permeance variation of silica (SiC-10) membrane with heat treatment temperature.

In order to investigate the effect of organic ligands as micropore templates, silica membranes (SiD) were prepared from sols which contained 10 mol % MTES/TEOS and their permeances were determined for all tested gas molecules showed very low permeance values. The permeance results shown in Figure 7.77 seems to be largely independent of heat treatment temperature, though the permeance may be slightly higher at 400 °C treated membrane while permselectivities nearly remained unchanged. These results indicate that methyl ligands remained unreacted in the membranes after calcination at 400 °C as can be seen in TGA curve of SiD (Figure 7.19).
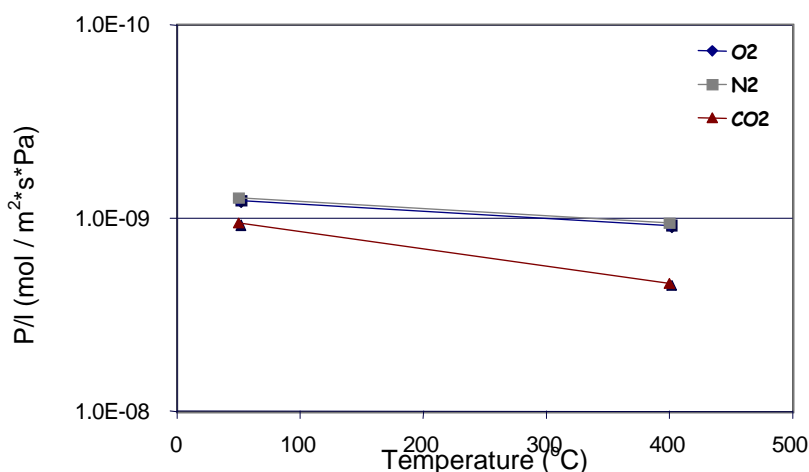
**Figure 7.77. Permeance variation of silica (SiD-10) membrane with heat treatment temperature.**

Kusakabe et al., (1999) also prepared organic templated membranes with TEOS and alkyltriethoxysilanes. They reported permeance of $8*10^{-9}$ mol $m^{-2}s^{-1}Pa^{-1}$ (CO_2) and $2.8*10^{-9}$ mol $m^{-2}s^{-1}Pa^{-1}$ (CH_4).

CHAPTER VIII

CONCLUSIONS AND RECOMMENDATIONS

This report gives an overview about the preparation, structure and transport (permeance) properties of composite ceramic membranes consisting of mesoporous (γ-Al_2O_3) and microporus (SiO_2) layers on top of a macroporous ZrO_2 substrate.

Thin membranes of γ-Al_2O_3 and SiO_2 with relatively sharp-fine pore size distribution were produced by sol-gel processing. Pinholes and cracks on membrane surfaces were eliminated by repeated dipping-drying-firing procedure.

In the preparation of alumina sols and membranes by the sol-gel method many factors, such as type of acid, acid concentration and water content can affect the particle sizes of the alumina sols and pore size distributions of the membranes. The increase in the acid content of the sols caused decreases in sol particle sizes however increase of water content had a contrary effect on particle size. Particle diameters in the sols containing 0.07 to 0.4 mol HNO_3 per mol alkoxide as water content is constant and 100 to 180 mol water per mol alkoxide as acid content is constant, measured by DLS were expressed in terms of Stokes diameter assuming spherical particles. All sols were clear and transparent but the sol of 0.25 HNO_3/Al mole ratio had the smallest mean particle size of about 30 nm and 12 nm in terms of hydrodynamic diameter and number based particle diameter, respectively.

Thermal analysis results were used to determine the dehydration behavior of dried boehmite gels and the required temperature of the phase change to γ-Al_2O_3.There are primarily four stages in the weight loss curves. These were concluded to be due to the removal of water from pores, the removal of adsorbed-chemically bound water, the NO_3 removal and the decomposition of the boehmite to γ-Al_2O_3 at about 427^oC. The TGA analysis of the silica unsupported membranes have shown a two stage thermal behaviour, the removal of physical water from pores and adsorbed-chemically bound water.

X-Ray diffraction was used for phase identification. X-Ray patterns of the 200 ^oC dried film which was prepared by using a sol containing 0.25 mol HNO_3 per mol alkoxide (A08) corresponds the γ-AlOOH (boehmite) phase, and the crystallite size was

calculated by Scherer's equation. For boehmite the transformation sequence upon heating is,

$$\gamma\text{-AlOOH} \rightarrow \gamma \rightarrow \delta \rightarrow \theta \rightarrow \alpha\text{-Al}_2\text{O}_3$$

However, the diffraction peaks of samples which were heat treated at 500, 600,700, 800, and 900 ^{o}C, very broad because of poor crystallinity and no distinction could be made between polytypes. Moreover, only the (400) and (440) reflections can be used for the determination of the crystallite size. XRD patterns of 1200 ^{o}C heat treated sample attributed to the $\alpha\text{-Al}_2\text{O}_3$ peaks so complete transformation occurred at 1200 ^{o}C.

N_2 adsorption-desorption isotherms of all $\gamma\text{-Al}_2\text{O}_3$ membranes are almost similar in shape and they were classified as Type IV isotherms. The pore diameters were calculated from desorption branch by using BJH method and were in the range of 28-45 ^{o}A. The increase in the acid content of the sol caused almost a proportional decrease in both the sol particle size and the membrane pore diameter. This obviously indicates the fact that packing of smaller particles results in finer pore structures. The significant implication of this would be the ability of designing the microstructure of the membrane. Also one of the advantages of sol-gel processing for preparing membranes is the ability to vary the pore size with firing temperature. This fact may permit the choice of a desired calcination temperature for special applications. A08 sample that had the smallest particle size leads to the largest BET surface area and the smallest pore size (2.8 nm) when calcined at 500 ^{o}C. Increasing the calcination temperature to 600 ^{o}C caused to slight increases in the pore size. As a result pore size of the alumina membranes can be tailor made, by varying the calcination temperature and acid concentration of the sol.

Permeability measurement with alumina and silica membranes have been carried out on a pressure controlled dead-end mode membrane system with N_2, O_2 and CO_2. First the permeability of the slip-cast zirconia supports were measured as a function of front pressure. Alumina layers were formed on top of the support by using A08 sols. The N_2 permeability decreased by 11 % , 56 % and 63 %for 600 ^{o}C, 550 ^{o}C and 500 ^{o}C treated one layer alumina membrane, respectively. In addition, N_2 permeability of the support decreased by % 76 for the two layer and %94 for the three layer alumina membrane .

For all gases permeance through $\gamma\text{-Al}_2\text{O}_3$ membranes were independent of the mean pressure across the membrane except the 600 ^{o}C treated one layer alumina

membrane. This implies that no laminar flow occurs as could be excepted in these small pores. Because of pressure independent permeability, it can be concluded that for these gases Knudsen diffusion is the dominant transport mechanism in the alumina membranes prepared in this work.

The crack free alumina membrane thickness was 3.2 μm after two dipping-drying and heating procedure when a dilute sol (A08) of 0.2 M was used. The surface morphology and its change on calcination temperature were clarified using high-resolution SEM.

Silica membrane were prepared on ZrO_2 support with silica sols. However the sol penetrated into the substrate and SEM examination of fractured cross-sections showed that discrete silica layers were not formed on to surface of the substrate. That seepage causes increase the effective thickness which reduces the permeability.

The hydrolysis ratio is an important factor because of its effect on pore microstructure of membranes produced by sol-gel process. As can be expected an increase in the acid content increased the porosity (shown by an increase in permeability) which consequently reduced the selectivity of gases.

Silica membranes were heat treated from 50^oC to 400 ^{o}C in order to investigate the effect of heat treatment temperature on gas permeability. The increase in heat treatment temperature increased the permeability of gases. However, as the hydrolysis ratio was increased this effect became smaller. Permeance of gases investigated in this work through silica membranes were independent of the mean pressure across the membranes.

The variation of the permeability through 50 ^{o}C and 400 ^{o}C heat treated silica membranes with sol aging time was investigated up to 16h. After the 16h sol became more viscous and gelling was observed. Aging of silica sols prior to membrane formation caused the increase in permeability of O_2 due to change in the pore microstructure of membranes.

The permeability measurement through Titania, Zirconia and composite membranes including TiO_2, SiO_2, ZrO_2 and Al_2O_3 would yield valuable information on the gas separation ability and pore structure of ceramic membranes. Permeation measurements can be performed at certain temperatures as a function of kinetic diameters of different gases (He, H_2, CH_4, C_3H_8) to understand the transport properties and separation efficiency of membranes.

REFERENCES

1. Alie C., Benhaddou A., Pirard R., Lecloux A.J., Pirard J.-P., "Textural Properties of Low Density Xerogels", Journal of Non-Crystalline Solids, 270 pp:77-90 (2000).

2. Ayral A., Balzer C., Dabadie T., Guizard C., Julbe A., "Sol-gel Silica Membranes with Tailored Microporous Structures", Catalysis Today, 25 pp: 219-224, (1995).

3. Bhave, R. R., "Inorganic Membranes, Synthesis, Characteristics and Applications", (1991).

4. Brinker, C. J. and Scherrer G.W., " Sol-Gel-glass: I. Gelation and Gel structure", J. Non Crystalline solids, 70 pp: 301-322, (1985).

5. Brinker C.J., Sehgal R., Hietala S.L., Deshpande R., Smith D.M., Loy D. and Ashley C.S., "Sol-gel Strategies for Controlled Porosity Inorganic Materials", Journal of Membrane Science , 94, pp:85-102, (1994).

6. Brinker, C. J. and Scherrer G.W., " Sol-Gel Science: The Physics and Chemistry of Sol-gel Processing", Academic Press, (1990).

7. Burggraaf A.J., Vroon Z.A.E.P., Keizer K., Verweij H., " Permeation of Single Gases in Thin Zeolite MFI Membrane", Journal of Membrane Science, 144, pp: 65-76, (1998).

8. Chai M., Machida M., Eguchi K., Arai H., " Preparation and Characterization of Sol-gel Derived Microporous Membranes with High Thermal Stability", Journal of Membrane Science, 96, pp: 205-212, (1994).

9. Chane-Ching J.Y., and Klein Lisa C., "Hydrolysis in the Aluminium sec-Butoxide-Water-Isoprpyl Alcohol System: II, Aging and microstructure", J. Am. Ceram. Soc., 71,(1), pp: 86-90 (1998).

10. Chang C.-H., Gopalan R., Lin Y.S. , "A Comparative Study on Thermal and Hydrothermal Stability of Alumina, Titania and Zirconia Membranes", Journal of Membrane Science, 91, pp: 27-45, (1994).

11. Changrong X., Feng W., Zhaojing M. Fanqing L., Dingkun P., Guangyao M., " Boehmite Sol Properties of Two-layer Alumina Membrane by a Sol-gel Process" Journal of Membrane Science, 116, pp: 9-16, (1996).

12. Charpin j., Brgez P., Valin F., "Inorganic Membranes: Preparation, Characterization, Specific Application", High Tech. Ceramics, Elsevier Publication, pp: 2211-2225 (1987).

13. Cho Y.K., Han K., Lee K.H., "Separation of CO_2 by Modified γ-Al_2O_3 Membranes at High Temperature", Journal of Membrane Science, 104, pp: 219-230, (1995).

14. Choi J.G., Do D.D., Do H.D., "Surface Diffusion of Adsorbed Molecules in Porous Media: Monolayer, Multilayer, and Capillary Condensation Regimes", Ind. Eng. Chem. Res.,40, pp:4005-4031, (2001).

15. Curran M.D., Stiegman A.E., "Morphology and Pore structure of Silica Xerogels Made at Low pH", Journal of Non-Crystalline Solids, 249 ,pp:62-68 (1999).

16. Da Costa, J. C. D., Lu G.Q., Zhu H.Y. and Rudolph V., "Novel Composite Membranes for Gas Separation: Preparation and Performance", Journal of Porous Materials 6, pp. 143-151 (1999).

17. Da Costa, J. C., Lu G. Q., Rudolph V., Lin Y. S., "Novel Molecular Sieve Silica Membranes: Characterisation and Permeation of Single and Two Step Sol-gel Membranes", Journal of Membrane Science 198, pp. 9-21 (2002).

18. De Lange R.S.A., Keizer K., Burggraaf A.J., "Formation and Characterization of supported Microporous Ceramic membranes Prepared by Sol-gel Modification Techniques", Journal of Membrane Science ,99, pp. 57-75 (1995a).

19. De Lange R.S.A., Keizer K., Burggraaf A.J., "Analysis and Theory of Gas Transport in Microporous Sol-gel Derived Ceramic Membrane", Journal of Membrane Science ,104, pp: 81-100, (1995b).

20. De Lange R.S.A., Hekkink J.H.A, Keizer K., Burggraaf A.J.," Permeation and Separation Studies on Microporous Sol-gel Modified Ceramic Membranes", Microporous Materials ,4, pp:169-186 (1995c).

21. De Vos R. M., Verweij H., "Improved Performance of Silica Membranes for Gas Separation " Journal of Membrane Science , 143, pp: 37-51, (1998).

22. Fujiii, T., Yano T., Nakamura K., Miyawaki O., " The Sol-gel Preparation of Nanoporous Silica Membrane with Controlled Pore Size", Journal of Membrane Science, 187, pp. 171-180 (2001).

23. Hsieh H.P., Bhave R.R., Fleming H.L., "Microporous Alumina Membranes", Journal of Membrane Science , 39 (3)., pp:221-241, (1988).

24. Huang X., Meng G., Huang Z., Geng J., "Preparation of Unsupported Alumina Membrane by Sol-gel Techniques", Journal of Membrane Science , 133, pp:145-150, (1997).

25. Iler, R. K., "The Chemistry of Silica", John Wiley & Sons (1979).

26. Jia M.D., Chen B., Noble R. D., Falconer J. L., "Ceramic-zeolite Composite Membranes and Their Application for Separation of Vapor/Gas Mixtures", Journal of Membrane Science , 90, pp:1-10, (1994).

27. Kang B. S., Hyun S.H., " γ-Alumina Composite Membranes Modified with Microporous Silica for CO_2 Separation", J. Mater. Sci., 34, pp:1391-1398 (1999).

28. Keizer K., Uhlhorn R.J.R., Van Vuren R.J., Burggraaf A.J., "Gas Separation Mechanisms in Microporous Modified γ-Al_2O_3 Membranes", Journal of Membrane Science , 39, pp:285-300, (1988).

29. Klein L.C., Gallagher D., "Pore Structure of Sol-gel Silica Membranes", Journal of Membrane Science , 39 (3)., pp:213-220, (1988).

30. Koros W.J., Ma Y.H., Shimidzu T., " Terminology for Membranes and Membrane Processes" Journal of Membrane Science , 120, pp:149-159, (1996).

31. Kuraoka, K., Kubo N., Yazawa T., "Microporous Silica Xerogel Membrane with High Selectivity and High Permeance for CO_2 Separation", Journal of Sol-gel Science and Technology 19, pp., 515-518 (2000).

32. Kusakabe K., Sakamoto S., Saie T., Morooka S., "Pore Structure of Silica Membranes Formed by a Sol-gel Technique Using Tetraethoxysilane and Alkyltriethoxysilanes", Separation Science and Tech., 16 pp:139-146 (1999).

33. Larbot A., Alami-Younssi S., Persin M., Sarrazin J., Cot L., "Preparation of a γ-Alumina Nanofiltration Membrane", Journal of Membrane Science , 97, pp:167-173, (1994).

34. Larbot A., Fabre J.P., Guizard C., Cot T., "Inorganic Membranes Obtained by Sol-gel Techniques", Journal of Membrane Science , 39 (3)., pp:203-212, (1988).

35. Leenaars A.F.M., Keizer K., Burggraaf A.J., "The Preparation and Characterization of Alumina Membranes with Ultra-Fine Pores, Part I: Microstructural Investigation on Non-Supported Membranes", Journal of Mater. Science , 19, pp:1077-1088, (1984).

36. Lenza R.F.S., Vasconcelos W.L., "Synthesis and Properties of Microporous Sol-gel Silica Membranes", Journal of Non-Crystalline Solids, 273 ,pp:164-169 (2000).

37. Lin, Y.S., de Vries, J. and Burggraaf, A.J., "Thermal Stability and Its Improvement of the Alumina Membrane top layers Prepared by Sol-Gel Methods", J. Mater. Sc,., 26 pp: 715-720, (1991a).

38. Lin Y-S., Burggraaf, A.J., "Preparation and Characterization of High-Temperature Thermally Stable Alumina Composite Membrane",J. American Ceram. Soc.,74 (1), pp:219-224 (1991b).

39. M-Aguado M.J., Gregorkiewitz M., Bermejo F.J., "Structural Characterization of Silica Xerogels", Journal of Non-Crystalline Solids, 189 ,pp: 90-100 (1995).

40. Meixner D.L., Dyer P.N., "Characterization of the Transport Properties of Microporous Inorganic Membranes", Journal of Membrane Science , 140, pp:81-95, (1998).

41. Morooka, S. and Kusakabe K., "Microporous Inorganic Membranes for Gas Separation", MRS Bulletin 24(3), pp.25-28 (1999).

42. Munoz-Aguado M.J., Gregorkiewitz M., "Preparation of Silica-based Microporous Inorganic Gas Separation Membranes", Journal of Membrane Science , 111, pp:7-18, (1996).

43. Nair B. N., Yamaguchi T., Okubo T., Sumatsu H., Keizer K., Nakao S-I. " Sol-gel Synthesis of Molecular Sieving Silica Membranes", Journal of Membrane Science , 135, pp:237-243, (1997a).

44. Nair, B. N., Elferink J. W., Keizer K., Verweij H., "Preparation and Structure of Microporous Silica Membrane", Journal of Sol-gel Science and Technology 8, pp., 471-475 (1997b).

45. Naito M., Nakahira K., Fukuda Y., Mori H., Tsubaki J., "Process Conditions on the Preparation of Supported Microporous SiO_2 Membranes by Sol-gel Modification Techniques", Journal of Membrane Science , 129, pp:263-269, (1997).

46. Okubo T., Watanabe M., Kusakabe K. and Morooka S., "Preparation of γ-Al_2O_3 Thin Membrane by Sol-gel Processing and It's Characterization by Gas Permeation", J. Mater. Science, 25, pp:4822-4827, (1990).

47. Ramsay J.D.F., "Characterization of the Pore Structure of Membranes", MRS Bulletin, pp:36-40, March, (1999).

48. Rey N. L., Shemilt J.E.,Ralph B., Williams H.M., "A Novel Method for the Evaluation of Thin Ceramic Membranes", J. Mater. Sci.,32, pp:3913-3920 (1997).

49. Scherer G. W., "Aging and Drying of Gels", Journal of Non-Cryst. Solids, 100, pp:77-92, (1988).

50. Scherer, G.W., "Theory of Drying", J. American Ceramic Soc., 73, pp:77-92, (1990).

51. Shi L., Tin K-C., Wong N-B., "Thermal Stability of Zirconia Membranes", J. Mater. Sci., 34, pp:3367-3374 (1999).

52. Tsai C.Y., Tam S.Y., Lu Y., Brinker C.J., "Dual-layer Asymmetric Microporous Silica Membranes", Journal of Membrane Science ,169, pp:255-268, (2000).

53. Uhlhorn R.J.R., Huis In't Veld M. H. B., Keizer K., Burggraaf A.J., "Synthesis of Ceramic Membranes Part I: Synthesis of Non-Supported   and Supported γ-Al_2O_3 Membranes Without Defects", J. Mater. Science, 27, pp:527-537, (1992).

54. Vercauteren, S. and Keizer K., Vansant E. F., Luyten J. and Leysen R., "Porous Ceramic Membranes: Preparation, Transport Properties and Applications", Journal of Porous Materials 5, pp. 241-258 (1998).

55. Vroon Z.A.E.P., Keizer K., Burggraaf A.J., Verweij H., "Preparation and Characterization of Thin Zeolite MFI Membranes on Porous Supports", Journal of Membrane Science , 144, pp:65-76, (1998).

56. Wang P., Huang P., Xu N., Shi J., Lin Y.S., "Effects of Sintering on Properties of Alumina Microfiltration Membranes", Journal of Membrane Science , 155, pp:309-314, (1999).

57. Ward D. A., Ko E.I., "Preparing Catalytic Materials by the Sol-gel Method", Ind. Eng. Chem. Res. ,34, pp:421-433 (1995).

58. Webb, P. A. and Orr C., "Analytical Methods in Fine Particle Technology", Micromeritics Instrument Corp. (1997).

59. West, G.D., Diamond G. G., Holland D., Smith M. E., Lewis M. E., "Gas Transport Mechanisms Through Sol-gel Derived Templared Membranes", Journal of Membrane Science 5175, pp. 1-17 (2002).

60. Wu J.C.S., Sabol, H. , Smith G.W., Flowers D.L., Liu P.K.T., "Characterization of Hydrogen-Permselective Microporous Ceramic Membranes", Journal of Membrane Science , 96, pp:275-287, (1994).

61. Yelken G., "Preparation and Characterization of Inorganic Membranes by Using Sol-gel Techniques", MS Thesis, IYTE,2000.

62. Yoldas B. E., "Transparent Porous Alumina", Ceramic Bulletin, 54,3,pp: 286-288 (1975a).

63. Yoldas B. E., "Alumina Sol Preparation from Alkoxides", Ceramic Bulletin, 54,3,pp: 289-290 (1975b).

64. Yoshioka, T., Nakanishi E., Tsuru T., Asaeda M., "Experimental Studies of Gas Permeation through Microporous Silica Membranes", AlChE Journal, 47(9), pp. 2052-2063, (2001).

65. Zarzyckı, J., "Past and Present of Sol-Gel Science and Technology", Journal of Sol-gel Science and Technology,8, pp: 17-22 (1997).